



<https://theses.gla.ac.uk/>

Theses Digitisation:

<https://www.gla.ac.uk/myglasgow/research/enlighten/theses/digitisation/>

This is a digitised version of the original print thesis.

Copyright and moral rights for this work are retained by the author

A copy can be downloaded for personal non-commercial research or study,
without prior permission or charge

This work cannot be reproduced or quoted extensively from without first
obtaining permission in writing from the author

The content must not be changed in any way or sold commercially in any
format or medium without the formal permission of the author

When referring to this work, full bibliographic details including the author,
title, awarding institution and date of the thesis must be given

Enlighten: Theses

<https://theses.gla.ac.uk/>
research-enlighten@glasgow.ac.uk

Investigations and Developments
Relevant to a Prototype Laser
Interferometric Gravitational Wave
Detector

by

David Ian Robertson

Department of Physics and Astronomy
University of Glasgow.

Presented as a thesis for the degree of
Ph.D. in the University of Glasgow.

May 1990.

©David Ian Robertson 1990.

ProQuest Number: 11007393

All rights reserved

INFORMATION TO ALL USERS

The quality of this reproduction is dependent upon the quality of the copy submitted.

In the unlikely event that the author did not send a complete manuscript and there are missing pages, these will be noted. Also, if material had to be removed, a note will indicate the deletion.



ProQuest 11007393

Published by ProQuest LLC (2018). Copyright of the Dissertation is held by the Author.

All rights reserved.

This work is protected against unauthorized copying under Title 17, United States Code
Microform Edition © ProQuest LLC.

ProQuest LLC.
789 East Eisenhower Parkway
P.O. Box 1346
Ann Arbor, MI 48106 – 1346

Contents

1	Gravitational Radiation - Production and Detection	1
1.1	Introduction	1
1.2	Sources	2
1.2.1	Supernovae	3
1.2.2	Binary Coalescence	4
1.2.3	Periodic Sources	5
1.2.4	Stochastic Background	6
1.3	Detectors	6
1.3.1	Resonant Bar Detectors	7
1.4	Laser Interferometric Detectors	9
1.4.1	Photon Shot Noise	12
1.4.2	Frequency Noise	13
1.4.3	Other Optical Noise	13
1.4.4	Displacement Noise	13
2	Methods of Frequency Stabilisation	15
2.1	Sources of Noise	15
2.1.1	Fundamental Noise	15
2.1.2	Technical Noise	16
2.2	Active Stabilisation	18
2.3	Frequency References	18
2.4	Feedback Transducers	22
2.5	Conclusions	24
3	A Frequency Stabilisation System	26

3.1	Frequency Noise	26
3.2	The Optical Cavities of the Prototype Detector	27
3.3	Passive Stabilisation	27
3.4	Previous Frequency Stabilisation System	27
3.5	Method of Feedback	30
3.6	Two Loop System	31
3.7	First Loop	32
3.7.1	Results	34
3.8	Second Loop	35
3.8.1	Frequency Response	35
3.8.2	Other Feedback Paths	36
3.8.3	Results	37
3.9	Problems	39
4	Servo Analysis	40
4.1	Introduction	40
4.2	Stability	41
4.3	Changes in GH	42
4.4	Bypass Design of Electronics	42
4.5	The First Loop	44
4.6	The Second Loop	51
4.7	Total Gain	54
4.8	Limitations	55
5	Data Collection	56
5.1	Introduction	56
5.2	Signals to be Recorded	57
5.3	Sampling Analogue Signals	58
5.4	Analogue Signals	59
5.5	Digital Signals	63
5.6	Other Information	65

6	Data Analysis	66
6.1	Introduction	66
6.2	Duty Cycle	66
6.3	Tape Checking	67
6.4	Displacement Noise Level	68
6.5	Noise Statistics	70
6.5.1	Improved Analysis	72
6.5.2	Limitations	73
6.6	Coherence Function	75
6.6.1	Microphone Signal	75
6.6.2	Seismometer Signal	77
6.7	Conclusions	78
7	Seismic Isolation and Thermal Noise	79
7.1	Suspension Systems	79
7.1.1	Single Pendulum	80
7.1.2	Double Pendulums	81
7.1.3	Wire Resonances	86
7.2	Measuring Suspension Quality Factors	88
7.2.1	End Masses	88
7.2.2	Centre Masses	90
7.3	Measurement of the Q of the Test Masses	91
A	Circuits	93
A.1	Diode Clipping	93
B	Intensity Noise Measurements	99
C	Two Data Analysis Programs	103

List of Figures

1.1	Induced Displacement of Test Masses	7
1.2	Michelson Interferometer	9
1.3	Multipass Michelson Interferometer	10
1.4	Fabry-Perot Detector	11
3.1	Previous Frequency Stabilisation Scheme	29
3.2	Diagram of Laser Rear PZT Mount	30
3.3	Block Diagram of the Two Loop Stabilisation System	32
3.4	Details of the Two Loop Stabilisation System	33
3.5	Mirror Resonance	35
3.6	Acousto-Optic Modulator	36
3.7	Laser Frequency Noise	38
4.1	Simple Servo	40
4.2	Split Feedback System	43
4.3	Bode Plot (gain) for the First Loop	46
4.4	Bode Plot (phase) for the First Loop	47
4.5	Nyquist Plot for the First Loop	48
4.6	Unstable Nyquist Plot	50
4.7	Second Loop Electronics	52
4.8	Nyquist Plot for the Second Loop	53
4.9	Total Gain	54
5.1	Bessel Filter Response	59
5.2	Data Acquisition System	60
6.1	Tape Duty Cycle	67

6.2	Typical Sensitivity Measurement	69
6.3	Sensitivity against Time	70
6.4	Pulse Height Graph	71
6.5	Improved Pulse Height Graph	74
6.6	Coherence Function (microphone signal)	76
6.7	Coherence Function (seismometer signal)	77
7.1	Simple Pendulum	80
7.2	Double Pendulum	82
7.3	Thermal Noise	84
7.4	Transfer Function	85
7.5	Wire Resonances	87
7.6	Suspension of Centre Mass	90
7.7	Test Mass Resonance	92
A.1	Diode Clipped Amplifier	94
A.2	Circuit of First Servo (part1)	95
A.3	Circuit of First Servo (part2)	96
A.4	Circuit of Second Servo (part1)	97
A.5	Circuit of Second Servo (part2)	98
B.1	Intensity Noise	101

Acknowledgements

I would like to thank my supervisor Jim Hough for his help and guidance during the period of this work.

Thanks are also due to the other members of the gravitational waves group Harry Ward, Gavin Newton, Brian Meers, Norna Robertson, Graham Kerr, John Mangan, Norman Mackenzie, Peter Veitch, Kenneth Strain, Caroline Cantley, Allan Carmichael, Jennifer Logan and Euan Morrison for their advice and encouragement.

I am grateful for the interest and support of Prof. I. Hughes and Prof. R. Ferrier.

Technical support was ably provided by Jim Pittillo, Allan Latta, Angus McKellar, John Jarvis and David Edwards.

I am grateful to SERC for financial support.

Lastly I would like to thank my family and friends for all their help, encouragement and support.

This thesis was written using the \LaTeX document preparation system.

Preface

The construction of a 10m interferometer for the detection of gravitational radiation was started in Glasgow University in 1978 and work is still continuing on the development of the detector. In addition there are plans to build a large scale detector with a 3km baseline and techniques relevant to such a detector are also under development. This thesis describes work done in the period October 1986 to September 1989.

Chapter 1 is an introduction to gravitational radiation. The first part is a short review of the sources of gravitational radiation most likely to be detected by terrestrial interferometric detectors operating in the frequency range from a few tens of Hz to ~ 10 kHz. The second part of the chapter is a brief review of the properties of both resonant bar detectors and laser interferometric detectors.

Chapter 2 is a review of methods used to stabilise laser frequency.

Chapter 3 covers the development of a narrow band frequency stabilisation system for the laser used to illuminate the prototype detector. This work was carried out in collaboration with Dr. Harry Ward and Dr. Brian Meers.

Chapter 4 is an analysis of the servo loops used in the frequency stabilisation system developed in the previous chapter. I wrote a computer program to calculate the gain of the nested two loop system and then used it to investigate the gain and stability of the system under a variety of conditions.

Chapter 5 describes the signals recorded during a 100 hour data run with the prototype detector. I was responsible for organising which signals to record. The signals were chosen in consultation with the rest of the group who also helped instrument the data acquisition system. I designed, built and tested the prototype data acquisition modules. Each module contained differential amplifier, signal shaping filters and anti-aliasing filters which conditioned the signals before they

were recorded.

Chapter 6 shows the results of my preliminary analysis of the data recorded during the 100 hour run. Two of my data analysis programs are given in Appendix C.

Chapter 7 is a summary of my work on the seismic isolation provided by some suspension systems, their thermal noise, and the thermal noise in test masses.

The intensity noise measurements in Appendix B were made mainly by myself with a little help from Prof. Jim Hough and Dr. Harry Ward.

Summary

Gravitational waves are travelling distortions in the curvature of space-time. They are a prediction of most relativistic theories of gravity, including general relativity. Their coupling to matter is extremely weak and the only sources likely to be detectable are violent astrophysical events where huge amounts of matter are accelerated very rapidly. Gravitational radiation is quadrupole in nature. It causes a tidal strain in space. With the prototype detector at Glasgow we aim to detect this strain by measuring the differential length change induced in two orthogonal reference arms. This is done using optical interferometry.

Chapter 1 is a general introduction to gravitational radiation. The first part is a short review of the sources likely to be detectable by terrestrial interferometric detectors and bar detectors. This is followed by a review of the main features of both resonant bar detectors and interferometric detectors, including a discussion of the main noise sources in both types of detector.

The frequency of the illuminating laser needs to be stabilised in interferometric gravitational wave detectors and this is dealt with in the next three chapters. Chapter 2 is a review of the methods used to improve the frequency stability of lasers. It concentrates on continuous, single mode gas lasers such as the argon ion laser used to illuminate the detector at Glasgow.

In our prototype detector the laser is frequency locked to one of the 10m long Fabry-Perot cavities. To achieve the desired sensitivity the residual frequency noise must be $< 10^{-4}\text{Hz}/\sqrt{\text{Hz}}$ at 1kHz. This requires a frequency stabilisation system with a gain of $> 2 \times 10^7$ at 1kHz. Chapter 3 describes a new frequency stabilisation system which achieves this performance. The system is narrow band, as would be required for a large scale detector. It employs two nested servo loops to achieve the desired gain.

Chapter 4 is an analysis of the gain and stability of the nested servo loop system described in the previous chapter.

The next two chapters concern a 100 hour data run with the prototype detector. Chapter 5 describes the preparation for the run. It includes details of the timing system used and a description of each of the signals that were recorded. Chapter 6 describes the preliminary analysis of the data taken during the run. This analysis was carried out to look at the behaviour of the detector rather than to look for signals from astrophysical sources. The variation of the noise level with time, noise statistics of the data and possible contamination of the data by acoustic and seismic noise were investigated.

Chapter 7 starts with a discussion of the results of some calculations of the seismic isolation and thermal noise in some single and double pendulum suspension systems. These show that thermal noise in the lowest stage of the suspension system is likely to be dominant. Measurements of the Q of the suspension of the test masses and of the test masses themselves are then described.

Appendix A contains diagrams of the circuits used in the frequency stabilisation system described in chapters 3 and 4, some of their special features are commented on.

In appendix B the results of intensity noise measurements in three large frame argon ion lasers are given. These show that the level of high frequency intensity noise varies widely depending on the type of plasma tube used. The measurements were taken in the range 0-7MHz.

Appendix C contains two of the data analysis programs.

Chapter 1

Gravitational Radiation - Production and Detection

1.1 Introduction

For the last two decades there has been considerable interest in searching for gravitational radiation and there are many laboratories around the world where active work on the development of gravitational wave detectors is being carried out.

Gravitational waves are ripples in the curvature of spacetime. They are a prediction of general relativity and other relativistic theories of gravity. They were first predicted by Einstein when he showed that, in a weak field approximation, the field equations of general relativity could be made linear and a wave equation solution obtained [Einstein 1916]. This showed that the waves propagated with the speed of light and carried energy away from a suitable system of accelerating masses. In general relativity gravitational radiation is generated by systems in which the mass has a time varying quadrupole moment. It has two polarisation states and its amplitude is characterised by a dimensionless strain h . The effect of a gravitational wave of amplitude h on a length l defined between two free test masses will be to alter the length by Δl , h is $\frac{2\Delta l}{l}$ for $l \ll \lambda_{GW}$.

While indirect evidence for the production of gravitational radiation at the level predicted by general relativity has come from observation of the pulsar PSR1913+16 [Taylor and Weisberg 1982] there has been no convincing direct observation of gravitational radiation. However experimental development is reaching

the stage where the researchers concerned can now see the way forward to building instruments capable of detecting the predicted levels of gravitational radiation from astrophysical sources.

This chapter is a brief introduction to sources and detectors of gravitational radiation. A much more detailed review is contained in [Thorne 1987] and there is a recent review of detectors [Blair 1990]. General relativity is taken to be the accepted theory of relativity throughout the rest of this thesis.

1.2 Production of Gravitational Radiation

The basic problem in both the production and the detection of gravitational radiation is that its coupling to matter is very weak, much weaker than, for example, electro-magnetic radiation. To give an idea of scale the gravitational force between two protons is a factor of 10^{36} weaker than the electrostatic force. It is thus very hard to generate or detect gravitational radiation. A further problem is that gravitational radiation is generated most efficiently by quadrupole radiation; monopole and dipole radiation are excluded by the conservation of mass-energy and the conservation of momentum respectively. This leads to the conclusion that it is unlikely that any detectable terrestrial source of gravitational radiation will be built in the foreseeable future. For example a bar of length 10m and mass 10^5 kg rotated about its centre at 1000 radians per second would only radiate $\sim 10^{-22}$ W of gravitational radiation. The most likely sources of detectable gravitational radiation are violent astrophysical events where huge amounts of mass are moving at large (relativistic) velocities and with very high accelerations.

The detection of gravitational radiation is interesting for two main reasons. The first is the confirmation of general relativity or other relativistic theories of gravity. This information will come from the amplitude, polarisation and speed of travel of the radiation. The second relates to the information carried by the waves about the regions where they are produced. Present day astronomy is based on electromagnetic observations. Electromagnetic radiation is easily scattered and absorbed and cannot escape from high gravity, high density regions without interacting with

the matter that generally surrounds such regions. In contrast gravitational radiation is emitted strongly in these regions and has virtually no interaction with the surrounding matter. The gravitational radiation carries information about violent astrophysical events which is unobtainable by other methods and which is qualitatively different from previous data. This previously unavailable information about the movement of matter should open up a whole new window on the universe.

This section is intended as a brief review of some of the first sources likely to be detected by a new generation of gravitational radiation detectors. It will however be disappointing if signals from some unexpected sources are not detected.

1.2.1 Supernovae

Supernovae were for a long time thought to be the most promising sources of gravitational radiation. The first bar detectors (see section 1.3.1) were optimised to look for signals from supernovae.

There are two types of supernovae. Type I supernovae occur in systems where a white dwarf accretes matter from a companion star. The white dwarf then undergoes a nuclear explosion and may produce a neutron star.

Type II supernovae occur in highly evolved massive stars when the radiation pressure from the nuclear reactions in the core is no longer sufficient to prevent gravitational collapse. The star then undergoes a rapid collapse to form a neutron star or a black hole.

The amount of gravitational radiation given off in either of the above cases depends on the sphericity of the event. The less spherically symmetric the event the greater the amplitude of the gravitational radiation emitted. Numerical simulations have been done to try to predict the waveforms of the emitted gravitational radiation [eg. Saenz and Shapiro 81]. Unfortunately little is known of the initial conditions in supernovae and any predictions of the strength or waveform of the emitted radiation are therefore highly uncertain and only broad generalisations can be made. It seems likely that the energy radiated in the form of gravitational waves will be some small fraction of a solar mass and the amplitude of this radiation can

be estimated. The characteristic amplitude of a burst source at a distance r_0 which emitted an energy ΔE_{GW} of a characteristic frequency f_c is given by Equation 1.1 [Thorne 1987].

$$h_c \sim 2.7 \times 10^{-21} \left(\frac{\Delta E_{\text{GW}}}{10^{-2} M_{\odot} c^2} \right)^{\frac{1}{2}} \left(\frac{1 \text{kHz}}{f_c} \right)^{\frac{1}{2}} \left(\frac{10 \text{Mpc}}{r_0} \right) \quad (1.1)$$

Where M_{\odot} is the mass of the sun, and 10Mpc is the distance to the Virgo cluster of galaxies.

There may also be gravitational radiation emitted by any newly formed object. For example the collapse may form a black hole in which the quadrupole modes are excited, these would then radiate, damping the oscillation.

1.2.2 Binary Coalescence

Systems of two objects orbiting each other will emit gravitational radiation at a frequency equal to twice the orbital frequency. In order to produce gravitational radiation at frequencies likely to be detectable by planned terrestrial detectors the system would have to consist of two compact objects such as neutron stars or black holes in close orbit. Two normal stars orbiting each other would coalesce well before the gravitational radiation reached a suitable frequency.

Two compact objects orbiting each other will lose energy by gravitational radiation. This loss of energy causes the orbits to decay. The objects spiral together and as this happens the frequency and amplitude of the emitted radiation increases. This produces a ‘chirp’ signal whose characteristics depend only on a few parameters (the total mass of the system ($M_{\text{T}} M_{\odot}$), its reduced mass (μM_{\odot}) and the distance from the source to the earth (r_{100}), measured in hundreds of Mpc).

$$\langle h_c \rangle = 10^{-23} M_{\text{T}}^{\frac{2}{3}} \mu f_{100}^{\frac{2}{3}} r_{100}^{-1} \quad (1.2)$$

$$\tau = \frac{f}{\dot{f}} = 7.8 M_{\text{T}}^{-\frac{2}{3}} \mu^{-1} f_{100}^{-\frac{8}{3}} \quad (1.3)$$

($\langle \dots \rangle$ represents an average over the source and detector orientations.)

Signals from coalescing compact binaries are likely to be the first signals detected by terrestrial laser interferometric detectors. They produce a highly predictable characteristic signal lasting for many cycles. Such signals may be searched for in the output of a detector using a series of matched filters.

The total mass and reduced mass enter Equations 1.2 and 1.3 in the same way. It is therefore possible to solve the equations to get the distance to the source [Schutz 1986]. If the source can be detected optically then this will allow a much more accurate determination of Hubble's constant than has previously been possible. If only the neighbourhood of the source can be identified then a statistical method should still allow an accurate measurement of Hubble's constant [Schutz 1986].

1.2.3 Periodic Sources

Compact binary systems will emit gravitational radiation at a virtually constant frequency and amplitude for most of their lifetime. The final increase in frequency and amplitude only occurs close to coalescence.

Other sources of periodic gravitational radiation are rotating neutron stars. These will emit gravitational radiation only if they are not symmetric about their axis of rotation. The amplitude of the radiation increases with both speed of rotation and the size of the deviation from axisymmetry. The crust of the neutron star may be deformed by the presence of a magnetic field that is not aligned with the axis of rotation [Zimmerman 1978]. Other deviations from axisymmetry could be caused by lumps in the solid crust of the star; these may be associated with 'starquakes' in older stars [Pandharipande *et al.* 1976] or asymmetric collapse in those that have been recently formed. If the period of rotation of the neutron star is short enough the star will be beyond the Chandrasekhar[70]-Friedman-Schutz[78] instability point and will emit gravitational radiation. The radiation is generated by hydrodynamic waves in the star travelling in the opposite direction to the stars rotation and being driven by the back reaction from the gravitational radiation. It is difficult to accurately predict the frequency of this radiation. The stars can

be either recently formed neutron stars or old neutron stars that have been ‘spun up’ by the accretion of mass, and therefore angular momentum, from a companion star.

1.2.4 Stochastic Background

A possible background of gravitational radiation will result from the superposition of gravitational radiation from many sources and may also result from stochastic processes in the early universe. It can only be detected by cross-correlation of the output of at least two independent detectors.

There are many possible sources of background radiation.

- There could be primordial gravitational radiation, analogous to the microwave background, but a remnant of an even earlier stage of the universe (10^{-43} second). This radiation would be far too weak to detect unless it was amplified by its interaction with the background curvature of space and its peak amplitude could well fall outside the bandwidth of planned detectors [Allen 1988]. There are too many unknowns to make any reliable estimate of the strength of such signals.
- A population of massive pre-galactic stars (Population III stars) which evolved very rapidly and ended their lives in supernovae could produce background gravitational radiation.
- Many Grand Unified Theories have closed loop cosmic strings acting as seeds for the formation of galaxies and galaxy clusters. A product of these models is background gravitational radiation. The predicted strength of the background varies between models. Searches for the background in large scale detectors are likely to place interesting limits on such models.

1.3 The Detection of Gravitational Radiation

A gravitational wave propagating in free space will produce a strain in space. This strain cannot be seen by a single observer since the waves produce no local effect,

but it can, in principle, be detected by measuring the separation of two test points. The effect of a gravitational wave can be visualised by imagining its effect on a ring of test masses (Figure 1.1). Any gravitational wave detector must measure this

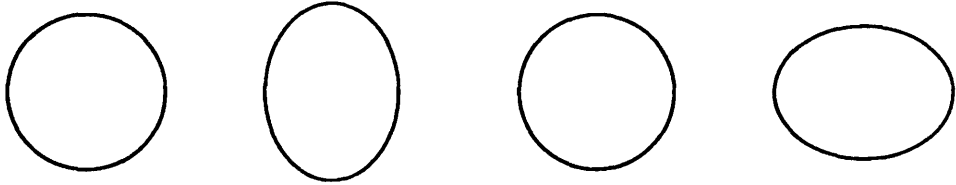


Figure 1.1: *The effect of a gravitational wave on a ring of test masses, one complete cycle of the wave is shown. The wave is propagating perpendicular to the page and has polarisation h_+ (the orthogonal polarisation h_x produces the same effect but rotated $\frac{\pi}{4}$ about the axis of propagation.)*

strain. There are two types of laboratory based detectors now operating which do this in somewhat different ways.

1.3.1 Resonant Bar Detectors

The first gravitational wave detectors were resonant bar detectors [Weber 1960] and there are many groups still using and developing these detectors. A bar detector consists of a massive bar, usually several tons of aluminium, with the resonant frequency of its first longitudinal mode at the frequency of the expected signal. The bar is isolated from the environment by a suspension system and is mounted in a vacuum chamber.

The principle of these detectors is that a gravitational wave of the correct orientation and polarisation will strain the bar, exciting oscillations at the Fourier frequencies of the gravitational wave signal. In particular the signals will excite the first longitudinal mode of the bar and can then be detected as changes in the amplitude of this mode. A number of different measurement methods have been used. The first transducers were piezo-electric elements glued to the bar but since then inductive, capacitive and parametric transducers have been used. Parametric

transducers use the mechanical motion of the bar to, for example, change the resonant frequency of a microwave cavity [Veitch 1990]. Most of the current types of transducer employ a resonant mechanical device of some form to increase the size of the signal.

The main noise sources in bar detectors are thermal noise in the bar and in the transducer, and amplifier noise. Thermal noise comes from the mean thermal energy kT of any mode of the system. This corresponds to a mean amplitude of the fundamental mode of

$$x = \left(\frac{kT}{m \omega_0^2} \right)^{\frac{1}{2}} \quad (1.4)$$

Where T is the temperature, k is Boltzmann's constant, m is the effective mass of the bar and ω_0 is the angular frequency of the fundamental mode. This gives a severe limit to the sensitivity that can be achieved. Fortunately this limit can be overcome.

For a mode with a high Q the damping time of the mode τ_d is much longer than the timescale of the gravitational wave signal t_{gw} . The mean change in amplitude of the mode in a time $t_{meas} (\ll \tau_d)$ is given by

$$x \sim \left(\frac{kT t_{meas}}{m \omega_0 Q} \right)^{\frac{1}{2}} \quad (1.5)$$

an improvement by a factor of $\left(\frac{Q}{\omega_0 t_{meas}} \right)^{\frac{1}{2}}$. Reducing the measurement time t_{meas} to equal the timescale of the signal (t_{gw}) would seem to maximise the sensitivity. Unfortunately reducing t_{meas} increases the bandwidth of the measurement amplifier ($\Delta f = \frac{1}{t_{meas}}$) and this increases the amplifier noise to a point where it dominates the detector's noise level, reducing the sensitivity. The sensitivity is thus optimised by choosing t_{meas} so that the noise contributions from the detector and the amplifier are equal. Amplifier noise presently limits the bandwidth Δf of the bar detectors to around $\frac{\Delta f}{f} = 0.01$. To reduce the noise level many groups cool their detectors to 1.5-4 K. The bars should also have as large a mass and as high a Q as possible. Groups in the University of Louisiana, the University of Maryland and in Stanford University now use bars of 2-5 tonnes made from an Aluminium alloy that has a Q

of 5×10^7 . The group in the University of Western Australia (Perth) use a 1.5 tonne Niobium bar with a Q of 2×10^8 and the group in Moscow State University use a much smaller (30kg) Silicon bar with a Q of 4×10^9 and a resonant frequency of 8kHz. The amplifier used by any group depends largely on the type of transducer employed.

The most sensitive bar detectors at present are those at Stanford and CERN¹ which have strain sensitivities of around $h \sim 10^{-18}$ for millisecond pulses.

An apparently fundamental limit to the sensitivity of bar detectors is given by the Heisenberg uncertainty principle. This will limit the present bar detectors to sensitivities of around 10^{-20} . However it is possible that this limit can be sidestepped by the use of back action evasion techniques [Caves *et al.* 1980] which should allow improvements beyond this limit.

1.4 Laser Interferometric Detectors

Laser interferometric detectors all measure the relative strain between two orthogonal directions. Conceptually the simplest system is a Michelson interferometer (Figure 1.2). The arms of the detector are formed between a beamsplitter and

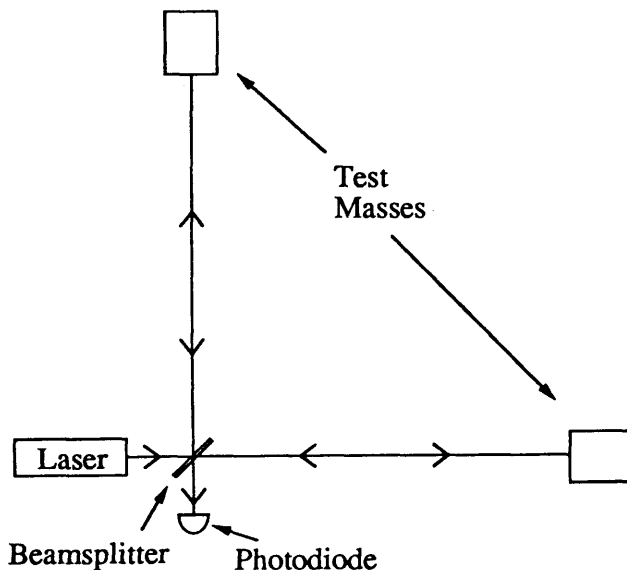


Figure 1.2: A schematic diagram of a Michelson interferometer.

¹University of Rome

two end mirrors. Light incident on the beamsplitter is split equally between the two arms. It is returned by the end mirrors and recombined at the beamsplitter. Any change in the relative length of the two arms will cause a change in the phase difference between the light from the two arms. This phase difference will cause a change in the intensity of the detected light. This system is particularly appropriate to the detection of gravitational radiation since, because of its quadrupole nature, the gravitational wave signal will cause opposite sign phase changes in the two arms. The sensitivity can be increased by making the arms longer and by bouncing the beams up and down the arms a number of times before recombining them (Figure 1.3). The time the light spends in the arms of the detector should

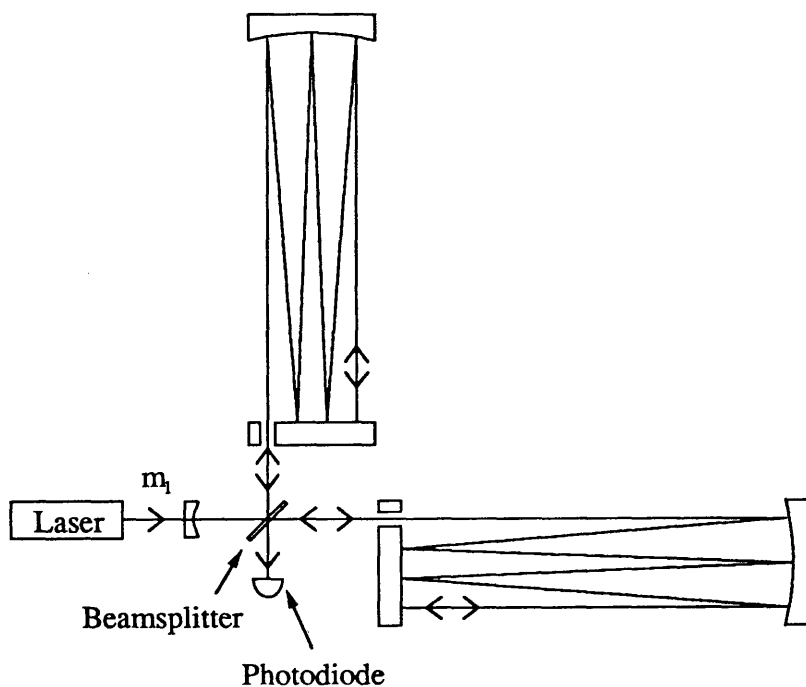


Figure 1.3: A schematic diagram of a multipass Michelson interferometer.

be less than half the period of the gravitational wave signal since after half a cycle its effect changes sign and starts reducing the accumulated phase shift.

The first interferometric detector [Forward 1978] was a Michelson interferometer. There are a number of groups who now have working prototype detectors of this type. These include groups at Max Plank Institute for Quantum Optics (MPQ) [Shoemaker *et al.* 1988] and Massachusetts Institute of Technology

[Livas 1987]. The other type of interferometric detector is similar to the Michelson but it replaces the multiple beams in each arm by a resonant Fabry-Perot cavity (Figure 1.4). When the cavity is close to resonance the phase of the re-

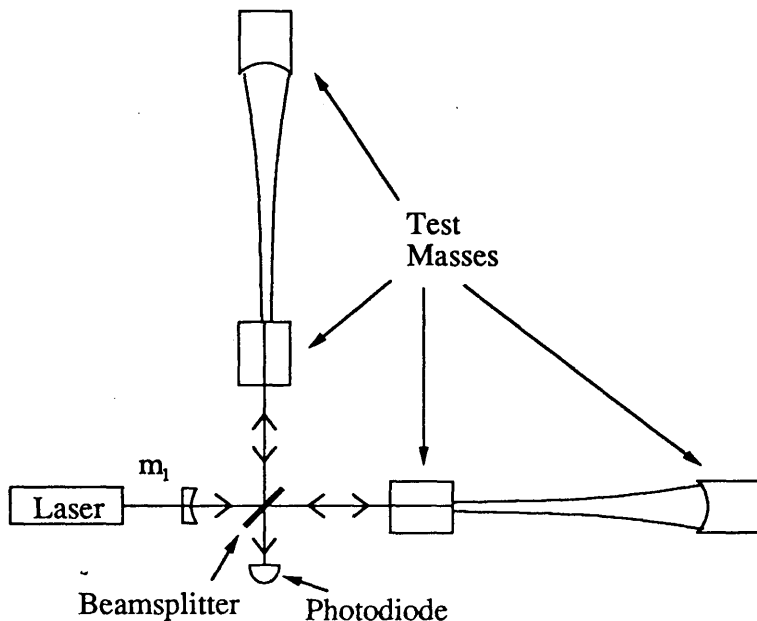


Figure 1.4: A schematic diagram of a Fabry-Perot interferometer.

flected light is a sensitive function of the length of the cavity. Any change in the phase difference between the light from the two cavities will produce a change in the intensity of the light at the photodiode.

The Fabry-Perot system is used in the prototype detector at Glasgow University². Here the laser is frequency locked to one cavity and the other cavity is held on resonance with the stable light. A gravitational wave signal will cause a change in the relative lengths of the two cavities, effectively trying to move the second cavity away from resonance. This change is resisted by the second servo system which produces a compensating feedback signal to keep the cavity on resonance. The gravitational wave signal thus appears in this feedback signal.

The prototype detector at MPQ currently has the best sensitivity of any interferometric detector with a noise level equivalent to a strain of $1.1 \times 10^{-19}/\sqrt{\text{Hz}}$ above 1.5kHz. The sensitivity of the prototype detector at Glasgow is $1.7 \times 10^{-19}/\sqrt{\text{Hz}}$ at the same frequency. The detector at MPQ is approximately three

²and in the prototype detector at the California Institute of Technology

times less sensitive than the best bar detector but it is sensitive over a much wider bandwidth. The planned large scale detectors aim to achieve sensitivities of 10^{-22} for millisecond pulses; a noise level of $\sim 10^{-24}/\sqrt{\text{Hz}}$.

There are many sources of noise that are common to both types of detector. A brief list of some of the more important is given below. A fuller examination of possible noise sources can be found in the plans for large scale interferometric detectors submitted by the various groups to their funding authorities [Hough *et al.* 1989, Vogt *et al.* 1989, Giazotto *et al.* 1989, Blair *et al.* 1989].

1.4.1 Photon Shot Noise

The minimum detectable phase shift is given by the minimum detectable change in intensity. This is governed by photon counting statistics (photon shot noise). This noise is minimised by operating with the detector on a dark fringe and with as high a contrast as possible [Hough *et al.* 1990]. The noise falls with increasing laser power ($\propto I_0^{-\frac{1}{2}}$). Large scale detectors will need high laser power (100W) to achieve the desired sensitivities.

With the use of high quality mirrors the amount of light absorbed or scattered in the interferometer is very small. Most of the input light is returned to the beamsplitter and, because the detector is operating on a dark fringe, most of the light power is returned towards the laser and is wasted. By placing a mirror (m_1 in Figures 1.3 and 1.4) in a suitable position this 'waste' light can be coherently added to the the input light, increasing the light power in the interferometer [Drever *et al.* 83b]. Optical techniques have also been developed to enhance the signal size in particular frequency bands [Meers 1988].

It has also been suggested that shot noise could be suppressed using squeezing techniques [Caves 1980, GeaBanacloche and Leuchs 1990]. This would increase the radiation pressure noise on the test masses but that would not be a problem with any present or foreseeable laser power.

1.4.2 Frequency Noise

In principle a Michelson interferometer with equal arm lengths is insensitive to laser frequency noise. In practice some frequency stabilisation is necessary to reduce the effects of unequal arm lengths and of scattered light in the interferometer.

In a Fabry-Perot interferometer the cavities must be kept on resonance with the laser light. In the prototype detector at Glasgow the laser is frequency locked to one cavity and the other cavity is kept on resonance with this stable light. To achieve the desired displacement sensitivity requires a frequency stability of order 1 part in 10^{19} in a 1Hz bandwidth at 1kHz. The natural frequency stability of the argon ion laser used to illuminate the detector needs to be improved by a factor of $\sim 10^8$ to reach this level. Chapter 3 describes work carried out to provide a new frequency stabilisation system for the prototype detector.

1.4.3 Other Optical Noise

Variations in the laser intensity, beam size and beam direction can also cause noise in the detector and must therefore be controlled. In the prototype detector at Glasgow a servo system stabilises the intensity [Mangan 1987]. The beam size and direction are controlled by transmission through a monomode optical fibre. The alignment of the optical cavities is maintained by local control of the orientation of the test masses [Mackenzie 1989].

1.4.4 Displacement Noise

Seismic noise is a problem, particularly at low frequencies, in all interferometric detectors. To reduce its effect much passive isolation is used. The isolation includes the suspension of the test masses and the use of lead/rubber stacks.

Thermal noise in both the suspension system for the test masses and in the test masses themselves could be a problem, particularly in a large scale detector. This noise can be minimised by ensuring that the Q of their resonances is as high as possible.

Chapter 2

Methods of Frequency Stabilisation

A laser is normally thought of as a source of monochromatic light. This, however, is not quite the case. There will still be some frequency jitter of the laser light. Many applications which require a stable light source will be limited by this frequency noise. There has therefore been a fairly continuous effort to improve the frequency stability of lasers and this chapter contains a brief review of the methods used to carry out the frequency stabilisation. It concentrates on continuous, single mode gas lasers such as the argon ion laser used to illuminate the detector at Glasgow.

2.1 Sources of Noise

2.1.1 Fundamental Noise

There are sources of noise in both the lasing and the detection process that arise from quantum-mechanical considerations. These noise sources are always present and will provide a lower limit to the frequency stability of a free-running laser.

Spontaneous Emission Noise

We will assume here that the pumping of the lasing medium is noiseless. Atoms in the gain medium will emit photons of the laser frequency either by stimulated emission or by spontaneous emission. In a laser operating well above threshold stimulated emission will be the dominant process. There will, however, still be

some photons in the output light produced by spontaneous emission. These photons will have random phase relative to the 'laser' light and will cause small, random phase changes in the output light. The effect of this process on the frequency stability of the output light can be calculated [Yariv 1985]. For the large frame Ar⁺ laser presently used to illuminate the detector this limits the linewidth to $\sim 1\mu\text{Hz}$. (This was calculated for an output power of 1W at $\lambda = 514\text{nm}$ with a cavity length of 2.2m and an output mirror reflectivity of 97%). This corresponds to a wideband white noise level of $5.6 \times 10^{-4}\text{Hz}/\sqrt{\text{Hz}}$. This is the best stability that can be achieved by a free running laser. However technical noise usually makes the actual noise level in the laser many orders of magnitude worse than this. Active stabilisation is therefore necessary.

Shot Noise

To stabilise a laser's frequency it is necessary to have a frequency discriminator. This is a device that produces an optical signal which indicates in what direction, and by how much, the laser frequency is different from the reference frequency. This optical signal is detected by a photodiode. The photocurrent that is generated by this signal will have a certain noise level. This noise is due to the randomness with which the charge carriers are generated by the optical signal. This noise, shot noise, will limit the size of optical signal, and hence frequency fluctuation, that can be detected.

2.1.2 Technical Noise

Technical noise is the term used to cover all non-fundamental sources of noise. There are a wide variety of such noise sources. They can be roughly divided into two categories, those that change the length of the laser cavity and those that change the refractive index of the medium in the cavity.

Length Changes

Changes δl in the length l of the laser cavity will cause changes δf in the laser frequency f that are given by $\frac{\delta f}{f} = \frac{-\delta l}{l}$.

In a large frame argon ion laser the plasma tube is cooled by enclosing it in a 'jacket' through which cold water is pumped. This water flow produces considerable mechanical excitation of the plasma tube and laser resonator. This causes motion of the Brewster windows of the plasma tube and motions of the mirrors, which are mounted on the resonator. Seismic and acoustic noise will also cause length changes of the resonator. Much of this noise, particularly that below $\sim 3\text{kHz}$, can be reduced by careful design [Kerr *et al.* 1985]. The Brewster windows can be damped to reduce their motion. The resonator can be separated and mechanically isolated from the plasma tube and from the ground. The resonator should also be damped to reduce the amplitude of its mechanical resonances. To reduce the frequency change caused by changes in the ambient temperature the resonator can be built from a material of low thermal expansion and any residual expansion can be compensated by using a short length of a material with a high rate of thermal expansion.

Changes in Refractive Index

Fluctuations in the refractive index or density of the plasma will cause changes in the optical length of the laser cavity and so cause changes in the laser frequency. At low frequencies such fluctuations are mainly due to noise from the power supply and may be reduced by modification of its circuitry. The effects of such modifications on the laser *intensity* noise can be seen in [Schilling 1986]. At higher frequencies they result from genuine plasma instabilities and little can be done to reduce these. Acoustic noise will also cause density variations in all parts of the laser cavity and acoustic shielding may be necessary.

2.2 Active Stabilisation

Passive stabilisation methods, some of which have been described above, are effective and are necessary to build a stable laser. They do, however, leave the frequency stability many orders of magnitude worse than is required for many purposes. It is therefore frequently necessary to provide some form of active frequency stabilisation. To do this we require some form of frequency reference and a method of altering the laser frequency.

2.3 Frequency References

Frequency references are either optical cavities, frequency sensitive interferometers or spectral absorption lines of ions, atoms or molecules.

Spectral Lines

In a gas laser it is possible to use the lasing medium to provide the reference. This can be done by locking the laser to the peak of the gain curve or, for an inhomogeneously broadened laser, to the center of the Lamb dip [Lamb 1964]. For both of these methods the laser frequency is modulated, usually by driving one of its mirrors by a piezo-electric device. The power output is measured and coherently demodulated to provide a suitable error signal. This only works below the modulation frequency and this imposes an upper limit on the bandwidth of the servo system. The transitions used in both these cases are very broad (up to ~ 200 MHz) and so these techniques have a poor sensitivity to frequency fluctuations. A further problem is that the reference frequency may drift as the composition or pressure of the gas changes. Another scheme is to use Zeeman splitting of energy levels of the gas in the lasing medium [Umeda *et al.* 1980, Baer *et al.* 1980]. This again locks to the peak of the gain curve. It too will suffer from drifts of this reference frequency. Improvements can be obtained by using a molecular gas (*eg* I_2 , CH_4) in a separate intra-cavity cell to provide the reference [Wallard 1972]. This gives both a much narrower transition (~ 10 MHz) and a more easily reproduced refer-

ence frequency. These techniques all suffer from the large width of the transitions used and so their sensitivity is poor. However they can provide very high DC stability with very reproducible frequencies.

Optical Cavities

It is possible to make Fabry-Perot cavities of very high finesse (>20000) and so of very narrow linewidth ($<1\text{kHz}$ for a 10m long cavity) [Anderson *et al.* 1984]. This makes them very attractive as frequency references as this narrow linewidth provides a frequency discriminator of great sensitivity. To provide good stability such cavities must be carefully designed and isolated from environmental noise.

Cavities in Transmission

The simplest way to use such a cavity is in transmission. When the laser frequency is close to the cavity resonant frequency the intensity of the transmitted light is strongly frequency dependent. For example consider a reference frequency corresponding to a point halfway up one side of the fringe. Any deviation in the frequency of the illuminating light from this reference frequency will produce a change in the intensity of the transmitted light. This signal is then compared with the original laser intensity, measured by another diode. The difference between these two signals is directly proportional to the frequency difference between the laser and the reference and is a bipolar error signal from which a suitable correction signal can be derived.

This is a simple technique but it does suffer from several disadvantages. It relies on the two photodiodes having closely matched responses at all frequencies of interest. There are also problems with the dynamic range of the system. If the laser frequency shifts by more than the cavity linewidth then, if the frequency shift is 'up' the fringe, the error signal will change sign. This will drive the laser frequency away from the locking point, causing the servo to lose lock. If the frequency shift is in the opposite direction the error signal will be of the correct sign to bring the laser frequency back to the locking point.

Another technique using a cavity in transmission is to frequency modulate the reference cavity or the laser frequency and then coherently detect the amplitude modulation of the transmitted light [White 1965]. This system provides a symmetrical error signal and allows locking to the fringe center. It uses only one photodiode and so avoids the matching problems above. The dynamic range of this system is still limited. The error signal falls to zero a few cavity linewidths away from the fringe center making the system unable to recover from frequency jumps of this size. There is also a compromise between the sensitivity of the frequency discriminator and the bandwidth of the servo. The servo bandwidth is limited to less than the modulation frequency. It, in turn, has to be less than the cavity linewidth for a significant amount of the modulated light to be transmitted through the cavity. The servo bandwidth must therefore be less than the cavity linewidth for such a system. Modulation of the cavity is limited to frequencies below $\sim 10\text{kHz}$. The mirror is driven by a piezo-electric element (PZT) and its movement above this frequency tends to become distorted. This distortion allows the excitation of other modes in the reference cavity and these will increase the noise level. This limits the bandwidth of the servo system.

Cavities in Reflection

It is also possible to use the light reflected from the reference cavity. One technique uses a reference cavity with an internal linear polariser and monitors the polarisation of the reflected light [Hänsch and Couillaud 1980]. This provides a symmetrical error signal and allows locking to the centre of the fringe. It avoids the need for any modulation. The signal well away from resonance is larger than in the previous cases giving a greater chance of recovery from large frequency jumps in the laser. This system uses two photodiodes and so has the problem of matching their responses.

Another technique using the light reflected from the cavity is *rf* reflection locking [Drever *et al.* 1983a]. The light from the laser is phase modulated at an *rf* frequency (f_m) greater than the cavity linewidth before entering the cavity. The

light reflected from the cavity is then split off and examined. This light consists of two components, the light reflected directly from the front of the cavity and the 'leakage' light from the cavity. The 'leakage' field will only be present when the laser frequency f_l is close to the cavity frequency f_c . It will contain only the laser frequency f_l . The modulation sidebands will be well outside the cavity linewidth and will not resonate in it. The phase of this light depends strongly on how close f_l is to the cavity frequency f_c . The directly reflected light will consist of the laser 'carrier' frequency f_l and sidebands at frequencies $f_l \pm f_m$ plus higher orders. The two beams are combined on the photodiode. If $f_l \neq f_c$ the detected signal will be amplitude modulated at f_m . The amplitude and phase of this modulation depends on $(f_l - f_c)$. Demodulating this signal against the *rf* source provides a suitable, bipolar error signal. There is also a DC component in the detected light. It can be minimised by the choice of suitable cavity mirrors.

This system uses only one photodiode, avoiding any matching problems and it locks to the center of the fringe. Its main advantage is the wide servo bandwidth that can be obtained independent of the cavity linewidth. At frequencies below the cavity linewidth the error signal is proportional to frequency difference between the cavity and the laser light and above this it is proportional to phase difference between the cavity 'leakage' light and the laser light. The transition between the two states is smooth and, provided allowance is made for the 90° phase shift of the signal above the cavity linewidth, the servo bandwidth may be many times larger than the cavity linewidth. This feature is particularly useful as it allows the use of reference cavities with very narrow linewidths, and consequently high discriminator sensitivity, without compromising the servo bandwidth, and thus the accuracy with which the servo will hold lock. The servo bandwidth will be limited either by the modulation frequency, which may be tens of MHz, or by the speed of the photodetectors, electronics and transducers used to detect and control the laser frequency.

The recovery of this servo from large laser frequency shifts is not limited by the cavity linewidth; the error signal is of the correct sign up to one modulation frequency away from the fringe.

Optical cavities can, if suitably isolated, provide good frequency references but for adequate long term stability a high level of temperature stability is required. To avoid the problem of long term drifts it is possible to use a hybrid system. The optical cavity is frequency locked to a spectral line at low frequencies and the laser is then locked to this stable, wide bandwidth, frequency reference [Hackel *et al.* 1977].

2.4 Feedback Transducers

It is possible to control the laser frequency in two ways. It can be done either by changing the frequency of oscillation of the laser cavity, *ie.* changing its optical length, or by altering the frequency of the light after it has left the cavity.

External Frequency Control

External frequency control can be achieved using an acousto-optic modulator (*aom*) or an electro-optic modulator (*eom*).

The *aom* is a transparent material through which acoustic waves are passed. Light passing through the material perpendicular to the direction of the acoustic wave will be diffracted by the variation in density caused by the acoustic wave. The acoustic wave is a travelling wave and so the diffracted light will be frequency shifted by an amount equal to the acoustic frequency. It is thus possible to control the frequency of the diffracted light by controlling the acoustic frequency. The angle of diffraction also depends on the acoustic frequency and this means that large frequency shifts will produce angular shifts in the output beam; *eg.* the *aom* used in the next chapter gave $\Delta\theta = 0.3^\circ$ for a 40MHz frequency shift. This effect can be greatly reduced by double passing the beam through the *aom*. The diffracted beam is reflected back through the *aom* by a curved mirror placed a distance equal to its radius of curvature away from the *aom*. This produces twice the frequency shift of a single pass but it does reduce the transmitted power.

The main limitation of the *aom* for this purpose arises from the speed of sound in the material. This produces a time lag between a change in the driving frequency

and that change reaching the laser beam. The acoustic signal will also take a certain time to cross the laser beam. These effects will limit the bandwidth of the *aom*. Bandwidths of up to $\sim 1\text{MHz}$ have been achieved [Hall *et al.* 1977].

The electro-optic modulator is a crystal such as AD*P (ammonium-dideuterium phosphate) which has, in the correct orientation, an electrically controllable refractive index. When used outside the laser cavity this allows the phase of light passing through the crystal to be altered. Since the frequency change δf depends on the induced phase change $\delta\phi$ ($\delta f = \frac{1}{2\pi} \frac{d\delta\phi}{dt}$) the frequency of the light can be controlled. The *eom* can operate at very high frequencies and so can provide a very wide bandwidth feedback element. The frequency change caused by the *eom* depends on the rate of change of the phase shift, ϕ , where ϕ is directly proportional to the voltage applied to the *eom*. The frequency change δf induced by a sinusoidal voltage of angular frequency ω and amplitude V is given by

$$\delta f = \omega \frac{V}{V_\lambda} \sin \omega t$$

where V_λ is the voltage required to produce 2π phase change in light passing through the *eom*. We can see that while frequency correction at high frequencies is relatively easy, at low frequencies it becomes progressively more difficult; for example to provide a constant frequency shift requires the voltage on the *eom* to increase linearly with time. As this is obviously impracticable, extra-cavity *eoms* are therefore used along with some other method of laser frequency control that works at low frequencies such as an *aom* [Hall and Hänsch 1984] or a piezo-driven laser mirror [Kerr *et al.* 1985].

Internal Frequency Control

There are many ways to achieve internal frequency control. For correction signals at low frequencies it is possible to use a heating element attached to the laser resonator to change the cavity length. This can be made to operate in servo systems with unity gain frequencies of up to $\sim 100\text{Hz}$ [Niebauer *et al.* 1988] but it is usually used for lower frequency operation.

Another method for applying low frequency correction signals is to use a glass plate inserted into the laser cavity at Brewster's angle. Rotation of this plate varies the optical length of the cavity, altering the laser frequency. This method is only used at frequencies below $\sim 1\text{kHz}$. It also has the disadvantage of introducing a lossy element into the laser cavity, reducing the output power.

Faster control may be obtained by driving one or more of the laser cavity mirrors with a piezo-electric element (PZT). This does not use an intra-cavity device and avoids any loss of laser power. The limit to high frequency operation is usually the presence of a mechanical resonances in the mirror/PZT/support structure combination. These resonances produce large amplitude and phase deviations from the ideal response and are difficult to compensate for in the servo electronics. The PZT's frequency of operation is thus limited to below the first of these resonant frequencies. First resonance frequencies of up to 350kHz have been reported [Jitschin and Meisel 1979].

The fastest way to control the laser frequency is to use an intra-cavity *eom*. This has the same wide bandwidth as the extra-cavity *eom* and can now easily produce DC frequency shifts. This is because the applied voltage produces a change in the refractive index of the *eom*, causing a change in the optical length of the cavity and hence a change in the laser frequency. The disadvantage of this scheme is that it again involves an extra, lossy, element in the laser cavity and so it will not be appropriate if maximum output power is required.

2.5 Conclusions

There are a large number of possible techniques to frequency stabilise lasers. The technique or combination of techniques used will depend on the intended application.

When stabilising a laser it may be found that noise in its intensity and in its beam direction, size and mode structure couple into the frequency stabilising system to produce unwanted noise. It may then be necessary to build separate systems to stabilise these parameters. Intensity stabilisation can be done using an *aom*

Chapter 3

A Frequency Stabilisation System

3.1 Frequency Noise

In the prototype gravitational radiation detector at Glasgow the laser is frequency locked to a Fabry-Perot cavity, the primary cavity, which forms one arm of the detector. The length of the other cavity, the secondary cavity, is then locked to this stable illuminating source. Residual frequency noise Δf in the illuminating light will be seen as differential displacement noise Δl in the detector output at a level given by

$$\frac{\Delta l}{l} = \frac{-\Delta f}{f}$$

l :- length of the cavity (10m)

f :- laser frequency (5.8×10^{14} Hz)

To ensure that this was not a noise source at the present level of sensitivity of $1.7 \times 10^{-18}\text{m}/\sqrt{\text{Hz}}$ the laser frequency had to be stabilised to the primary cavity with a residual frequency noise $\Delta f < 1 \times 10^{-4}\text{Hz}/\sqrt{\text{Hz}}$.

The frequency noise for the laser used to illuminate the detector (Spectra Physics 170) is shown in Figure 3.7. The unstabilised frequency noise is around $2\text{kHz}/\sqrt{\text{Hz}}$ at 1kHz . This is a typical noise level for a large frame argon ion laser. A servo loop of gain $> 2 \times 10^7$ at 1kHz is thus required to give adequate frequency stability.

3.2 The Optical Cavities of the Prototype Detector

The primary and secondary cavities of the prototype detector are each formed between two mirrors optically contacted onto fused silica test masses. These masses are hung as pendulums to reduce the effect of seismic noise. The whole assembly is in a vacuum system of pressure $\sim 10^{-3}$ Torr. This is necessary to reduce the random fluctuations in the refractive index of the air in the cavity to a level where they are no longer significant; it also provides isolation from acoustic noise. Both cavities have storage times that vary between 50 and $130\mu\text{s}$ depending on how clean the mirrors are. The fringe visibility is 50-60%. Each cavity is illuminated by $\sim 30\text{mW}$ of light. This light is phase modulated at 12MHz with a modulation index of 0.7.

3.3 Passive Stabilisation

It has been previously shown that the noise levels of Ar^+ lasers can be reduced by careful design and that this is necessary if good frequency stability is required. The laser used here had been suitably modified. The resonator was built separately from the support structure for the plasma tube and was mechanically isolated from it. The Brewster windows of the plasma tube were surrounded by damping compound to reduce their motion. The resonator was built from Invar rods to reduce the effects of thermal expansion. Aluminium plates were fixed between the rods at various points to restrict their resonances. The end plates, on which the mirrors were mounted, were of lead to keep the amplitude of any resonance small. The rods were covered in damping compound and then in a lead/foam sandwich to damp any resonances and to reduce any acoustic noise effects. The noise level shown in Figure 3.7 is the remaining noise after this passive stabilisation.

3.4 Previous Frequency Stabilisation System

The system of frequency stabilisation used until recently is shown in Figure 3.1. The error signal between the laser frequency and the cavity frequency was gener-

ated by the rf reflection locking technique described in the previous chapter. This error signal was then suitably amplified, filtered and applied to the feedback transducers. The main transducer was an intra-cavity electro-optic modulator (*eom*). A piezo-electrically driven laser front mirror was also used to provide large dynamic range below a few hundred Hz. At frequencies below a few Hz feedback was applied to the suspension points of the cavity masses. This was done to damp out any large motion at the ~ 1 Hz pendulum frequency of the suspended masses. This means that at these frequencies the length of the primary cavity is locked to the length of the laser.

The main advantage of this system is the large bandwidth of the *eom* of >1 MHz. This means that the gain of the frequency controlling servo had to be reduced from 3×10^7 at 1 kHz to 1 at 1 MHz, ie over three decades of frequency. This is possible with a reasonably sophisticated design of servo system.

A disadvantage of this system is that it employs an intra-cavity device, the *eom*. This introduces extra losses into the laser cavity and so reduces the power output from the laser. The reduction here was up to 50%. The losses in the *eom* rise as the laser power is increased. This limits the output power to <2.5 -3W. Trying to increase the laser power above this level will not work and is liable to damage the *eom*. There was also evidence that the *eom* caused short bursts of extra radial modes in the laser which produced excess noise in the detector output.

A further incentive to change the frequency stabilisation system was provided by plans to build a large scale detector. In such a detector the optical cavities in the arms would be greater than 1 km in length and so would have free spectral ranges of less than 150 kHz. An optical cavity has a null in its response to frequency noise at a frequency f_{FSR} given by its free spectral range (FSR) ($f_{FSR} = c/2l$: l cavity length, c velocity of light). The output signal above this frequency has an extra phase lag of 180° . A frequency controlling servo that used the cavity as a frequency discriminator would also have this null and phase shift in its response at this frequency. With the present 10 m cavities the FSR is 15 MHz which is well outside the bandwidth of the servo but in a large scale detector this would not be the case. This null would mean that at that frequency the servo would have no

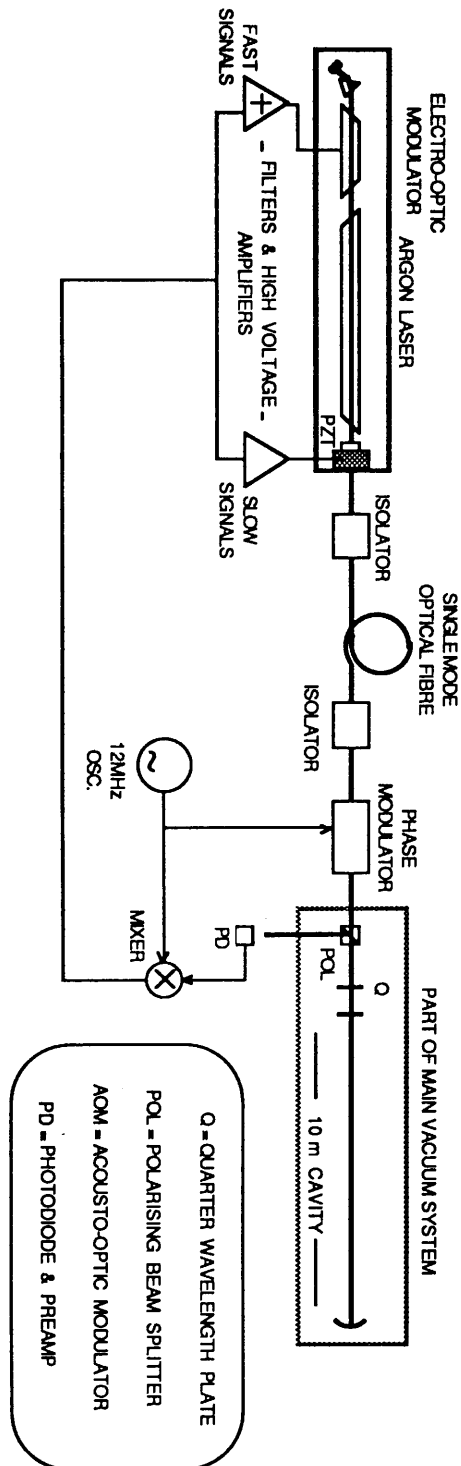


Figure 3.1: A diagram of the old system of frequency stabilisation using an in-cavity electro-optic modulator.

gain, producing a peak of frequency noise and possibly preventing the servo from locking stably. The phase shift would have to be compensated for in the servo electronics. This would be difficult as the phase shift happens over a frequency span similar to the cavity linewidth.

3.5 Method of Feedback

For all of the above reasons it was decided to build a frequency stabilisation system that did not employ an intra-cavity device and had a bandwidth of $<150\text{kHz}$. To do this required a replacement for the intra-cavity *eom* that had previously provided fast feedback to the laser. The replacement feedback device was chosen to be a piezo-electrically driven rear laser mirror. The mirror was glued onto a piezo-electric disc (PZT) and this was in turn glued onto a special mount (Figure 3.2). The mount was designed and supplied by A.Brillet and colleagues at Orsay and later modified at Glasgow. It consists of a damped transmission line which acts as an impedance matched terminator for acoustic signals generated by the PZT. This ensures that the acoustic signals are absorbed by the mount and not reflected from it to set up unwanted resonances in the mirror-PZT-mount assembly. This greatly

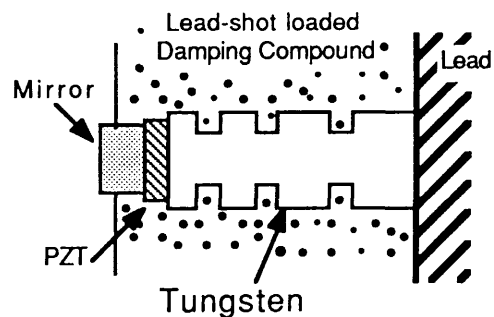


Figure 3.2: Diagram of Laser Rear PZT Mount

increases the bandwidth of the PZT feedback element which would otherwise be severely limited by resonances in the mount assembly. Resonances cause problems for the servo loop because the gain of the signal changes near the resonant frequency and above this frequency the signal has a phase shift of 180° . Resonances in the mirror/PZT structure are still going to limit its bandwidth; these were searched for by looking at the frequency change induced in the laser frequency by a test

signal applied to the PZT. The first resonance was found at $\sim 140\text{kHz}$, it had a very low amplitude and was a resonance of the PZT-mirror combination only. It could have been moved to a higher frequency by using a mirror with a thinner substrate but it limited the servo to the required bandwidth and so this was not pursued. The next resonance was at $\sim 200\text{kHz}$ and was of much larger amplitude ($Q \sim 3$).

3.6 Two Loop System

To try to reduce the bandwidth of the original servo by a factor of ten while still maintaining the gain at 1kHz of 3×10^7 is a very difficult task. It would be possible to design a servo system to do this but such a system would have a very small range of gain over which it would be stable. The gain of the servo loop is changed by alterations in the visibility of the optical cavity which are caused by changes in its alignment. Thus alignment changes caused by seismic and acoustic disturbances and by thermal expansion would frequently change the gain enough to make the servo unstable, causing it to oscillate or even to lose lock. There would also be a problems in the acquisition of lock by this servo.

The solution to these problems was to do the frequency stabilisation in two stages. The laser is first frequency locked to a reference cavity. This system has an input that allows the frequency of the light out of it to be controlled by an external signal. This system now acts as a source of relatively stable light. This combination is then frequency locked to the detector's primary cavity as before (Figure 3.3). The gain of this system at any frequency is the product of the gains of the two loops at that frequency. This allows two servos of gain $\sim 10^4$ at 1kHz and each of bandwidth $\sim 100\text{kHz}$ to provide a final frequency stability at least as good as that provided by the single, wide bandwidth, servo loop.

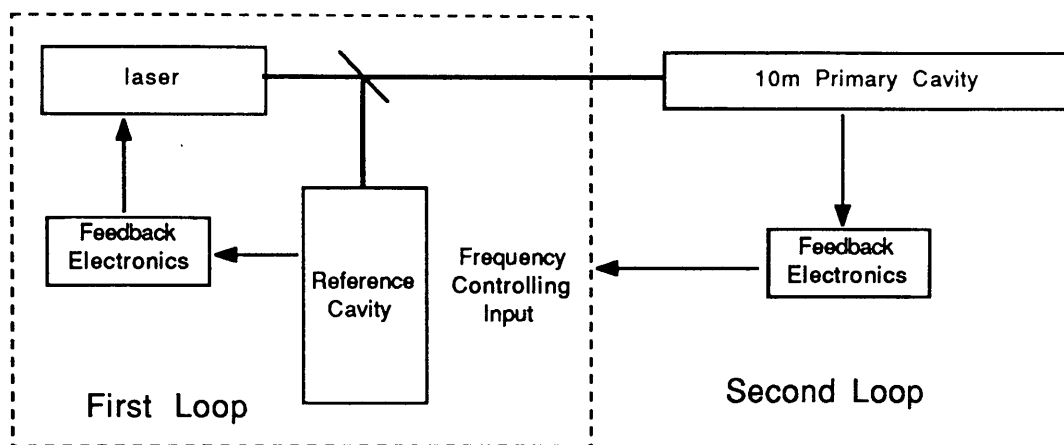


Figure 3.3: Block diagram of the two loop stabilisation system

3.7 First Loop

The scheme implemented is shown in Figure 3.4, with the first loop inside the dotted box. The reference cavity is formed from a tube of Zerodur 227mm long (external diameter 76mm, internal diameter 23mm) with the mirrors mounted on either end. The cavity is mechanically isolated from the optical bench by three layers of rubber and is in a vacuum tank to reduce its coupling to acoustic noise. It is illuminated by $\sim 1\text{mW}$ of light phase modulated at 24.3MHz with a modulation index (β) of 0.7. The cavity linewidth was measured by scanning the cavity length and looking at the demodulated signal. It was $(4.5 \pm 0.5)\text{MHz}$ which corresponds to a finesse of ~ 135 . The fringe visibility is $\sim 90\%$ with no modulation. One mirror is mounted on a PZT stack. This allows the length of the cavity to be adjusted so that its resonance is near the laser frequency when trying to lock the servo loop. It also allows the cavity to be scanned, which is useful when aligning the input beam.

The light is double passed through an acousto-optic modulator (*aom*) before entering the reference cavity. It is double passed to reduce the variation in beam direction produced as the frequency of the *aom* changes. The presence of the *aom* has no effect on the operation of the first loop as it only produces a static frequency shift on the light entering the reference cavity. It is the main feedback element for

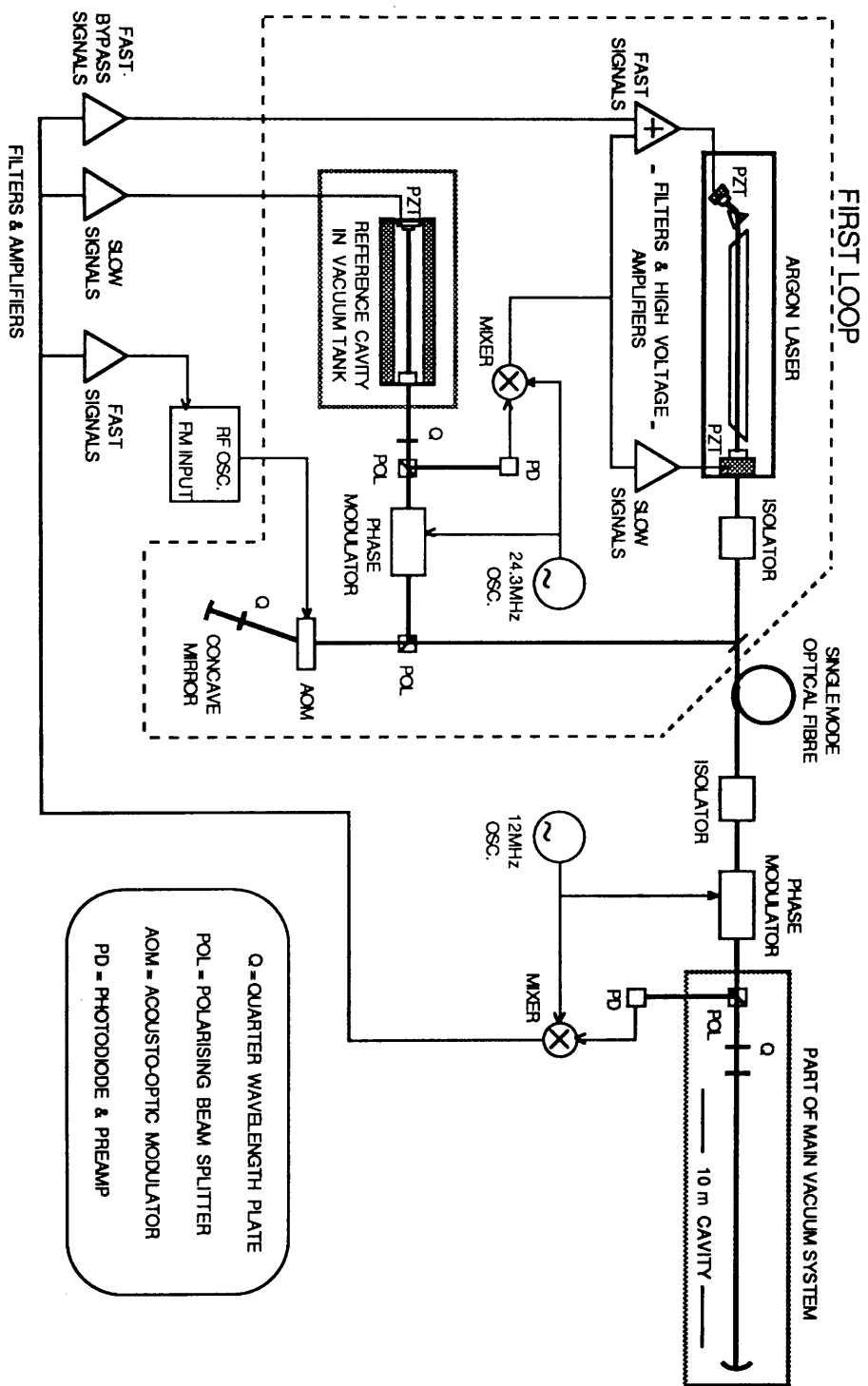


Figure 3.4: Details of the two loop stabilisation system

the second loop.

3.7.1 Results from the First Loop

When the laser is frequency locked to the reference cavity we want to know the level of stability achieved. This is most easily seen by looking at the residual frequency noise measured at the error point of the servo loop. This gives the lower limit to the residual frequency noise achieved and, together with the the original frequency noise, gives the servo loop gain. It does not necessarily give the frequency stability of the light. This is because noise in the reference cavity and shot noise in the detection process will both be suppressed at the error point of the servo loop by imposing these signals onto the laser frequency. The error point is then ‘quieter’ than the laser frequency. A better way to determine the residual frequency noise is to lock the laser frequency to a second reference cavity. The signal required to do this gives an upper limit to the residual frequency noise. If the frequency of the input light is more stable than that of the cavity then it will be the cavity noise that dominates the feedback signal. In the case here the second reference cavity is the detector’s primary cavity.

When the first loop was first stably locked the performance achieved was less than had been hoped for. To avoid exciting the 200kHz resonance of the rear PZT the unity gain frequency of the loop had to be reduced. This limited the gain at 1kHz. A notch filter was added to the drive to the PZT. This filter greatly reduced the 200kHz signals at the PZT and eliminated this problem.

The system now worked well apart from a large peak of noise at 1kHz in the primary cavity error point (Figure 3.5). This was caused by a resonance in the adjustable mirror mount on the front of the reference cavity. The amplitude of the motion was $\sim 5 \times 10^{-14}$ m. The mount was changed for one which was more solidly constructed and this cured the problem.

With the system now working well the feedback circuitry of the first loop was adjusted to increase the gain at 1kHz. This resulted in a frequency stability of $\sim 0.3\text{Hz}/\sqrt{\text{Hz}}$ below $\sim 3\text{kHz}$. The stability achieved was limited by shot noise.

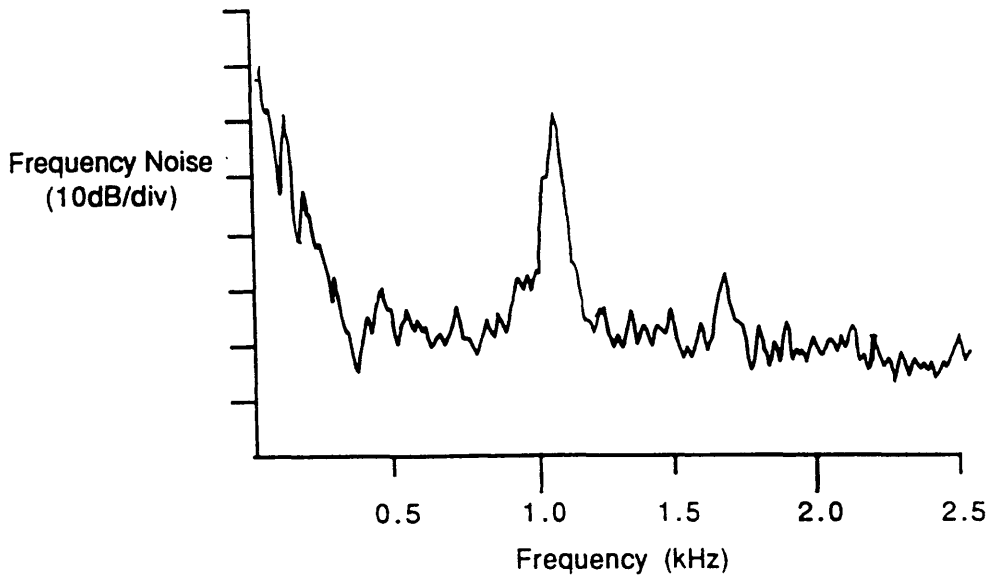


Figure 3.5: *A graph of the error point of the second loop showing the peak of noise caused by the resonance of the reference cavity mirror mount*

Above 3kHz the frequency noise rises as the gain of the servo loop begins to fall more rapidly than the laser's frequency noise. The gain of the servo at 1kHz was $> 10^4$.

3.8 Second Loop

The *aom* is the main feedback method from the second loop. When the frequency of the drive signal to the *aom* is changed by δf the light entering the reference cavity suffers a frequency shift of $2\delta f$. This is detected by the first servo loop which shifts the laser frequency by $-2\delta f$ to keep it on resonance with the cavity. The *aom* thus effectively changes the frequency of the reference cavity. The frequency of the *aom* is controlled by a signal derived from the error point of the primary (10m) cavity.

3.8.1 Frequency Response

The *aom* works in the manner described above only on timescales longer than its response time and only where the gain of the first loop is large enough.

If the first loop has a gain $G(f)$ that varies with frequency, then, for a perfect *aom*, a frequency change of δf_{aom} at a frequency f will produce a change in the laser frequency of δf_{laser} given by

$$\delta f_{laser} = \frac{-G(f)}{1 + G(f)} 2\delta f_{aom}$$

If the first loop has a 6dB/octave slope as it passes through its unity gain frequency f_1 then the response of the laser frequency to changes in the frequency of the *aom* will have an integration with its -3dB point at f_1 . This will only be the case for frequencies below the first resonance of the rear PZT assembly so the bandwidth achievable by this method will still be limited, as would be expected, by the PZT resonant frequency. The unity gain frequency f_1 of the first loop was around 80kHz.

The response of the *aom* is limited by the finite velocity of sound v_s in the crystal. This causes a time delay between a signal on the driving PZT and the same signal in a different part of the crystal (Figure 3.6). There is therefore a

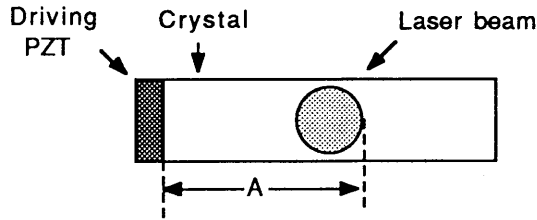


Figure 3.6: *Diagram of Acousto-Optic Modulator*

time delay $\delta t_1 (= A/v_s)$ between signals on the PZT and these signals appearing on the laser light. This can be reduced by ensuring that when the laser beam passes through the crystal it is focused down and is as close to the driving PZT as is possible without the beam ‘clipping’ on the edge of the crystal. The distance can be kept to $\sim 3\text{mm}$ making the frequency limit of the *aom* substantially higher than the bandwidth of the first loop.

3.8.2 Other Feedback Paths

There are three methods of applying feedback from the second loop apart from that using the *aom*. At frequencies near the unity gain frequency of the first loop

(f_1) some signal is applied to the laser rear mirror PZT. This bypass signal does not suffer the phase shift caused by the first loop going through its unity gain frequency. This gives a signal with a predictable phase rather than one whose phase depends on the exact unity gain frequency of the first loop, making it easier to keep the second loop stable. Signals at frequencies below $\sim 10\text{Hz}$ go to the PZT on the reference cavity. This greatly reduces the need for the *aom* to have large dynamic range at low frequencies. As in the previous system there is feedback to the suspension point of one of the test masses to damp out its $\sim 1\text{Hz}$ motion (the other test mass in the 10m cavity is now damped to ground). This means that at low frequencies the length of the primary cavity is locked to that of the reference cavity.

3.8.3 Results from the Two Loop System

With the first loop working well the feedback circuitry of the second loop was modified to increase the gain at 1kHz. This achieved a residual frequency noise of $\sim 2 \times 10^{-5}\text{Hz}/\sqrt{\text{Hz}}$ at 1kHz (Figure 3.7), — a loop gain of 10^8 . The error point noise was again below shot noise at 1kHz.

With this frequency stabilisation system the detector reached its previous best sensitivity level of $1.7 \times 10^{-18}\text{m}/\sqrt{\text{Hz}}$ where it was limited by some unknown noise source. The level of frequency stability achieved would allow the sensitivity to be increased by a factor of ~ 3.5 before being limited by frequency noise.

In a detector in which the frequency stability is not limited by shot noise, frequency noise causes a common signal in the detector's two cavities. This signal can be subtracted from the detector's output either electrically or by optical recombination of the beams from the two cavities. The amount of subtraction depends on how similar the two cavities are. This should allow a further increase in the sensitivity by a factor ≥ 10 in this case.

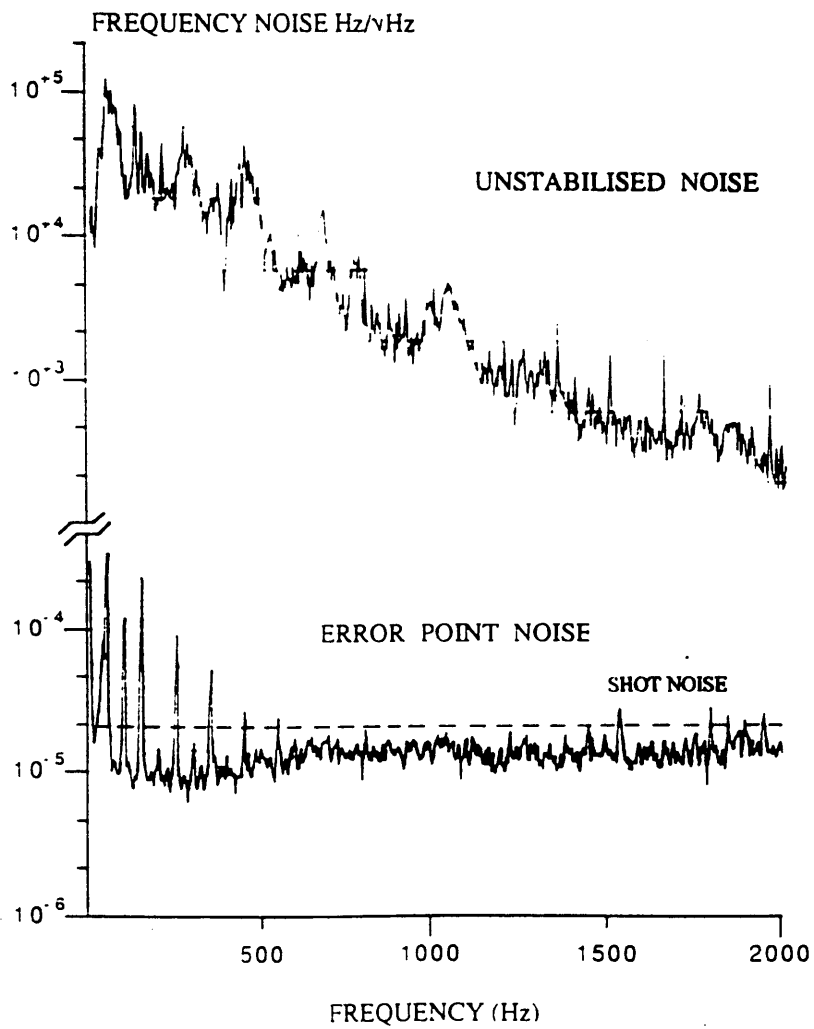


Figure 3.7: A graph of frequency noise against frequency for unstabilised and stabilised laser

3.9 Problems

There were some problems with the system. Spikes of frequency noise at $\sim 200\text{kHz}$ were causing dynamic range problems in the electronics used to lock the secondary cavity to the laser frequency. This noise had been suppressed by the old frequency stabilisation system but was well outside the bandwidth of the new one. To reduce this high frequency noise an extra-cavity *com* was added to the first loop. This greatly increased its bandwidth and reduced the troublesome frequency noise. The bandwidth of the second loop, which used the primary cavity as its frequency discriminator, was not changed and so this system could still be used on a large scale detector.

Chapter 4

Servo Analysis

4.1 Introduction

In the previous chapter we examined the frequency stability achieved by a two loop servo system. In this chapter we shall examine in more detail the behaviour of the combined servo system.

A servomechanism, or servo loop, is a closed loop control system which has to produce an output to follow and cancel some reference input which may be varying. In the previous chapter the laser frequency had to be kept on resonance with a cavity that was varying in length. Figure 4.1 shows a diagram of a simple control system. There are a number of conditions that must be met for such a system

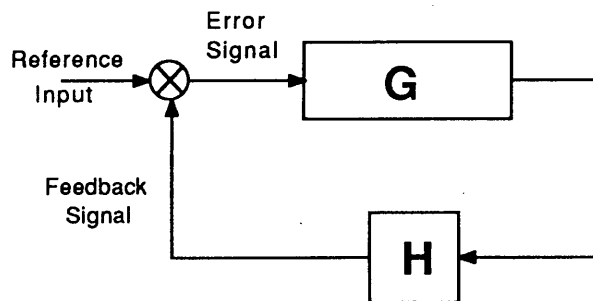


Figure 4.1: *Diagram of a simple servo system.*

to perform adequately. It must be stable: when it is perturbed it should settle to a steady value and not oscillate with a constant or increasing amplitude. The gain must be high enough to ensure that, at the frequencies of interest, the output signal follows the reference signal to the required accuracy. It is also preferable

to have a system that is not unduly sensitive to small changes in the open loop response.

4.2 Stability

The stability of a closed loop system can be found from its open loop response GH . Two possible ways of viewing GH are the Bode and Nyquist plots. From each of these plots the stability of the system can be assessed and the gain and phase margins measured.

Phase Margin

The phase margin is a measure of how much extra phase lag must be added to make the system unstable. It is defined as 180° minus the number of degrees phase lag at the frequency where $|GH| = 1$ (unity gain). Systems with a positive phase margin are stable and those with a negative phase margin are unstable. The larger the phase margin the more stable the system and the less likely it is to oscillate at a frequency near its unity gain frequency.

Gain Margin

The gain margin is a measure of how large a gain change is required to make the system unstable. It is defined as the amount the gain of the system must be changed by to make it 0dB (*ie.* unity gain) at a frequency where the phase is -180° .

Bode Plots

Bode plots are graphs of $|GH|$ against frequency and the phase of GH against frequency. In the plots here the frequency axes are logarithmic, the amplitude of GH is in dB and the phase is linear. The gain and phase margins can be calculated from the two, complementary, graphs.

The Nyquist Plot

The Nyquist plot is a polar plot of the gain and phase of GH . It is normal to plot the gain using a linear scale but because of the large range of gain in the systems here it is plotted in decibels. The condition that must be met for the closed loop system to be stable is that the plot of GH must not encircle the point $(0\text{dB}, -180^\circ)$. The phase margin can be easily seen and is the angle between the line corresponding to -180° and the vector from the origin to the point where the gain is 0dB . The gain margin is the distance between the point where the graph crosses the -180° line and $(0\text{dB}, -180^\circ)$.

4.3 Changes in GH

The gain and phase margins are also useful because they give a measure of how sensitive the system is to variations from the calculated open loop transfer function GH . This is useful because no system will have exactly the GH that was hoped for. Variations from the calculated GH may be caused by imperfect detectors, amplifiers and transducers. There may also be some variation in GH with time, for example as the temperature changes. In the case of the frequency stabilisation system the largest changes may be the cavity linewidth and visibility changing slowly with time as the mirrors become dirty. The visibility will also change at a much faster rate as the test masses move, particularly at their pendulum frequency.

4.4 Bypass Design of Electronics

We have seen in the previous chapter (Figure 3.7) that the frequency noise of the laser increases at low frequencies. At 2kHz the noise is $\sim 300\text{Hz}/\sqrt{\text{Hz}}$ and at 200Hz it has increased to $\sim 30\text{kHz}/\sqrt{\text{Hz}}$. The feedback signal required to suppress this noise will also vary in exactly the same way. We can see that at low frequencies the feedback electronics must have much higher gain and much larger range than at higher frequencies. To have one chain of amplifiers performing this function would be extremely difficult. Amplifiers that have large gains or large output voltage

swings have much larger time delays associated with them than those with low gain or low output voltage swings. They are thus inherently slower. To overcome this problem and achieve the required performance from the electronics it was decided to use a split feedback system. The low frequency signals, which require high gain and high voltages on the PZT, are supplied by one chain of amplifiers and the high frequency signals, which require much smaller gains and final voltages, are supplied by another (Figure 4.2).

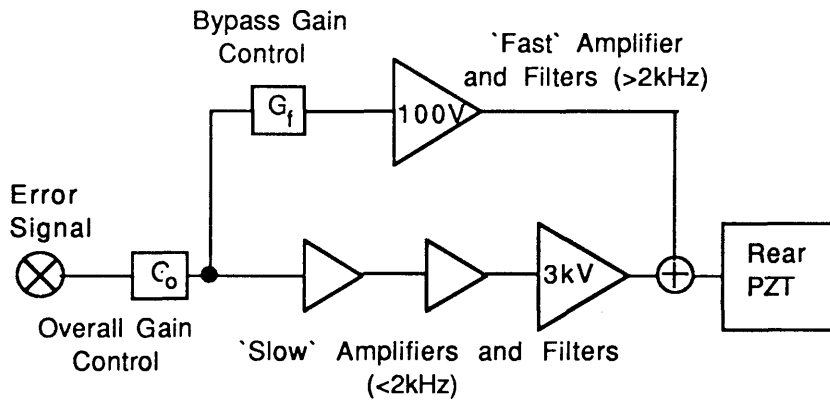


Figure 4.2: A diagram of the split feedback system.

This bypass design greatly simplifies the design of the electronics. It also has advantages over simpler designs in the acquisition of lock. When the optical cavity is off resonance the 'slow' feedback electronics will be driven into saturation. The DC gain of the system ($\gg 10^8$) means that a typical DC offset from the mixer of $< 1\mu\text{V}$ will cause saturation. When the cavity comes on resonance the feedback electronics will get signals that correspond to the frequency difference between the laser and the cavity. The 'fast' electronics will respond quickly to the signal, and will try to keep the laser on resonance with the cavity. The 'slow' electronics will respond much more slowly and will eventually come out of saturation. If the laser is still on resonance with the cavity the system should lock. If the feedback was done with only one amplifier chain then it would take as long as the 'slow' chain above to come out of saturation and so the

chances of the system acquiring lock would be much reduced.

The bypass design does have one problem. At some frequency the signals from the two amplifier chains will be equal and above this frequency the signals from the 'fast' amplifiers will start to dominate over those from the 'slow' amplifiers. Care must be taken at this crossover frequency to ensure that the two signals have a similar phase lag. The difference in phase lag must be $< 180^\circ$ and should, ideally, be $< 90^\circ$. If the phase difference is $> 180^\circ$ the resulting servo system will be unstable. An example of this can be seen in Figure 4.6.

4.5 The First Loop

To obtain the open loop response GH_1 of the first loop we need to know the response of every element within the loop. The transfer function of the electronics is relatively simple to obtain but we also need to know the gain and frequency response of the feedback elements, the optical cavity and the detection system.

Feedback Elements

In this loop the feedback elements are all PZTs which are capacitive in nature below their resonant frequencies. These, together with the resistor through which they are driven, act as integrators; their corner frequencies and conversion factors (from volts to Hz) are shown in Table 4.1.

In practice the bandwidth of the servo is limited by the lower resonance of the rear PZT. The effect of this resonance was simulated by having the phase effect of a notch filter in the transfer function at 140kHz. This only affects the phase of the signal and is a good approximation to the effect of this resonance. In the Bode plot of $|GH|$ the position of the resonance was marked by allowing the notch to effect the signal amplitude. This is meant only to mark the position of the resonance on this plot.

Element	Constant	Units	Corner frequency	Upper limit
Front PZT	4.1E+5	Hz/Volt	100Hz	16kHz (resonance)
Rear PZT	1.4E+5	Hz/Volt	17kHz	140kHz (resonance)
Reference Cavity	1.3E-6	Volt/Hz	2.5MHz	

Table 4.1: *The corner frequencies and conversion constants for the feedback elements and detection system of the first loop*

Detection System

The optical cavity has an integration in its response to frequency noise. The corner frequency of this integrator is given by half the linewidth of the optical cavity.

The photodetector circuit employs resonant enhancement of the signal at the modulation frequency. This resonance is of finite width and so there will be a phase shift for signals well away from the resonant frequency. The resonance width (2MHz) is much larger than the bandwidth of the servo and its effect may be neglected. The conversion constant of the optical cavity and detection system is also shown in Table 4.1. This is the conversion constant from a frequency change in the light to the corresponding voltage change out of the mixer.

Electronics

We have seen that the servo system requires high voltages at low frequencies. To provide these voltages the final amplifier in the ‘slow’ chain can provide an output voltage of up to 3kV. This amplifier is also the one that limits the frequency response of the ‘slow’ chain, its output falling rapidly above 8kHz. In the ‘fast’ chain the final stage is a 100V amplifier; it works well to beyond 100kHz and does not cause any problems.

It can be seen from Figure 4.2 that there are two gain controls in the system, G_F and G_O . G_F controls the relative gain between the two chains. This controls the crossover frequency. With G_F set to some suitable value G_O controls the gain of

the whole system. The crossover frequency here was set to around 2.5kHz. Trying to increase the gain at 1kHz by increasing the crossover frequency would quickly cause the servo to become unstable (Figure 4.6).

Bode and Nyquist Plots

Figures 4.3, 4.4 and 4.5 show the Bode and Nyquist plots

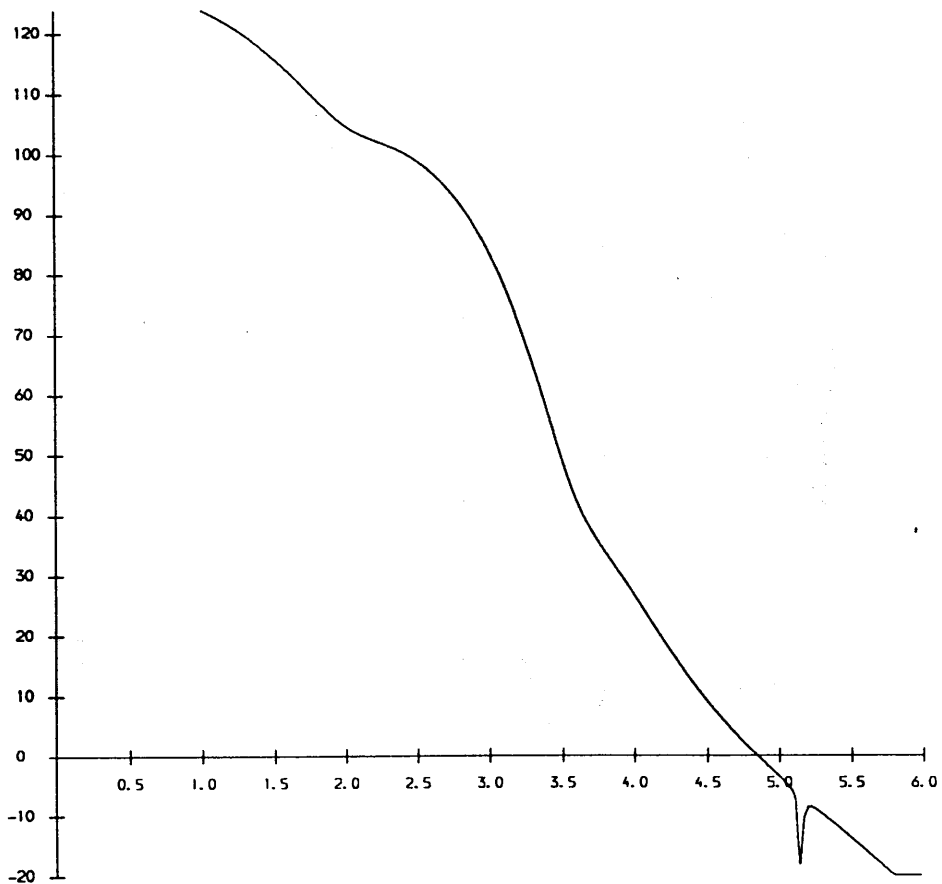


Figure 4.3: *The Bode plot of the gain of the first loop. The vertical axis is gain in dB and the horizontal axis is log(frequency). The notch is at 140kHz and marks the position of the PZT resonance.*

for the first loop. It can be seen that this servo is conditionally stable —

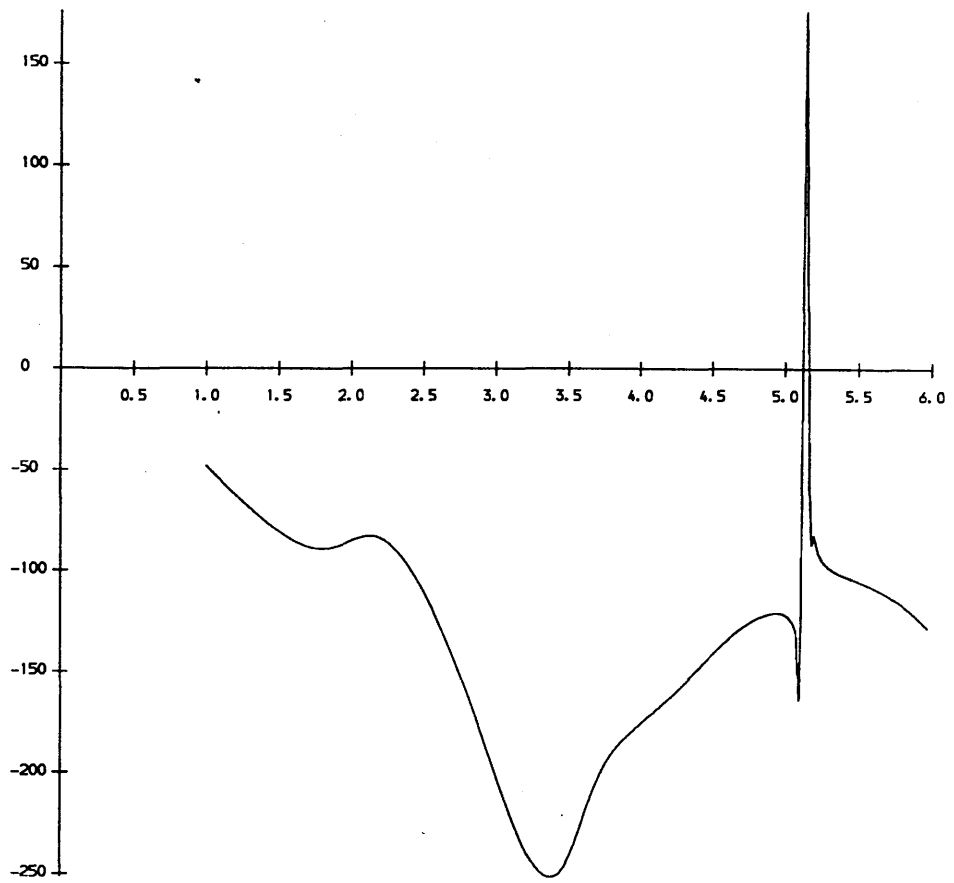


Figure 4.4: *The Bode plot of phase (in degrees) against log(frequency) for the first loop. The 'spike' is at 140kHz and marks the position of the PZT resonance.*

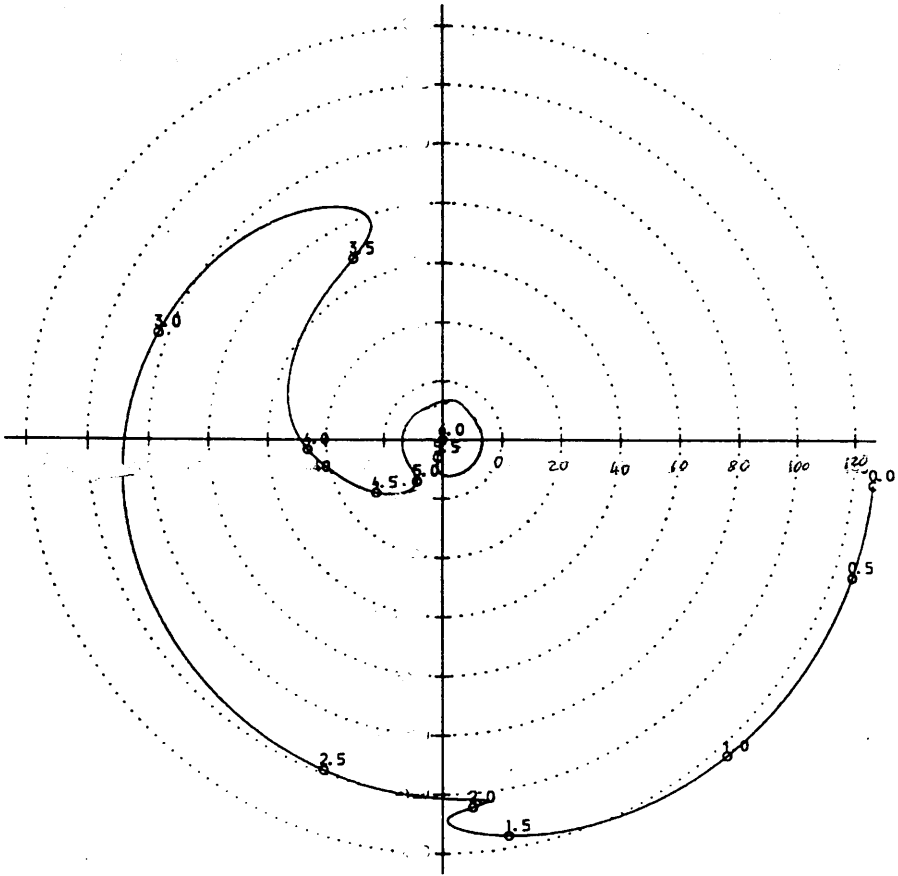


Figure 4.5: *The Nyquist plot for the first loop. The radial axis is in dB with the centre of the plot at -20dB. The circles on the plot are of radii 0dB, 20dB, 40dB, etc.*

it is possible to make it unstable by increasing or decreasing the gain. For this application the upper gain margin is set to be much smaller than the lower one as changes in the gain caused by movement of the masses are much more likely to decrease the gain than to increase it. The lower gain margin is $\sim 28\text{dB}$ and the upper one is $\sim 6\text{dB}$. We can see that the gain at 1kHz is 83dB .

The phase margin is $\sim 56^\circ$. This is slightly less than the ideal of $> 76^\circ$ required for critical damping in an ideal second order system [Marshall 1978]. It means that this system is slightly underdamped. The behaviour of the system near its unity gain frequency can be estimated by modelling it as a second order system. This model shows that there is a very small ($\sim 0.8\text{dB}$) enhancement of the noise near the unity gain frequency. Plotting $\frac{1}{1+GH_1}$ shows the enhancement of the noise to be $\sim 1.5\text{dB}$. This model also gives the $1/e$ damping time for oscillations at this frequency to be ~ 1.5 cycles.

Figure 4.6 shows the effect of increasing the crossover frequency to a point where the difference in phase lags between the 'fast' and 'slow' sides is $> 180^\circ$. The Nyquist plot encloses the $(0\text{dB}, -180^\circ)$ point showing the system to be unstable.

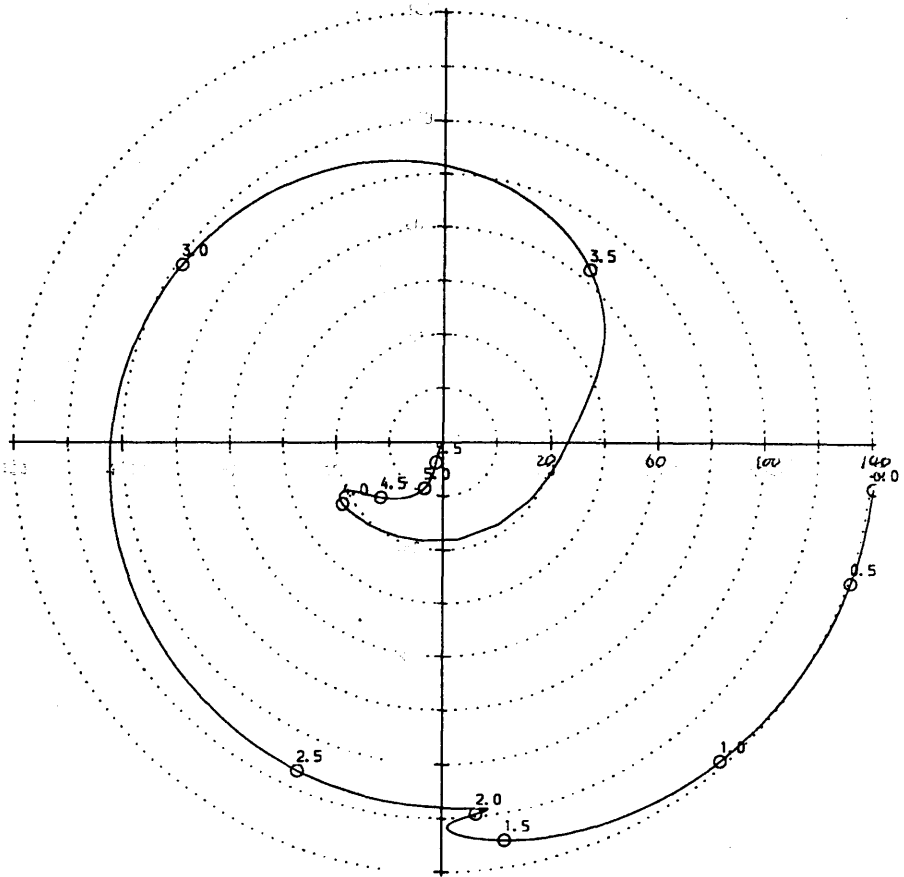


Figure 4.6: *The Nyquist plot for the first loop in an unstable state, the curve encloses the point (0dB, -180°).*

4.6 The Second Loop

We have seen in the previous chapter that this loop also has several channels of feedback. The responses of some of these elements are more complicated than those above as they will depend on the behaviour of the first loop.

The Acousto-Optic Modulator

The acousto-optic modulator is the main feedback element. It introduces a frequency shift Δf_s on the light going to the reference cavity. This will produce a frequency shift on the laser light Δf_l that depends on the open loop gain of the first loop GH_1 .

$$\Delta f_l = \frac{GH_1}{1 + GH_1} \Delta f_s$$

This only deviates significantly from $\Delta f_l = \Delta f_s$ where $|GH_1| \leq 1$, *ie.* near the unity gain frequency of the first loop. Above this frequency the gain falls and the phase lag increases.

The Rear PZT

The ‘bypass’ signal is applied directly to the rear PZT. This signal is treated by the first loop in the same way as laser frequency noise and will be similarly suppressed. A signal Δf_s will produce a frequency shift on the laser light Δf_l that is given by

$$\Delta f_l = \frac{1}{1 + GH_1} \Delta f_s$$

It will only approach $\Delta f_l = \Delta f_s$ when $GH_1 \leq 1$. This signal does not have the loss of gain and increased phase lag suffered by the *aom* signal near the unity gain frequency of the first loop. It is used to compensate for the bandwidth limitation imposed by the first loop.

Reference Cavity PZT

The signal to the reference cavity PZT will be effected by the first loop in the same way as the signal to the acousto optic modulator (*aom*). Here, however, the signal is only applied at frequencies where $|GH_1| \gg 1$ and so we can take $\Delta f_1 = \Delta f_s$.

The Electronics

In this loop we do not have to apply the large voltages that were needed in the first loop, this simplifies the design of the electronics.

The feedback operates through several channels, the gain of each of these relative to the main channel (the *aom*) is adjustable (Figure 4.7). There is also an overall gain control and a switch that when closed increases the gain below 200Hz.

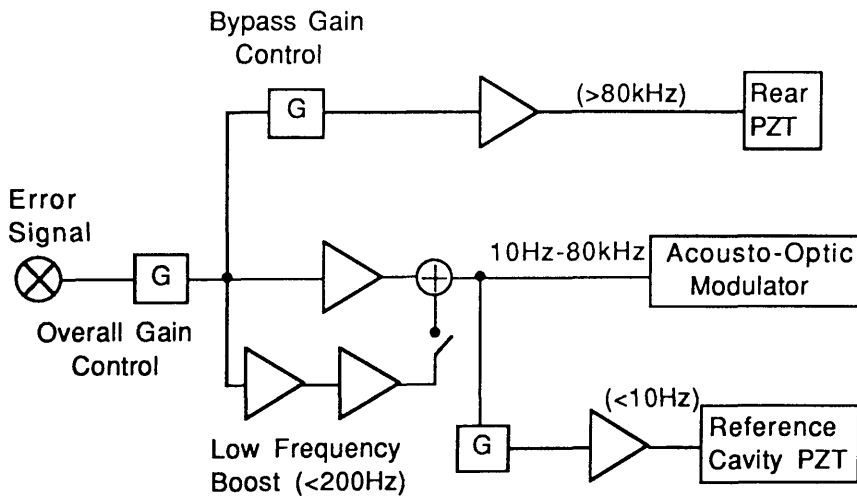


Figure 4.7: Diagram of the feedback electronics of the second loop.

Nyquist Plots

Figure 4.8 shows the Nyquist plot for the second loop. This was calculated for the first loop in the state shown previously (Figures 4.3,4.4 and 4.5). The low frequency boost and the feedback to the reference cavity PZT were both turned

off. Neither of these effect the stability of the servo, they only increase the low frequency gain. We can see from Figure 4.8 that the servo is again conditionally

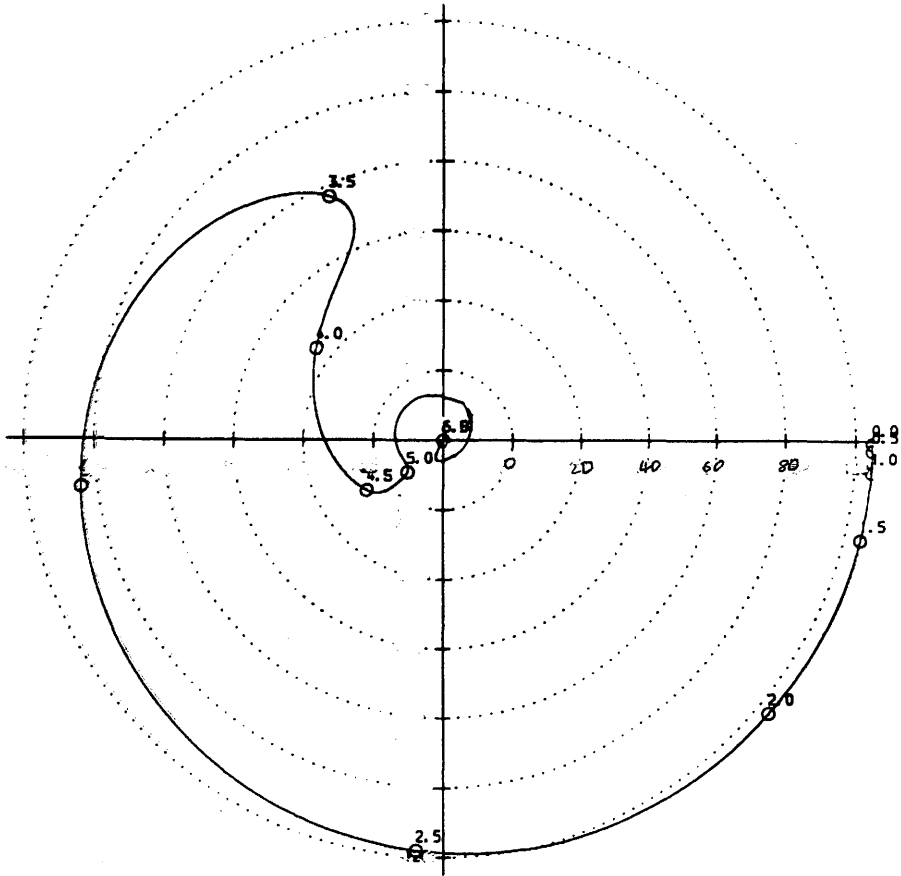


Figure 4.8: *The Nyquist plot for the second loop.*

stable. The lower gain margin is 14dB and the upper one is 6dB. The gain at 1kHz is 84dB.

The phase margin can be seen from the Nyquist plot to be $\sim 43^\circ$. This is again less than ideal and gives an underdamped system. The behaviour of the system near its unity gain frequency can again be estimated by modelling it as a second order system. The model gives a $\sim 2.7\text{dB}$ enhancement of the noise near the unity gain frequency. Plotting $\frac{1}{1+GH_2}$ shows the enhancement of the noise to be $\sim 3.5\text{dB}$. The model gives the $1/e$ damping time for perturbations at this frequency to be

~ 2.2 cycles. The combined system is less well damped than the initial, single loop, system.

4.7 Total Gain

It is possible to plot the total gain of the combined system (Figure 4.9). This is taken as $|GH_1 \times GH_2|$. It represents the maximum amount of frequency stabilisation achievable from the combined system and does not take into account noise limitations *eg.* shot noise in both systems.

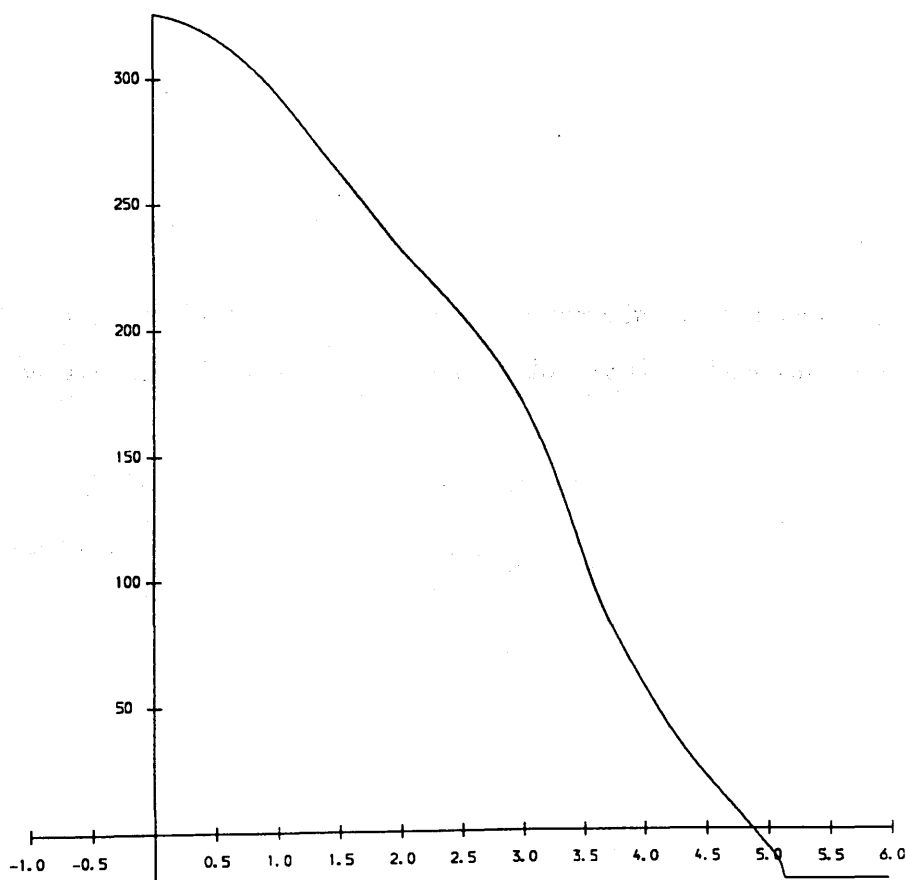


Figure 4.9: *The total gain of the two loop system. The vertical axis is in dB and the horizontal one is log(frequency). The gain is not shown below -20 dB.*

4.8 Limitations

Accuracy of Model

We can model the open loop transfer function of the servo system with reasonable accuracy and thus assess its gain and stability. The accuracy of the model depends on how accurately each component of the servo loop is modelled. It would be possible, for example, to increase the accuracy by carefully measuring the exact transfer function of each component in the system but there should be no need to do this provided the system has suitably large gain and phase margins.

All amplifiers apart from the 3kV amplifier were treated as ‘ideal’. The behaviour of the 3kV amplifier had a significant effect on the position of the crossover frequency between the ‘fast’ and ‘slow’ feedback channels and it was therefore modelled more carefully.

Noise and Dynamic Range

The model takes no account of the noise levels in the various components of the servo system. We saw in the previous chapter that these can limit the amount of frequency stability that can be achieved. Such problems can be avoided by careful design, although fundamental limits such as the shot noise limit cannot be overcome.

Acquisition of Lock

The model gives information on the gain and phase margins and large gain and phase margins make the acquisition of lock easier. It does, however, ignore the size of the signals in different parts of the feedback circuit. This is particularly important during the acquisition of lock when large signals are inevitable. This will drive amplifiers into saturation causing nonlinearities that are extremely difficult to model. The exact behaviour of each amplifier during this stage is critical to the acquisition of lock. Experimentation is the best way to overcome problems at this stage.

Chapter 5

Data Collection

5.1 Introduction

There are a number of plans to build large scale laser interferometric gravitational radiation detectors. These detectors will have to run, virtually continuously, for many months. Many hours of data have been recorded from the various interferometric detectors, including 94 hours of continuous data taking at the California Institute of Technology [Hereld 1984]. The optical discovery of SN1987a prompted the groups at California Institute of Technology, Massachusetts Institute of Technology and at Glasgow University to record several hours of data coincidentally [Mackenzie *et al.* 1987]. Apart from this short run no extended period of data taking had been tried with the prototype detector at Glasgow. It was therefore desirable to try running the prototype detector for a much longer time. This would indicate if continuous running of a full scale detector would present any previously unforeseen problems.

The period of the data taking had to be considerably greater than the few hours of previous runs. There was, however, little reason to record data for weeks or even months as this would produce a huge amount of data of little astrophysical interest. It would also stop any development work being done on the prototype detector. As a compromise between these two extremes it was decided to take data continuously for 100 hours. This was done in coincidence with the the German group at the Max Planck Institute for Quantum Optics in Garching.

The data taken during the run could be used in a variety of ways. It could provide information on how the sensitivity of the detector varied with time in a

way that had not previously been done. The data would be particularly useful in looking for spikes and transient bursts of noise. Finding the source of these infrequent bursts of noise is extremely difficult. The difficulty here should be greatly reduced by the large amount of auxiliary data that was recorded along with the sensitivity signal. Such noise sources would have to be eliminated for a large scale detector.

The data taken during the run could also be very useful in the development of the data analysis software that will eventually be required. The programs could now be written to take account of the ‘imperfections’ that will, inevitably, be present in the data. This would involve, for example, noticing when the detector was out of lock or when the data was particularly noisy and developing strategies to cope with these situations.

While developing the data analysis programs some searches could be made for gravitational wave signals. With the present level of sensitivity and with the current predictions of source strengths it is unlikely that any signals would be seen but a search might set some new upper limits on the strength of such signals.

5.2 Signals to be Recorded

The only signal that had to be recorded was the output of the detector. In addition to this as many other signals as possible were recorded. These signals came both from different parts of the detector and from other sensors in the room. These signals could then be analysed to see if there was any correlation between them and the output of the detector. This information could be used to reduce the number of unexplained ‘events’ in the data. It is important to reduce the number of spurious events as this reduces the ‘false alarm’ rate when doing cross-correlation experiments with other detectors. A signal that has no correlation with the recorded data is probably not worth recording in future runs.

The data acquisition program took samples at a rate of 60kHz (60,000 samples per second). The sampling rate was controlled by a Rubidium clock. Searches for signals, such as those from pulsars, that extend throughout the entire data set

require good stability of the sampling frequency. For example, a search for a signal at 4kHz in 100 hours of data would need the sampling frequency to be stable to 1 part in 6×10^9 over the 100 hours. The stability of the Rubidium clock was somewhat better than this at 1 part in 3×10^{11} over this period. The absolute time was taken from the MSF 60kHz time and frequency standard broadcast by the National Physical Laboratory. This should give absolute time to within a few milliseconds. The 60kHz sampling rate was divided between five 12 bit analogue channels, one 8 bit analogue channel and one 8 bit digital channel. Each channel was sampled at 10kHz. One of the 12 bit channels was made up of six channels multiplexed together so that each was sampled at 1.667kHz.

The ADC/multiplexer unit was a Cambridge Electronic Design (CED) 1401, the interfacing computer was a COMPAQ 386/25 and the data was recorded on an EXABYTE EXB-8200 8mm Cartridge Tape Subsystem. We recorded 1.39Gbytes of data on each tape.

5.3 Sampling Analogue Signals

The signals to be recorded came from many different sources and were of widely differing amplitudes and spectral shapes. To use the 72dB dynamic range of the analogue to digital converter (ADC) effectively it is best to have all the signals of roughly the same rms voltage level. For the same reason it is also useful to filter the signals to reduce the amplitude variations between components at different fourier frequencies before sampling them. This prewhitening of the data also helps reduce intermodulation distortion [Blackman and Tukey 1959].

The signals came from a wide range of sources and it was thus necessary to isolate the earth lines of the signals from each other to avoid introducing loops in the ground line. Each signal was therefore received by a differential amplifier.

Many of the signals to be recorded contain significant power at frequencies well above the Nyquist frequency of the sampling rate. The sampling process would alias this power down into the frequency band of interest (0Hz — sampling frequency/2 Hz). To avoid this it is necessary to provide some form of low pass

Signal	Type	Resolution (bits)	Sampling rate (kHz)
Secondary Feedback	Analogue	12	10
Secondary Error Point	Analogue	12	20
Primary Error Point	Analogue	12	10
Microphone	Analogue	8	10
Secondary Visibility	Analogue	12	1.67
Primary Visibility	Analogue	12	1.67
Seismometer	Analogue	12	1.67
Low Frequency Feedback	Analogue	12	1.67
Oscillation Detector	Analogue	12	1.67
Battery	Analogue	12	1.67
Multiplexer Synchronisation	Digital	1	10
Minute Mark	Digital	1	10
Calibration	Digital	1	10
Alarm	Digital	1	10
Mains Frequency	Digital	1	10
Lock Regained	Digital	1	10
Mains Pulse	Digital	1	10
Magnetic Pulse	Digital	1	10

Table 5.1: A table summarising the signals recorded during the data run.

anti-aliasing filter. This was done for all the channels being recorded. The filter used was an 8 pole low pass Bessel filter. For the signals sampled at 10kHz this filter had a response that was 6 dB down at 3kHz and a further 30dB down at 7kHz(Figure 5.1). This gave at least 30 dB of anti-aliasing for signals in the range

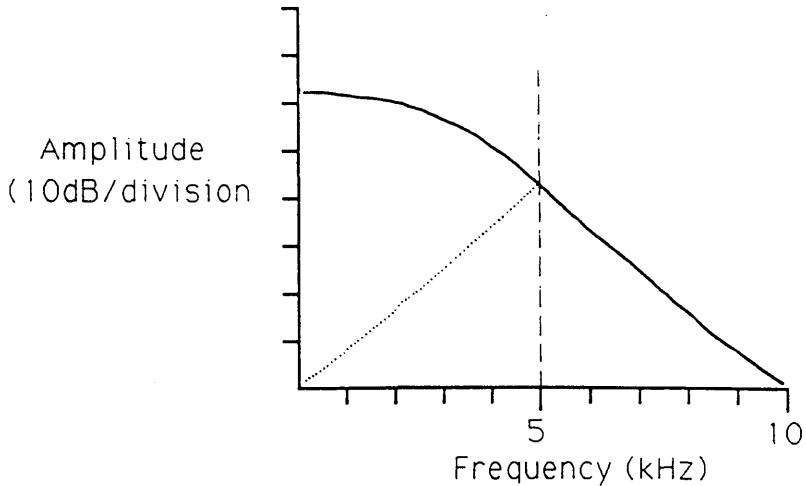


Figure 5.1: *The frequency response of anti-aliasing filter for signals sampled at 10kHz. The dashed line is at the Nyquist frequency. The dotted line shows how signals in the range 5–10kHz are aliased into the recorded spectrum.*

0 — 3kHz. This should be perfectly adequate provided the spectrum of the signal is roughly flat. For sampling rates other than 10kHz the above frequencies are simply scaled by the appropriate factor (sampling frequency/10kHz).

To simplify the building of the data collection instrumentation it was decided to build the differential amplifier, amplifier and filters and Bessel filter on one printed circuit board. This could then be duplicated, with changes to the values of a few components, for all the data signals. A simplified diagram of the data collection system is shown in Figure 5.2.

5.4 Analogue Signals

This is a list of the analogue signals that were recorded and the reasons for recording them.

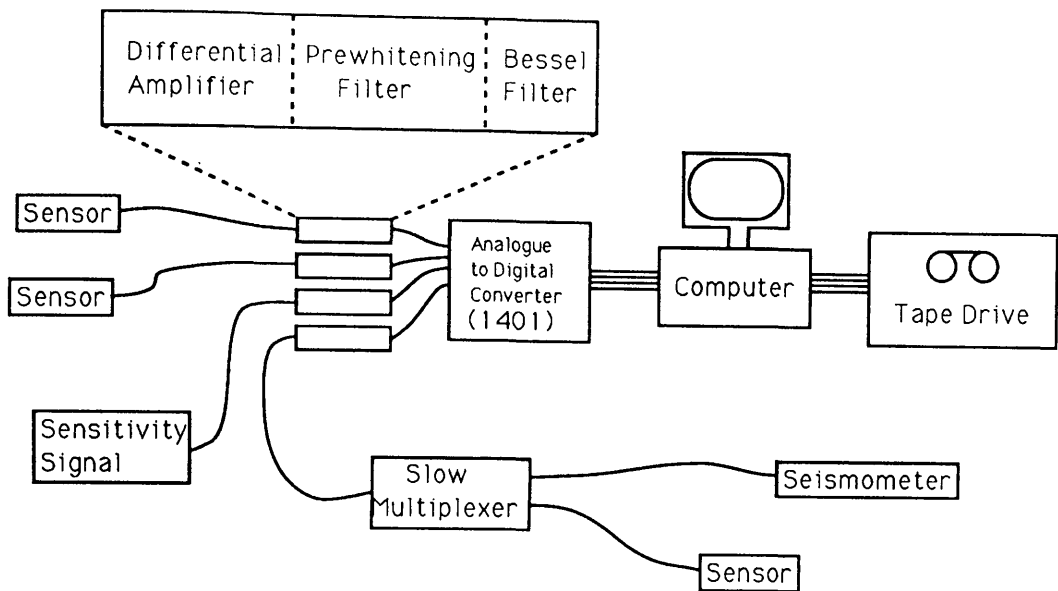


Figure 5.2: A simplified diagram of the data acquisition system.

Secondary Feedback (12bit resolution, 10kHz sampling rate)

This is the signal that keeps the secondary cavity on resonance with the laser light. At frequencies below the unity gain frequency of the secondary feedback servo this is a direct measure of the differential length changes between the two arms of the detector; *ie.* it is the sensitivity signal. Above this frequency the signal falls quite rapidly.

Secondary Error Point (12bit, 20kHz)

At frequencies above the unity gain frequency of the secondary feedback servo this is the sensitivity signal. To give a sensitivity signal with good anti-aliasing at frequencies greater than $\sim 3\text{kHz}$ it is sampled at 20 kHz. This is done by taking samples, symmetrically spaced in time, on two 10kHz channels.

Primary Error Point (12bit, 10kHz)

This is the error point of the servo that stabilises the laser to the primary (10m) cavity. Much of the misbehaviour of the laser that would cause extra noise in the sensitivity signal would also be expected to show up in this signal.

Microphone (8bit, 10kHz)

Three omnidirectional microphones were hung near the parts of the detector thought to be most sensitive to acoustic noise. These points were the two end tanks, in which test masses were hung, and above the optic table near both the laser and the center tank, in which the other test masses and the beam splitter are hung. The signals from these microphones were added and recorded. It was hoped that this signal would detect both bursts of acoustic noise and continuous signals. The continuous signals might not have been seen when measuring the sensitivity of the detector but they could show up in the data analysis where much longer, and therefore more sensitive, Fourier transforms will be done.

Secondary Visibility (12bit, 1.667kHz)

This is the intensity of the light reflected from the secondary cavity. It gives information on whether the cavity is locked on resonance with the laser frequency and on disturbances of the cavity. These disturbances may cause changes in the sensitivity of the cavity to frequency noise. Such changes vary the loop gain of the secondary cavity servo and so cause changes in the character of the recorded signal.

Primary Visibility (12bit, 1.667kHz)

This is the intensity of the light reflected from the primary cavity. It gives similar information to above. The secondary cavity can lock to the laser frequency with the laser locked to the reference cavity but *not* to the primary cavity. This signal allows this situation to be detected more easily than with the primary error point signal.

Seismometer (12bit, 1.667kHz)

Four seismometers were rigidly fixed to the vacuum system. These seismometers were all Teledyne Geotech short period seismometers (S-500) and were sensitive to accelerations below $\sim 500\text{Hz}$ along one axis. One was placed at each end tank, oriented parallel to the axis of the optical cavity. The remaining two were placed on the center tank, one parallel to the line bisecting the angle between the two optical cavities and the other oriented vertically. The function of this signal was similar to the microphone signal above but measuring mechanical rather than acoustic noise.

Low Frequency Feedback (12bit, 1.667kHz)

This is the signal that, at very low frequencies, controls the length of the primary cavity. It is recorded so that it is possible to detect when the feedback signal has drifted close to the end of its range. There are likely to be bursts of noise in this state as it is quite likely that the feedback electronics will be driven briefly into saturation but without causing the detector to lose lock.

Oscillation Detector (12bit, 1.667kHz)

The feedback loop that locks the laser to the primary cavity has a tendency to oscillate at two frequencies ($\sim 30\text{kHz}$ and $\sim 200\text{kHz}$). This

oscillation will increase the noise level. The oscillation will not be seen in the primary error point signal because it will be greatly attenuated by the anti-aliasing filter. To detect the oscillations a filter is used that has peaks in its response at the frequencies of oscillation. The rms value of the output of this filter taken. This signal is proportional to the amplitude of the oscillation and is recorded.

Battery (12bit, 1.667kHz)

The last of the multiplexed signals is the voltage from a battery. This voltage is large enough to saturate the ADC. This gives a signal of known size on the tape and allows easy checking of whether the position of the multiplexer channels has been changed by some disturbance of the clock pulses.

5.5 Digital Signals

Ground loops can be introduced by the wiring of the digital signals as well as by that of the analogue ones. To avoid this each digital signal is received through an opto-isolator. This also inverts the signal. The signals are all converted to be positive true by inverting them again where necessary. The clock signal is also isolated and inverted in the same manner.

Multiplexer Synchronisation

This is high when the first channel of the multiplexer is switched ON. It is also used to trigger the start of the data taking. This ensures that from tape to tape and from one run to the next each of the multiplexed signals is recorded at the same point in each block of data. This makes the reading of the data easier.

Minute Mark

The rising edges of this channel are separated by a minute. The timing is started by a minute mark from the MSF signal. Thereafter the time is kept by the 60kHz signal derived from the Rubidium clock. Rising edges of this signal should always be separated by exactly 10,000 samples. Anything other than this indicates that clock cycles have been missed or that extra, spurious, pulses have been added. This was used to check if there had been any interference with the clock signal. Only one such occasion was found in the 100 hours of data.

Calibration

This is high when the calibration signal is ON. Calibration was done automatically every 210 seconds for a period of 1.6 seconds. Extra calibrations, also 1.6 s long, could be added by the operator. This was usually done after lock had been regained.

Alarm

This signal is ON when any of the primary visibility, secondary visibility or oscillation detector signals exceed some threshold level. The thresholds were adjusted throughout the run. This signal also activated an alarm to alert the operator to the undesirable condition.

Mains Frequency

Much of the data recorded is contaminated by interference from harmonics of the ~ 50 Hz mains frequency. Removal of this contamination will depend on knowing the exact frequency of the mains. The time between rising edges of this signal should give the period of mains cycle.

Lock Regained

When, after some problem, the detector was again made to lock there was frequently some adjustment of the controls. When this was completed this line was supposed to be switched briefly ON by the operator. This indicates that the subsequent data was thought to be reliable.

Mains Pulse

This signal came from a box that detected fast 'spikes' in the mains power supply. These 'spikes' could be included in the data in many ways and might look like real signals.

Magnetic Pulse

This is recorded for similar reasons to the mains pulse signal. Some of the test masses in the detector are driven by coil and magnet devices. The detector will thus be sensitive to rapid fluctuations in the ambient magnetic field. This device detects such fluctuations. The threshold was set at a level corresponding to a movement of $1 \times 10^{-19} \text{m}/\sqrt{\text{Hz}}$ at 1kHz.

5.6 Other Information

There were two other methods used to record data during the run. A log book was kept in which things such as the tape number, temperature, adjustments to various controls, disturbances and anything else of note was recorded. A chart recorder was also running. The visibility in the primary and secondary cavities was recorded on it. There was also a bandpassed, rectified and smoothed form of the output of the detector which looked at the noise at frequencies around 1kHz. These signals allowed the operator to see how well the detector was operating. Tape changes and other information were also recorded on the chart.

Chapter 6

Data Analysis

6.1 Introduction

This chapter describes the work carried out at Glasgow on the analysis of the data taken during the 100 hour run. The data was recorded on tapes numbered B1-B12, C1-C12 and D1-D4, a total of 28 tapes. This work was only a preliminary analysis. It was done to find some of the characteristics of the data and of the detector. Copies of the data tapes have been sent to Cardiff where a more thorough examination of the data will take place. This should include the search for signals from both known and unknown pulsars. To obtain the best possible sensitivity such searches will have to use the entire data set. This will involve the manipulation of huge amounts of data both in the selection of the useful sections and in the resampling that is required to correct for the effects of doppler shifts on the signals. This is a large task and is beyond the scope of this initial analysis.

6.2 Duty Cycle

The first analysis done was to calculate the amount of valid data on each tape. This was done using the secondary visibility signal on the chart recorder. The data is assumed to be valid if the secondary cavity is locked. This will be true almost all the time; the exceptions will last for only a short time and can be safely ignored. The results are shown in Figure 6.1.

The data acquisition system crashed twice during the run (Tapes B7 and C6). The causes of the crashes are unknown but one was probably associated with

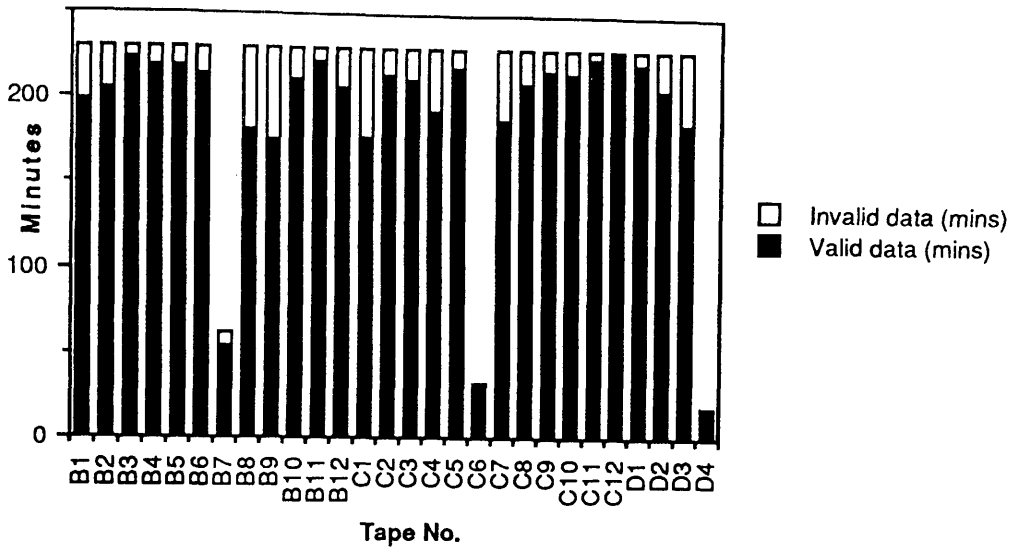


Figure 6.1: A diagram showing the amount of valid data on each tape.

interference caused by switching on nearby equipment. Tape D4 was stopped when a total of 100 hours of data had been taken.

The duty cycle of the detector over the whole of the run was 90.7% and the duty cycle of the recorded data was 90.8%. The effective duty cycle, allowing for the time between tapes was 88.3%. This was good and was better than might have been expected for a prototype detector not designed for continuous running. Improvements to these figures would be expected if the detector was made less sensitive to changes in the ambient temperature and if the four minute gap between the end of one tape and the start of the next one was eliminated.

6.3 Tape Checking

A program was written by a colleague to check that the data on the tape was both valid and readable. This program read every block of data and checked the time between minute marks. The minute mark signal is derived from the same source as the sampling clock and the minute marks should thus be exactly 10,000 samples apart. The only error detected by this program was in tape B12 where there appeared to have been an extra clock cycle. The program also calculated the

duty cycle for each tape, agreeing with the figures calculated earlier.

6.4 Displacement Noise Level

The output of the detector was calibrated regularly (page 64). This was done by a series of signals at different frequencies each producing a known displacement, applied to the primary cavity end mass. The signals were at odd multiples of 234.4Hz. The signal was applied for 1.6 seconds (2^{14} samples) every 210 seconds. Extra calibrations could be added by the operator.

The noise level of the detector at each calibration frequency could be calculated. To do this each block of data with the calibration signal in it was taken. The block was discarded if any of the digital signals *alarm*, *magnetic pulse* or *mains pulse* were *on* in any part of it. This should ensure that during the calibration the detector was locked stably and that there was no mains or magnetic pulse contamination of the data. Each remaining block of data was then Fourier transformed using a Fast Fourier Transform (FFT) routine (REALFT [Press *et al.* 1986]). The data was transformed in 8 blocks each of 2^{11} points. The power in each of the calibration peaks and in the 8 frequency bins (19.5Hz) on either side of it was averaged. The peak corresponded to a displacement of 1.19×10^{-16} m. From the ratio between the peak and the background noise level the actual displacement noise level at each calibration frequency could be found. If the calibration peak was less than 6dB above the background noise then it was assumed to be unreliable and was ignored. This occurred only rarely in the data that was analysed and only at the two lowest calibration frequencies. Figure 6.2 shows the results of a typical calibration measurement. The rise in the noise level near 5kHz is caused mainly by the aliasing of noise above 5kHz into this spectrum. The noise in the detector rises rapidly at low frequencies and the calibration peak at 234.4 Hz was therefore arranged to be 1000 times larger than the other peaks.

The fundamental frequency of the calibration signal was, like the 10kHz sampling frequency, derived from the 60kHz clock signal ($234.375 = \frac{10000 \times 3}{128} = \frac{60000}{256}$). This ensured that when calculating the displacement noise level each calibration

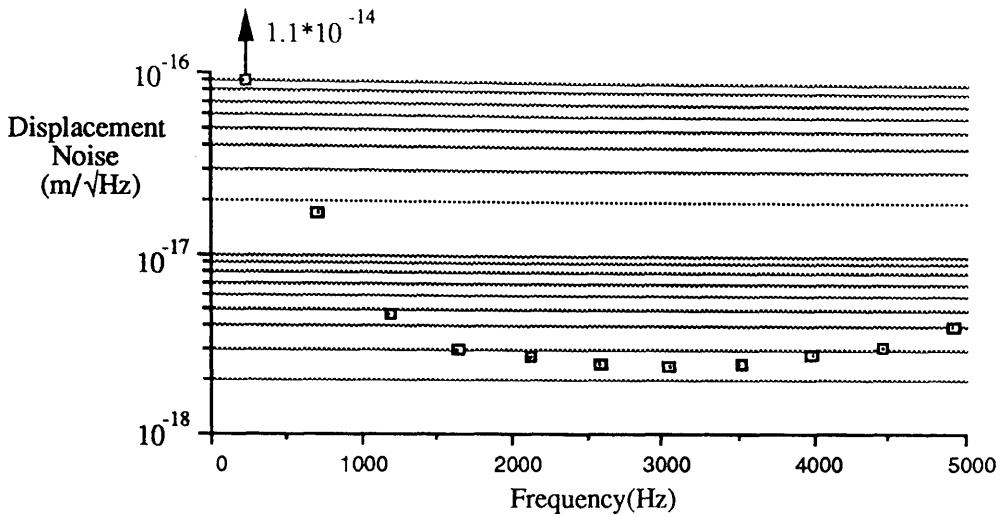


Figure 6.2: A typical plot of the displacement noise at each of the calibration frequencies (Tape B4). The vertical scale is logarithmic. The statistical uncertainty in the measurement is given by the height of the boxes.

signal was at the center of a frequency bin of the Fourier transform. There was therefore no leakage of power from the calibration peak into the neighbouring frequency bins when doing the transform. This simplified the calculation of the noise level.

To see how the sensitivity of the detector varied with time the displacement noise was calculated for all the calibrations on one tape (C12). This tape was chosen because it had a high duty cycle. The noise level at selected calibration frequencies is shown in Figure 6.3. The calibrations were not necessarily uniformly spaced in time. There are two reasons for this: some calibrations will have been ignored because of the veto signals explained earlier and some extra ones will have been added by the operator. The graph (Figure 6.3) shows how the sensitivity of the detector varies with time. The variation is larger than would be expected from purely statistical fluctuations implying that the noise level varies with time.

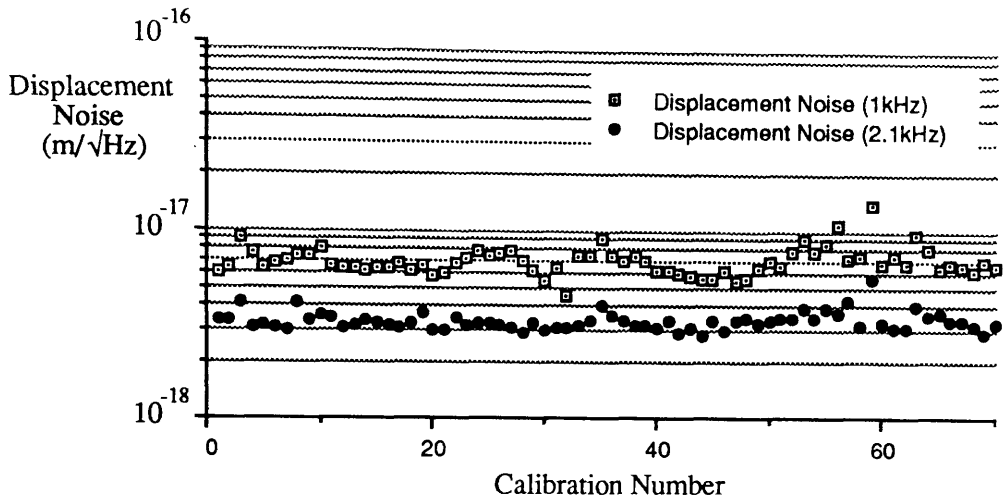


Figure 6.3: *A plot of the displacement noise against time at two particular frequencies. (Note that the calibrations are not necessarily evenly spaced in time.)*

6.5 Noise Statistics

One of the first signals likely to be searched for in the output of large scale detectors are pulses with timescales of around 1ms and of unknown shape. It is therefore useful to examine the output of the prototype detector to see what the noise statistics are for this type of signal. It is also interesting to see how the statistics may be improved using various veto signals derived from the auxiliary recorded data.

It can be seen from the typical noise measurement (Figure 6.2) that the lowest noise level is found in the frequency range 1.5kHz to 4kHz. Below 1.5kHz the noise level rises rapidly. The noise above 1.5kHz is similar in nature to that expected from a large scale detector. It was therefore decided to look at the noise statistics for signals in the range 1.33kHz — 1.96kHz. The data was filtered to include only signals in this frequency band by Fourier transforming it, zeroing all the unwanted frequency bins and retransforming it to get the bandpassed time series. Each point in the new time series was then squared to give a number proportional to the energy of that sample and a histogram of these values was accumulated. For a stationary Gaussian noise source a graph of $\ln(\sqrt{\text{bin no.} + 0.5} \times \text{bin contents})$

against bin number should be a straight line with equation

$$y = \ln \frac{N_1}{\sqrt{2\pi\sigma}} - \frac{\text{Bin No.}}{2\sigma^2}$$

Where N_1 is the total number of points, and σ^2 is the variance of these points. The $\sqrt{\text{bin no.} + 0.5}$ term is an approximation for the integral of the probability density function over the width of the bin. A more accurate approximation is used for the first few bins where the simpler approximation has errors of more than 1%.

When accumulating this data it was necessary to exclude periods when the detector was out of lock and other times when the output was expected to be unusual or unusually large. In the above case the data was discarded if the *calibration* or *alarm* signals were *on* or the *secondary visibility* signal exceeded a software set threshold. This program was then run on tape C12 (219 minutes of data). The resulting graph is shown in Figure 6.4. This found that even at energies corre-

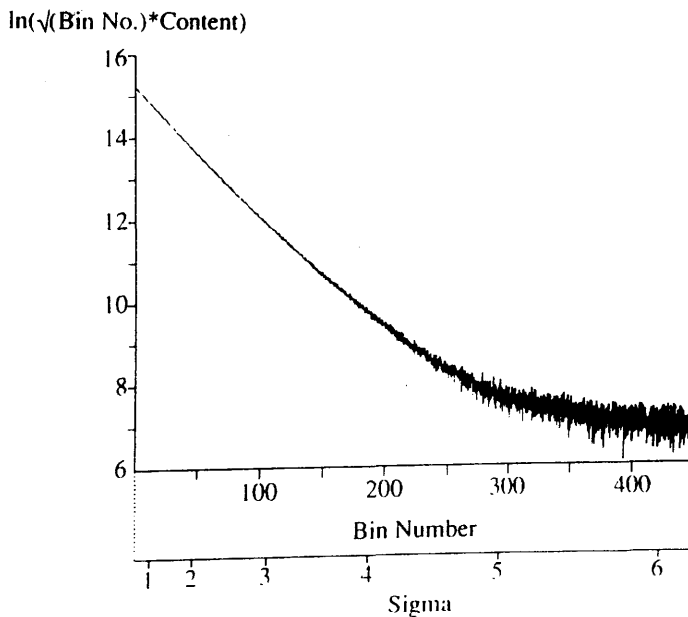


Figure 6.4: *The pulse height graph for tape C12. The horizontal axis is linear in energy. A Gaussian noise source would produce a straight line graph.*

sponding to a levels of a few σ there was a large excess of points over that expected for a Gaussian distribution. At the 3.5σ level there were 6.5 times as many points as expected and this factor increased at higher energies. The noise is not stationary Gaussian noise. There are two obvious features of the data that could produce

this effect: variation in the noise level and unusual signals associated with the loss and acquisition of lock by the detector.

Nonstationary Noise

We have already seen that the noise output of the detector varies with time (Figure 6.3). Variation in the noise level would produce a graph that, effectively, was the sum of several graphs of different variances. This would produce a curved shape similar to that of the graph in Figure 6.4.

Losses of Lock

When the detector is reacquiring lock there is frequently a period during which it will acquire lock, oscillate and lose lock several times before eventually acquiring lock stably. There may then be some adjustment of the controls before the operator is happy with its performance. Data from both the brief periods of lock and the period of adjustment will have been included in the above graph (Figure 6.4). The large amplitude signals produced by the detector in these states are probably the greatest contributor to the large number of high energy events seen. This period of noisy operation may also explain the high noise levels occasionally seen in the noise level against time graph (Figure 6.3).

6.5.1 Improved Analysis

The analysis procedure was then modified in several ways to try to eliminate identifiable spurious events.

The signals used previously to exclude noisy and unusual data were reused but with the addition of a period of dead time after the *alarm* signal had been *on*. This excluded the 32 seconds of data that followed the *alarm* signal going *off*. This should exclude the noisy data referred to in the *Losses of Lock* section above.

The absolute value of the signal recorded will vary with time as the gain of the secondary servo varies. To allow for this in the analysis the bandpassed time series

was taken in blocks of 3.2 seconds (4096 independent points) and the variance calculated. Each block was then normalised to a variance of 7.0. This procedure also normalises any genuine changes in the noise level such as those seen earlier (Figure 6.3) but the analysis is looking for excess noise above a Gaussian background and should not be affected by small changes in the background level.

The bandpassing of the data has reduced its bandwidth from 5000Hz to 625Hz. To use every point in the new time series would be oversampling the data. The data used to produce the first pulse height graph (Figure 6.4) was oversampled. This oversampling only affects the size of the statistical uncertainty that would be calculated for any point, it does not affect the shape of the graph. To avoid oversampling in the improved analysis only every eighth point in the bandpassed time series was used.

This modified program was then run on sixteen minutes of data from tape C12. This produced the graph shown in Figure 6.5. This shows the noise to be much more Gaussian than in the first graph. It is indistinguishable from Gaussian noise up to a level of $\sim 3\sigma$. Above this level there is still an excess of high energy points compared with that expected for pure Gaussian noise.

There are several possible explanations for this deviation from Gaussian behaviour at high energies. One is that the noise is not stationary over timescales of 3.2 seconds. This would lead to short bursts of noise in some blocks of bandpassed data. These bursts of noise would not be properly normalised and would show up as an excess of high energy samples. Another possible explanation is that the normalised noise is stationary and Gaussian but that some extra noise from a different source occasionally contaminates the data.

6.5.2 Limitations

Ideally the modified program would have been run on the full 219 minutes of data on tape C12. Unfortunately before this could be done there were technical problems with the tape drives and they had to be returned to their manufacturer. Before returning the drives 100 Megabytes (16 minutes) of data was copied from

$\ln(\sqrt{\text{Bin No.}} \cdot \text{Content})$

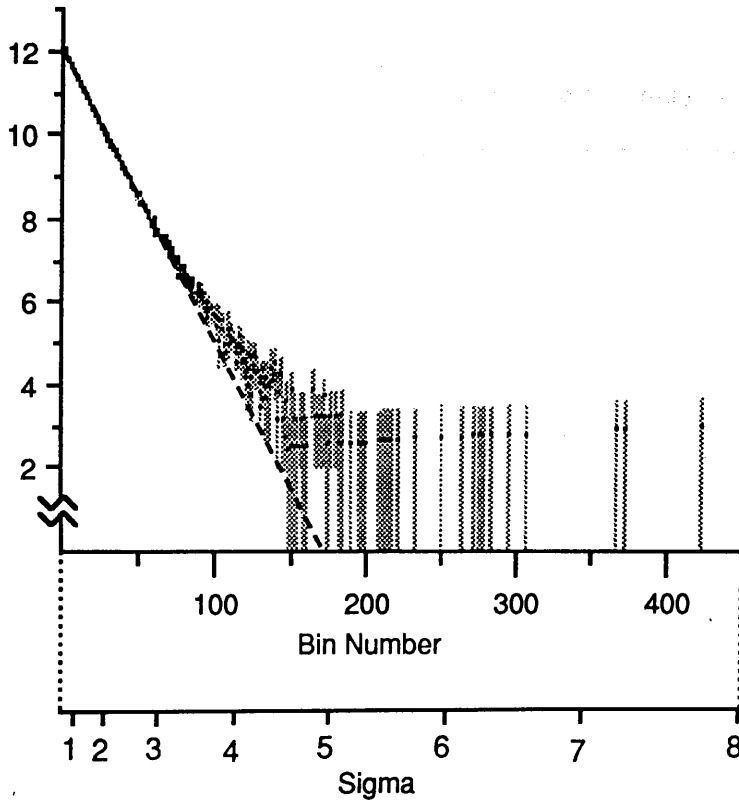


Figure 6.5: *The pulse height graph for 16 minutes of data from tape C12. The shaded bars are $\pm\sqrt{n}$ error bars. The dashed line is the distribution expected for Gaussian noise. To give an idea of scale 1σ corresponds roughly to a pulse of amplitude $h = 7 \times 10^{-17}$.*

tape C12 onto the hard disk in the data analysis computer. This data was taken from calibrations 40 - 45 in Figure 6.3 and was chosen because it was quiet and contained no losses of lock. The graph (Figure 6.5) was produced from this data. Using such a carefully selected subset of the data greatly improves the shape of the graph. The use of properly chosen veto signals over the whole data set should produce a similar effect. The normalisation gives a further improvement, producing the graph shown (Figure 6.5). There was no noticeable change when the dead time was introduced.

It would not be fruitful to continue this type of analysis on such a limited subset of the data and attention was turned to other methods of analysis.

6.6 Coherence Function

There are many possible sources of excess noise in the detector. Two likely sources of both short bursts of noise and continuous signals are seismic and acoustic noise. Both of these signals have been recorded and we wanted to know if there was any relationship between either signal and the output of the detector. Possible correlations were investigated using the coherence function.

The coherence function is a dimensionless frequency domain function that, at each frequency, gives the fraction of the output power of a system directly related to an input. It ranges in value from 0-1. It is easily calculated using Fourier transforms [Hewlett Packard].

6.6.1 Microphone Signal

The coherence between the microphone signal and the output of the detector was calculated. The results are shown in Figure 6.6.

The largest peak on the graph is at 100Hz and is related to the mains frequency. The 100Hz component of the two signals is thus related and is seen by the coherence function. The most likely explanation for the presence of this large peak is that both signals have large components at 100Hz that are caused by pickup of this harmonic of the mains frequency. There are also peaks at two other harmonics of

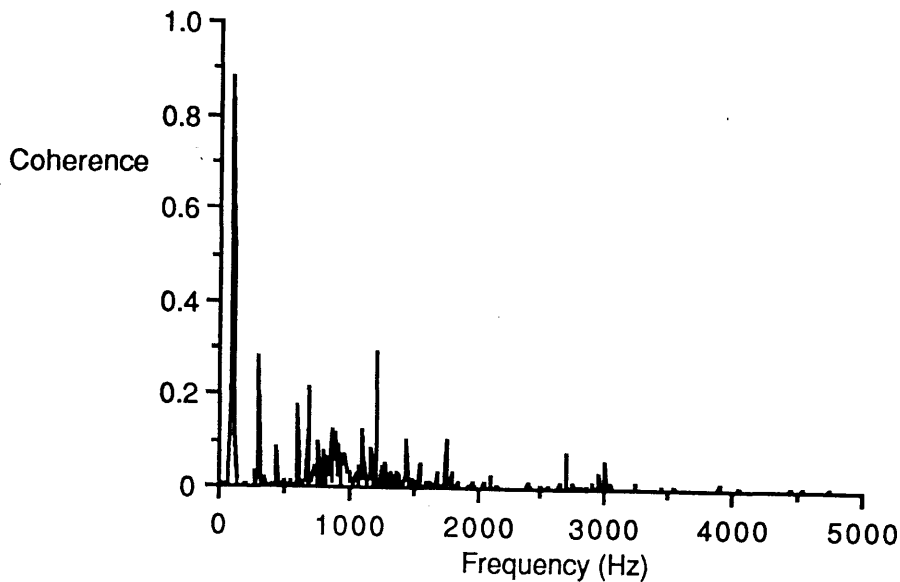


Figure 6.6: *The coherence function between the microphone signal and the detector's output. It was calculated for 9515 averages. There are 512 frequency bins, each 9.77 Hz wide.*

the mains frequency (300Hz and 600Hz). The graph contains several other peaks, the most prominent are at frequencies of 1211, 684, 1445 and 1748Hz. These are likely to be acoustic signals, generated by equipment near the detector, that couple in to the detector in some way.

We can also see from the graph that there is a region from 500Hz to 1.5kHz where up to 15% of the noise power (40% of the amplitude) out of the detector is directly related to the acoustic noise in the room. This is a lower limit to the level of acoustic pickup. The microphone signal is the combined signal from three microphones (page 61). The acoustic noise that is affecting the detector may only be picked up by one of these microphones, reducing its signal to noise ratio in the recorded signal. The coherence function would then be an underestimate of the magnitude of the contamination of the detector's output by acoustic noise. The coherence function is calculated for 16 minutes of data, the acoustic contamination may only occur for part of this time. The data used to produce this coherence function was recorded at about 5:30 am when the room would be expected to be acoustically quiet; the contamination may well be worse at other times.

6.6.2 Seismometer Signal

The coherence between the seismometer signal and the output of the detector was calculated. These signals were sampled at different rates. To match the sampling rates the output of the detector was filtered and every sixth sample of the new time series taken. The coherence function was then calculated using this resampled data and the seismometer signal. The output signal from the detector was filtered before resampling to avoid aliasing problems. The data was filtered by bandpassing it with a pass band of 0Hz — 830Hz. The method used was the same as in the *Noise Statistics* section.

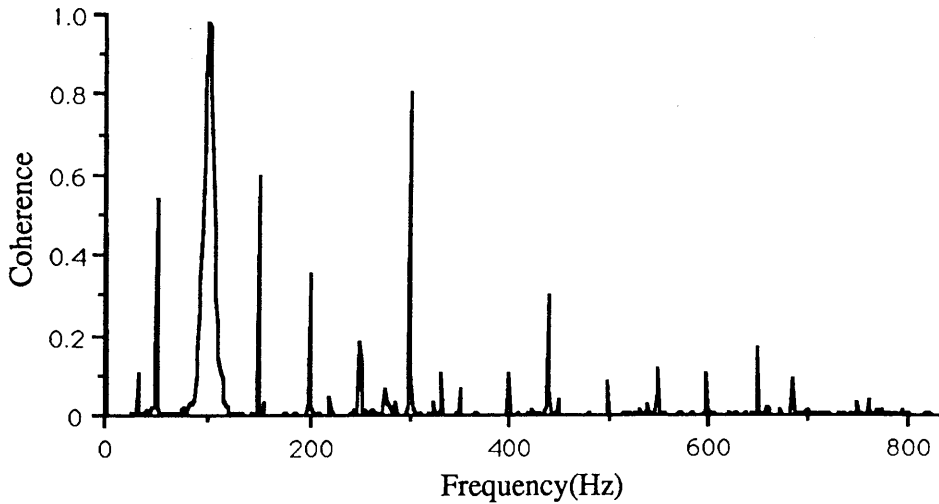


Figure 6.7: *The coherence function between the seismometer signal and the detector's output. It was calculated for 1582 averages. There are 512 frequency bins, each 1.63Hz wide.*

The results are shown in Figure 6.7. Unlike the previous graph this does not show a broad region of the spectrum where the two signals are correlated. The graph is dominated by signals at harmonics of the mains frequency. There are however several peaks at frequencies that are not multiples of 50Hz. The most significant of these is at 439.5Hz where 30% of the signal power (55% of the amplitude) is directly related to the seismic noise. The other frequencies at which signals are present at more than 20% of the signal amplitude are, in order of de-

creasing size, 32.6Hz, 322.0Hz, 684.4Hz, 275.1Hz and 219.7Hz. The seismometer signal is the combined output from four seismometers and this could again result in the measured value of the coherence function being an underestimate of the contamination by seismic noise.

6.7 Conclusions

This preliminary analysis of the data taken during the 100 hour data run has produced some interesting results which will be useful in later work. The data selection procedure used for the *Noise Statistics* section should provide the starting point for the selection of data to be used in other analysis *e.g.* pulsar searches. It is probably useful to further refine the selection procedure using some of the other auxiliary signals. The coherence function section shows that some continuous signals are contaminating the data and it also shows that acoustic noise may soon be a limiting factor over some parts of the detector's bandwidth.

Chapter 7

Seismic Isolation and Thermal Noise

7.1 Suspension Systems

In the prototype detector at Glasgow the test masses are hung as pendulums. Two possible sources of displacement noise of the mirror surfaces on the test masses are seismic noise and thermal noise. Two of the obvious sources of thermal noise are from the suspension system and from the internal modes of the test masses. This section will concentrate on the suspension system. The level of thermal noise from the suspension system and the amount of seismic isolation both depend on the characteristics of the suspension system.

There has recently been some interest in the development of many stage suspension systems. These are designed to lower the frequency at which a large scale gravitational radiation detector might work from $\sim 100\text{Hz}$ to $\sim 10\text{Hz}$. A prototype seven stage suspension system, the 'super-attenuator', has been built by a group at Pisa and is currently being tested [DelFabbro *et al.* 1988]. The work in this section was done when this 'super attenuator' was first proposed to see what constraints on the design of such a system were imposed by the expected thermal noise. This was done by modelling the seismic isolation and thermal noise expected from single and double pendulum suspension systems.

7.1.1 Single Pendulum

The simplest system for suspending the test masses is to use a simple pendulum (Figure 7.1).

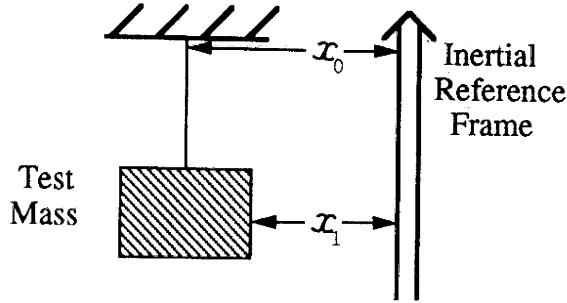


Figure 7.1: A simple pendulum suspension of length l m for a test mass of m kg. The pendulum has a resonant frequency $f_0 = \frac{1}{2\pi}\sqrt{\frac{g}{l}}$.

Thermal Noise

For any real suspension system there will be a resistive damping force (directly proportional to the velocity *i.e.* $-b(\dot{x}_1 - \dot{x}_0)$) that will damp any oscillation at the resonant frequency of the pendulum. It can be shown [Weiss 1972] that this damping force will have an associated noise force F_n which acts on the mass and whose spectral density (\tilde{F}_n) is given by Equation 7.1.

$$\tilde{F}_n^2 = 4kTb \quad (7.1)$$

Where k is Boltzmann's constant and T is the temperature. This thermal noise force produces displacement noise at a level given by Equation 7.2, where f ($\gg f_0$) is the frequency at which the displacement noise is measured and Q is the quality factor of the resonance ($Q = \frac{2\pi f_0 m}{b}$).

$$\text{Thermal Displacement Noise} = \left(\frac{4kTf_0}{8\pi^3 f^4 m Q} \right)^{1/2} \text{ m}/\sqrt{\text{Hz}} \quad (7.2)$$

This gives a limit of $Q > 7 \times 10^7$ ($f_0 = 1\text{Hz}$, $m = 400\text{kg}$) for detectors hoping to operate with a noise level of $10^{-20}\text{m}/\sqrt{\text{Hz}}$ at 100Hz and a much stricter limit of $Q > 7 \times 10^{13}$ for the same noise level at 10Hz.

Seismic Isolation

At a typical site, remote from traffic, the seismic noise level would be expected to be about $\frac{10^{-7}}{f^2}\text{m}/\sqrt{\text{Hz}}$ [Hough *et al.* 1986]. To reduce this noise to the level required by a large scale detector of $< 10^{-20}\text{m}/\sqrt{\text{Hz}}$ at 100Hz requires an isolation of $> 10^9$.

A simple pendulum (Figure 7.1) has a transfer function at a frequency f for movement of the suspension point to movement of the mass which is given by Equation 7.3.

$$\frac{x_1}{x_0} = \frac{mf_0^2 + jb'f}{m(f_0^2 - f^2) + jb'f} \quad (7.3)$$

Where $b' = \frac{b}{2\pi}$ and $j = \sqrt{-1}$. We can see that for $f \gg f_0$ this gives an isolation of $(\frac{f}{f_0})^2$ up to a frequency Qf_0 , above this frequency the transfer function will fall as $\frac{1}{f}$. A high Q 1Hz pendulum will give a factor of 10^4 isolation at 100Hz. One way to increase the isolation is to reduce the natural frequency of the pendulum (f_0). It is, however, unlikely that the natural frequency of the pendulum could be reduced much below 1Hz as this would require an unfeasibly long pendulum. Some other method must therefore be found for increasing the isolation.

7.1.2 Double Pendulums

Seismic Isolation

One way to increase the isolation is to use a double pendulum suspension system (Figure 7.2). The transfer function for the double pendulum shown in Figure 7.2 is given by Equation 7.4.

$$\frac{x_2}{x_0} = \frac{(m_2f_2^2 + jb_2'f)(m_Tf_1^2 + jb_1'f)}{(m_Tf_1^2 - m_1f^2 + jb_1'f)(m_2(f_2^2 - f^2) + jb_2'f) - m_2^2f_2^2f^2} \quad (7.4)$$

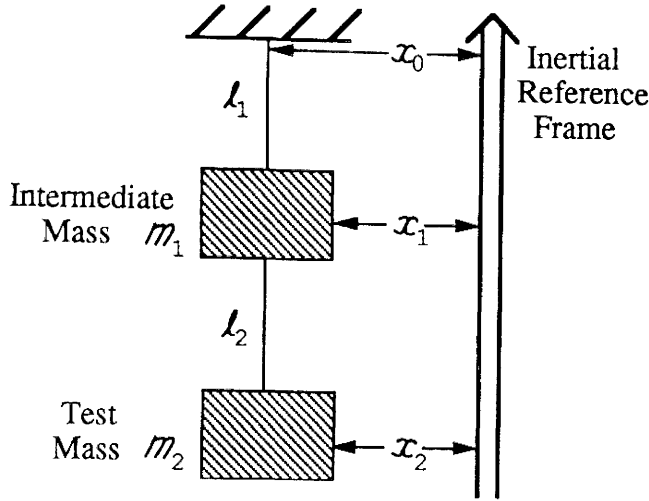


Figure 7.2: Diagram of a double pendulum suspension system

Where $f_{1,2} = \frac{1}{2\pi}\sqrt{\frac{g}{l_{1,2}}}$, $b'_{1,2} = \frac{b_{1,2}}{2\pi}$ and $m_T = m_1 + m_2$. The transfer function now falls as $\frac{1}{f^4}$ above the highest resonant frequency of the system, provided $f \ll Qf_1$ and Qf_2 . For example a system of two identical high Q , 0.7Hz pendulums will have a highest resonant frequency of 1Hz and will give an isolation of 2×10^8 at 100Hz. Further isolation can be achieved by adding more stages to the suspension system, by having the suspension point mounted on a stack consisting of alternate layers of lead and rubber, and by having the whole assembly mounted on air springs [Hough *et al.* 1989].

Thermal Noise

It is important to ensure that the thermal noise in the double pendulum case is no worse than for a single, high Q , pendulum. In a double pendulum suspension system the thermal displacement noise of the test mass will have two components. There will be noise from both the damping of the upper (intermediate) mass (7.5) and of the of the lower (test) mass (7.6). The two contributions are added in quadrature to get the resulting displacement noise of the test mass.

$$\frac{(m_2 f_2^2 + j b'_2 f) \frac{\dot{E}_{n1}}{(2\pi)^2}}{(m_T f_1^2 - m_1 f^2 + j b'_1 f)(m_2(f_2^2 - f^2) + j b'_2 f) - m_2^2 f_2^2 f^2} m / \sqrt{\text{Hz}} \quad (7.5)$$

$$\frac{(m_T f_1^2 + m_2 f_2^2 - m_1 f^2 + j b'_1 f) \frac{\tilde{F}_{n2}}{(2\pi)^2}}{(m_T f_1^2 - m_1 f^2 + j b'_1 f)(m_2(f_2^2 - f^2) + j b'_2 f) - m_2^2 f_2^2 f^2} m / \sqrt{\text{Hz}} \quad (7.6)$$

$$\tilde{F}_{n1,2} = \sqrt{4kTb_{1,2}} \quad (7.7)$$

We can see that above the resonances of the system the noise contribution from the damping of the intermediate mass will fall as $\frac{1}{f^4}$ (provided the lower mass is of high Q). The noise contribution from the damping of the test mass will only fall as $\frac{1}{f^2}$. It is thus possible to have a system in which a low Q intermediate mass does not degrade the noise performance above, say, 100Hz.

For example Figure 7.3 shows the displacement noise expected for a single 0.52 metre (0.7Hz) pendulum with a test mass of 1000kg and a Q of 10^8 and compares it with that expected for a double pendulum system with identical lower stage and an upper stage of length 0.52 metre, mass 1000kg and a Q of 1. Below 100Hz the noise in the double pendulum case is much worse than the single pendulum but above 100Hz the two noise levels are virtually identical. Figure 7.4 shows the seismic isolation achieved by the two systems. The transfer function of movement of the suspension point to movement of the test mass of the double pendulum is falling as $\frac{1}{f^3}$ above a few Hertz. This happens because the assumption that $f_0 Q \gg f$ no longer holds for the well damped pendulum. It, therefore, only contributes a $\frac{1}{f}$ term to the transfer function. In the example used here this results in a loss of a factor of ~ 40 in the isolation from seismic noise at 100Hz. However the upper pendulum is more highly damped than is likely in a real system: the loss in isolation can easily be reduced by increasing the Q of the first stage to a more realistic value of >100 . For a suspension system designed to work at 10Hz the constraints on the Q of the upper stage are more stringent. In the example above the Q of the upper stage would have to be $> 10^4$ to keep the noise level the same as in the case of the single pendulum.

The use of a relatively highly damped first stage greatly reduces the peaks in the transfer function that are present when both pendulums are of high Q. This means that these resonances are much less easily excited to large amplitude oscillations and the amplitude of the oscillations will have a much faster decay time. This

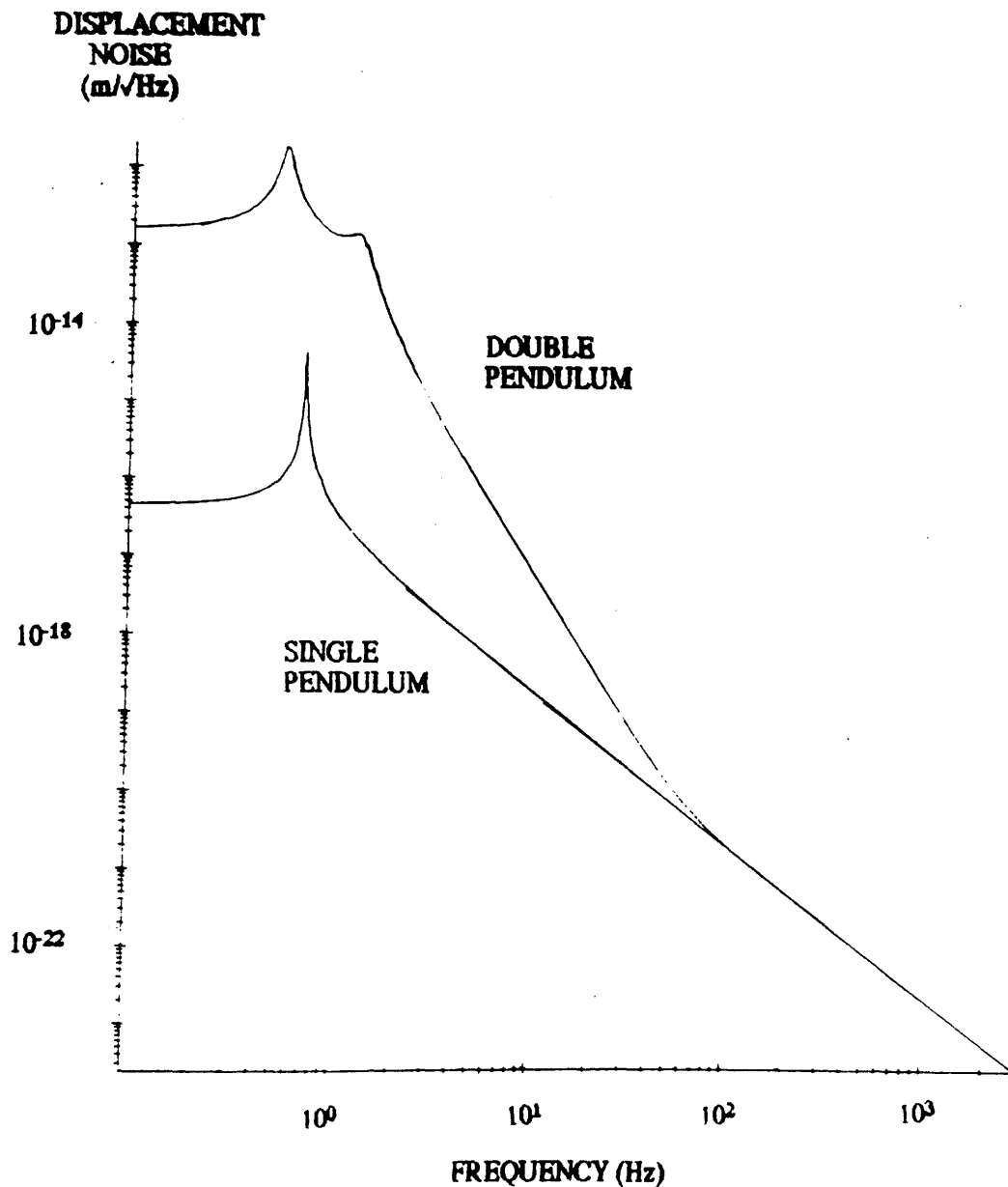


Figure 7.3: The thermal noise spectra for a single high Q pendulum and for a double pendulum with only the lower stage of high Q . Above 100 Hz the two graphs are identical. The peak at 1 Hz in the single pendulum graph has been truncated for clarity; it should rise to $3.5 \times 10^{-9} \text{ m}/\sqrt{\text{Hz}}$

TRANSFER
FUNCTION

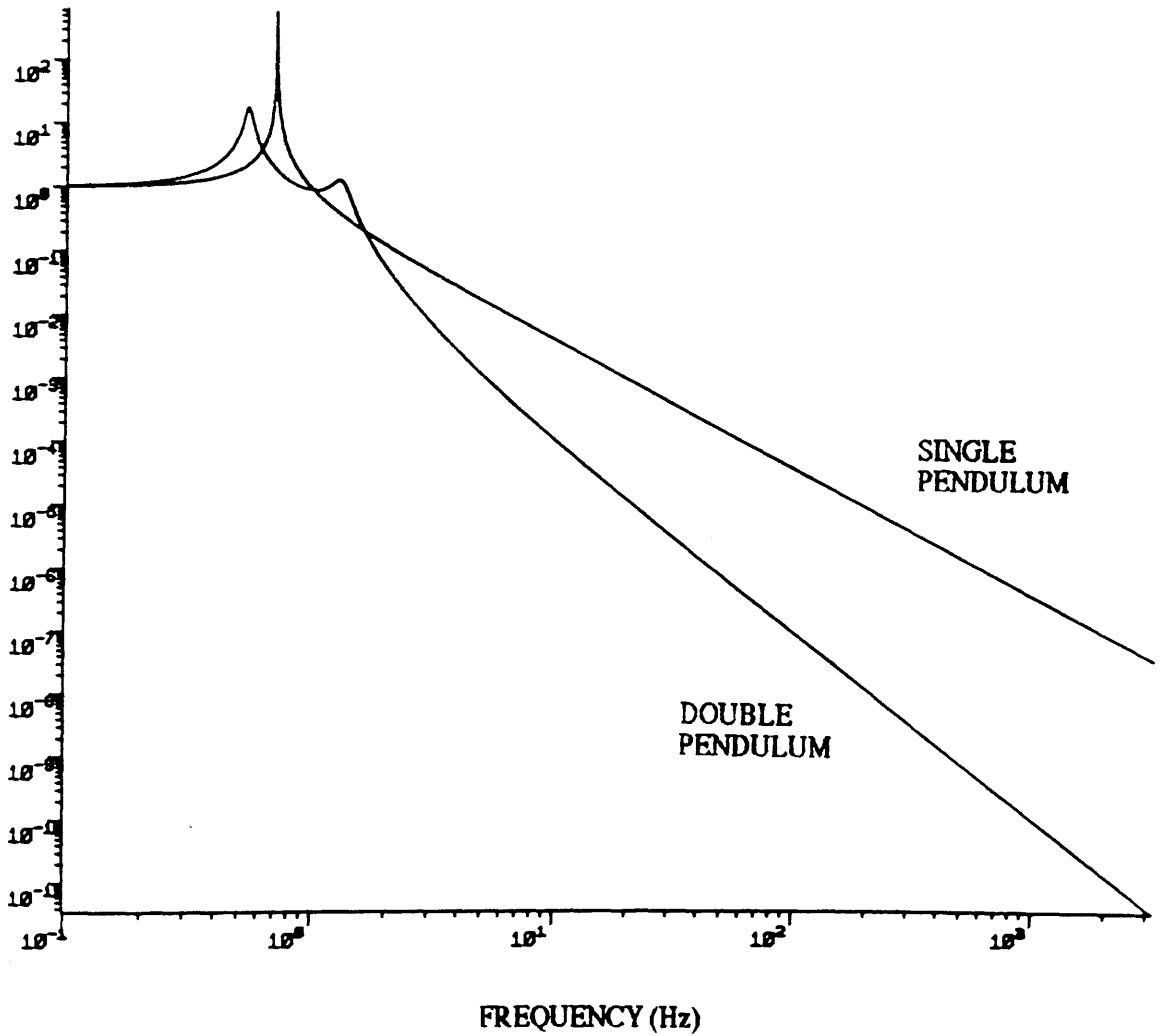


Figure 7.4: The transfer function for a single high Q pendulum and a double pendulum with only the lower stage of high Q . The peak at 1 Hz has again been truncated; it should rise to 10^8 . The peaks in the double pendulum graph are well damped.

makes control of the mass somewhat easier since the servo control systems will not have to have the very large dynamic range that would otherwise be required.

7.1.3 Wire Resonances

The preceding work has assumed that the suspension wire was massless and had no effect on the system. In practice there will be 'violin' modes of resonance in these wires. To give some idea of how the wire resonances might affect the system the simple pendulum model was compared with a model which took account of travelling waves in the suspension wire. The suspension was taken as a single length of steel piano wire loaded to a quarter of its breaking stress. This gave a wave velocity (v_w) in the wire of 310ms^{-1} independent of the load. The transfer function was calculated for an undamped system (Equation 7.8) with $k' = \frac{2\pi f}{v_w}$.

$$\frac{x_1}{x_0} = \frac{1}{\cos k'l - \frac{2\pi f}{v_w g} \sin k'l} \quad (7.8)$$

At low frequencies the two models gave exactly the same behaviour but at frequencies approaching $\frac{v_w}{2l}$ the effect of the first wire resonance becomes apparent (Figure 7.5). This produces peaks in the transfer function at multiples of $\frac{v_w}{2l}$ Hz and above the first wire resonance the transfer function falls only as $\frac{1}{f}$. The noise function for the 'wire resonance' model was also calculated (Equation 7.9). It assumes that the damping and noise force act on the mass and that the point of suspension is rigid.

$$\text{Displacement Noise} = \frac{\frac{\bar{F}_n}{m(2\pi)^2}}{f^2 - j \frac{f f_0}{Q} - \frac{g f}{2\pi v_w} \frac{\cos k'l}{\sin k'l}} \quad \frac{\text{m}/\sqrt{\text{Hz}}}{\text{m}/\sqrt{\text{Hz}}} \quad (7.9)$$

The two noise functions are the same except that there are very narrow peaks of noise at the resonant frequencies of the wire. These peaks are a factor of $\frac{fQ}{f_0}$ above the noise expected from the single pendulum.

The example used here is rather extreme since the masses in a real system are likely to be suspended by at least two wires. The wires will not act identically

TRANSFER
FUNCTION

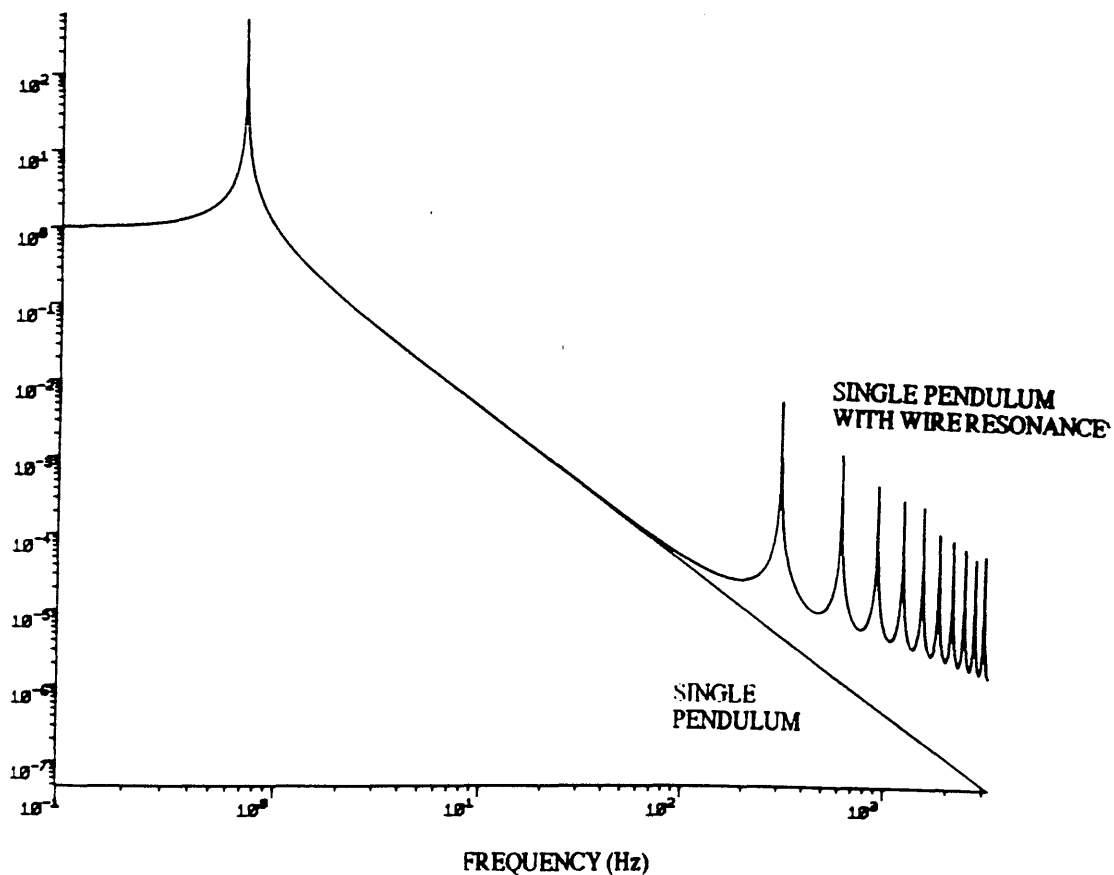


Figure 7.5: *The transfer function for single pendulum and single pendulum with wire resonances. All the peaks have been truncated. The wire resonance model only gives a $\frac{1}{f}$ dependence above the first wire resonance.*

in unison, this should reduce the size of the peaks in both the transfer and noise functions.

The results obtained in the earlier sections would be expected to agree with those of the more complicated 'wire resonance' model below the first wire resonant frequency. This should be at several hundred Hertz. If the detector is designed to operate at 100Hz then any loss in isolation above the resonant frequency should not cause any problems. The peaks of thermal and seismic noise caused by the wire resonances might produce some extra noise but this should only occur over very narrow frequency bands.

7.2 Measuring Suspension Quality Factors

When the measurements in this section were made in March 1988 the sensitivity of the prototype detector was limited by an unknown noise source at a level of $1.7 \times 10^{-18} \text{ m}/\sqrt{\text{Hz}}$. One possible source of noise was thermal noise in the suspension systems of the test masses. To eliminate this as a possible noise source the Q of the suspension system of each of the test masses was measured.

7.2.1 End Masses

The position of the end mass of the secondary cavity is controlled by a coil and magnet arrangement. Three magnets are glued to the mass. Each magnet is opposite a coil and the coils are wired in series. This system is normally used to keep the secondary cavity on resonance but it can also be used to measure the motion of the mass.

Movement of the mass will induce a voltage across the coils that is directly proportional to the velocity of the mass. The maximum velocity is directly proportional to the amplitude of the motion and we can thus measure the decay in the amplitude of the oscillation.

The mass was set in motion by briefly sending a current through the coils. The coils were then connected to an amplifier and the output voltage was recorded on a chart recorder. If the ratio of initial to final amplitudes is measured to be R over

a time t then, for a pendulum of natural frequency f_0 , the quality factor of the resonance (Q) is given by $Q = \frac{f_0 \pi t}{\ln(R)}$.

The Q of the secondary end mass was measured to be 160, much lower than expected. This corresponds to a thermal noise level of this mass of $4 \times 10^{-19} \text{m}/\sqrt{\text{Hz}}$ at 1kHz. This noise level was close enough to the displacement noise level of the detector of $1.7 \times 10^{-18} \text{m}/\sqrt{\text{Hz}}$ to be worrying. It was found that the low Q was caused by some damping compound on the suspension wires. When this was removed the Q increased to a value of 5,300. This, unfortunately, did not improve the sensitivity of the detector.

The Q of the other end mass was measured in the same way as that of the secondary cavity end mass. This gave an answer of $Q=2,700$.

The suspension points of all the test masses are mounted on lead/rubber stacks. This improves the seismic isolation but it does mean that the suspension points are not rigid. Energy from the pendulum resonance of the test mass can be transferred into this well damped suspension point. This effect could limit the measured Q even if the true Q , which governs the thermal noise level, was much higher. The measured Q is therefore only a lower limit and the thermal noise level calculated from it will be an upper limit on the actual thermal noise from the suspension system.

Another possible limit to the Q of the suspension is gas damping of the movement of the test mass. For the measurements here the pressure was $4 \times 10^{-3} \text{Torr}$. This pressure would limit the Q to around 500,000 [Ward 1983]. This, obviously, is not a problem at the moment. Another possible limit is given by the coil/magnet arrangement. The coils are driven by a low output impedance amplifier. This means that any voltage induced in the coils by a movement of the mass is effectively shorted to ground through a small resistance. This is a way of extracting energy from the system and thus lowering the Q . To simulate this effect the Q was measured with a 33Ω resistor across the coils (The internal resistance of the coils is 70Ω). This reduced the Q to 2,700. The damping effect of the low output impedance amplifier could easily limit the Q of the suspension system in a large scale detector. It will therefore be necessary to develop high output impedance

amplifiers for use in such a detector.

7.2.2 Centre Masses

The centre masses in both cavities have similar suspension systems which are different from those of the end masses. Each mass has a four wire suspension system that is attached to a cross which is itself suspended (Figure 7.6). The longitudinal position of the mass is controlled by a piezo-electric element (PZT) that acts on the cross.

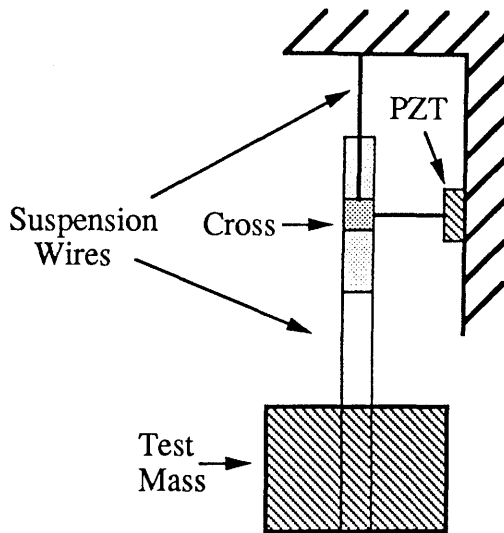


Figure 7.6: *The suspension system of the centre masses*

To measure the Q of this suspension system the mass was first excited by driving the PZT with a ~ 1 Hz sine wave. After a suitable time the drive was disconnected and the voltage across the PZT was recorded. This voltage is directly proportional to the displacement of the mass and so the decay in the amplitude of the oscillation can be measured.

The primary mass had a Q of 6,600 and the secondary had 11,600. The differences in the measured Q 's of the pairs of similarly suspended test masses are probably caused by differences in the rigidity of their suspension points rather than differences in the intrinsic Q 's of the suspension systems.

The PZT's are driven by amplifiers with high output impedance and this, with

the different type of transducer, reduces the effect of electrical resistive damping. Its effect could only be seen in the secondary mass where, with a suitable load resistor, the Q was reduced from 11,600 to 10,600.

7.3 Measurement of the Q of the Test Masses

The measurements in this section were taken in November 1986. At that time the sensitivity of the prototype detector was being limited by some unknown noise source. The test masses were aluminium spheres with one flat face onto which a mirror was glued. It had been found that the sensitivity of the detector depended on the type of glue used. The best sensitivity of $5 \times 10^{-18} \text{m}/\sqrt{\text{Hz}}$ was obtained using cyanoacrylate adhesive. One possible explanation for the noise in the detector was thermal noise from the internal modes of the test masses. To test if this was a problem the Q of the first internal mode of a test mass was measured. A piezoelectric ring (PZT) was glued onto the test mass and the mirror was glued onto the PZT. The electrical impedance of the PZT changes near the resonance of the test mass (Figure 7.7). From this change in impedance the Q of the resonance can be calculated.

In order to calculate the Q from the change in impedance of the PZT the test mass/PZT/mirror combination was modelled and the three parameters (f_0 the resonant frequency, \mathcal{R} the ratio of the energy stored in the mass to that stored in the PZT and the Q of the resonance) adjusted to fit the measured curve. This gave $\mathcal{R} = 975 \pm 25$ and $Q=7,500$.

To check accuracy of the model the ratio \mathcal{R} was calculated independently. This was done using the velocity of sound in the materials and their dimensions. This gave an answer of $\mathcal{R} = 1090$ which agrees well with the value obtained by the above method.

Equation 7.10 gives the thermal displacement noise level expected for a given Q value.

$$\text{Thermal Displacement Noise} = \left(\frac{4kT}{\pi^3 \rho v_s^3 Q} \right)^{\frac{1}{2}} \text{ m}/\sqrt{\text{Hz}} \quad (7.10)$$

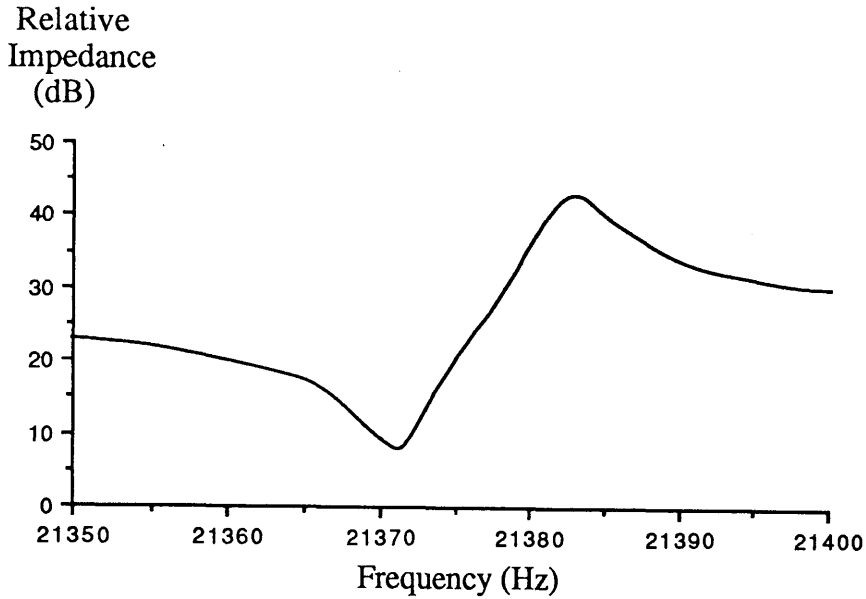


Figure 7.7: *The change in impedance of the PZT near the first acoustic resonance of the test mass.*

Where v_s is the velocity of sound in the test mass and ρ is its density. The equation (7.10) assumes that the first resonant frequency of the test mass is well above the frequency of interest.

The measured Q corresponds to a noise level of $1.9 \times 10^{-20} \text{m}/\sqrt{\text{Hz}}$ which was well below the noise level in the detector at that time of $5 \times 10^{-18} \text{m}/\sqrt{\text{Hz}}$. The aluminium test masses were later replaced by fused silica test masses with mirrors optically contacted onto them. The sensitivity then improved to $1.7 \times 10^{-18} \text{m}/\sqrt{\text{Hz}}$ before again being limited by an unknown noise source. These silica test masses have subsequently been replaced by solid, fused silica test masses with the dielectric mirror coating applied directly onto the test mass.

Appendix A

Circuits

This appendix contains the circuit diagrams of the laser frequency stabilisation system. In the design of the circuits various features such as noise performance and dynamic range have to be considered. In a conditionally stable servo system such as those used here the behaviour of the amplifiers when they saturate can greatly affect the acquisition of lock by the system. To prevent problems with saturation the signal size is limited in various parts of the circuits by diode clipping circuits.

A.1 Diode Clipping

Many operational amplifiers have undesirable characteristics when driven into saturation. For example the OP37 used in the example below (Figure A.1) produces voltage spikes and bursts of oscillation. Other operational amplifiers may, when driven into saturation, stay saturated for much longer than expected from their quoted slew rate. Amplifiers which when driven into saturation have these or other forms of inelegant behaviour can cause problems in a servo system. These problems are most likely to occur when the servo system is trying to acquire lock. The signals then are much larger than when the system is operating normally and saturation of some of the amplifiers is much more likely. The amplifiers may then prevent the system from locking stably. To avoid any such problems in the two circuits here the voltage swing is limited in various ways.

The simplest voltage limiter is two diodes of opposite polarity connected in parallel between the signal and ground (for an example see Figure A.5). This arrangement limits the voltage swing to less than the ($\sim 0.6V$) forward drop of

the diodes. A more adjustable limit can be obtained by using two Zener diodes connected 'back to back' in series (for an example see Figure A.2). The allowed voltage swing is then determined by the breakdown value of the Zener diodes.

These methods of limiting the voltage swing all work well at low frequencies. At higher frequencies the capacity of the diodes can cause undesirable phase shifts in the signal. To avoid this problem the diodes are used in a different way when high frequency signals are present (Figure A.1).

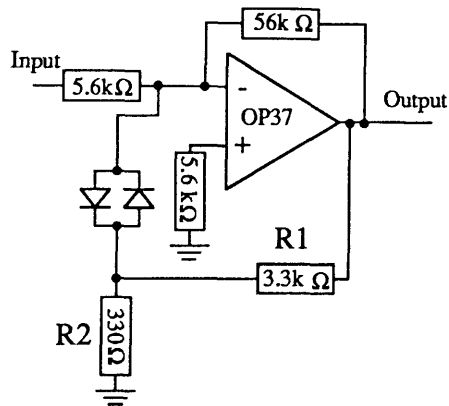


Figure A.1: *The diode clipping circuit used to modify the behaviour of some of the the feedback amplifiers in the servo systems.*

For small output voltages this circuit acts as a normal inverting amplifier with a gain of ten: all the feedback is done by the $56\text{k}\Omega$ resistor. The diodes will start conducting when the voltage across them is greater than about 0.6V . This happens when the output voltage exceeds a threshold set by the values of $R1$ and $R2$. In the case here the threshold is around 6V , an input of 0.6V . As the input voltage rises above this level the feedback is dominated by $R1$ and the diodes. This progressively reduces the gain of the amplifier as the signal amplitude increases above the threshold level: an input signal of 1V will produce an output of 5.8V , a 4V input will produce a 8.4V output. This progressive reduction of the gain greatly reduces the likelihood of the amplifier saturating in the unpleasant way described above.

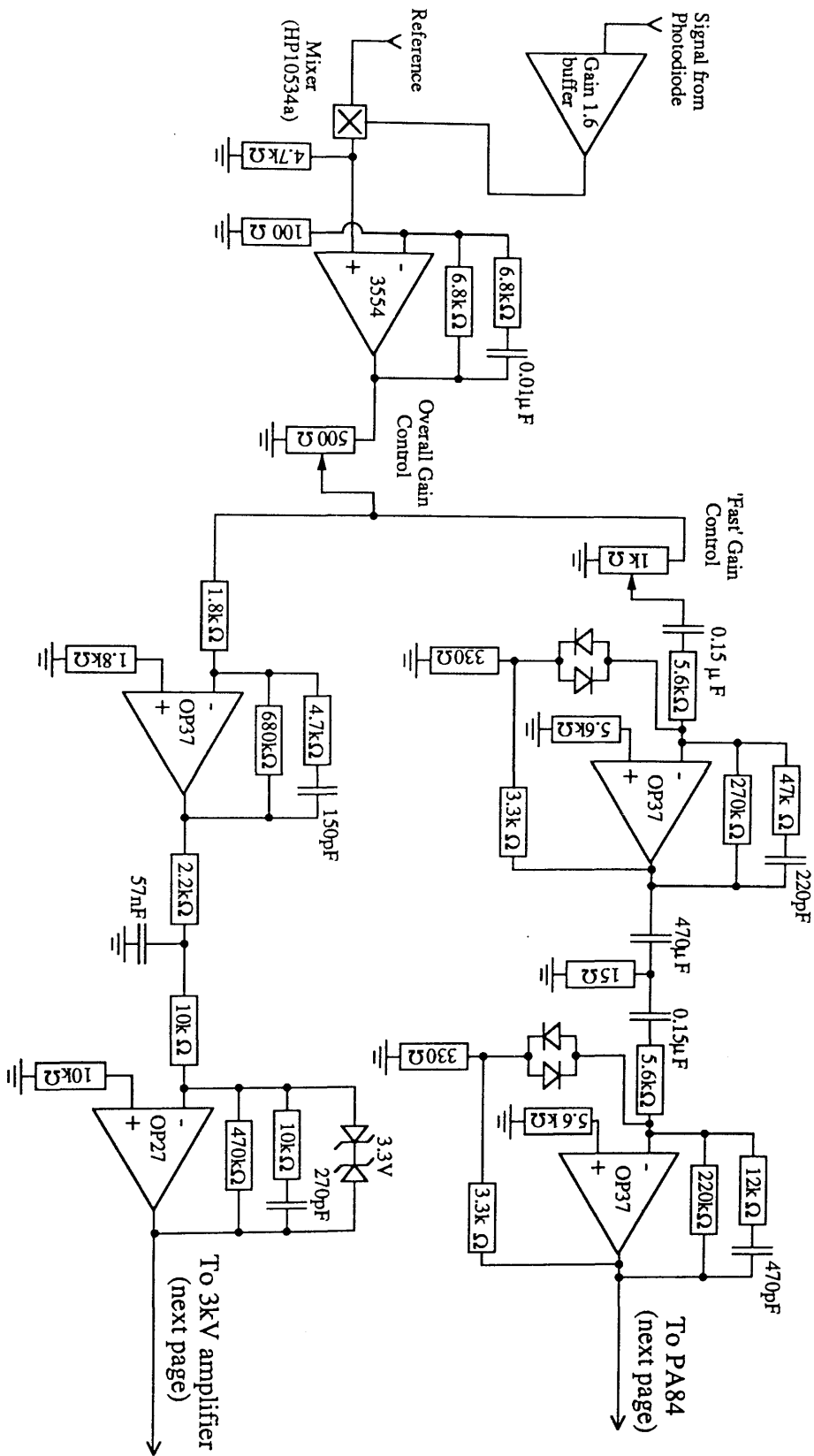


Figure A.2: The circuit diagram of the first part of first servo loop (continued on next page).

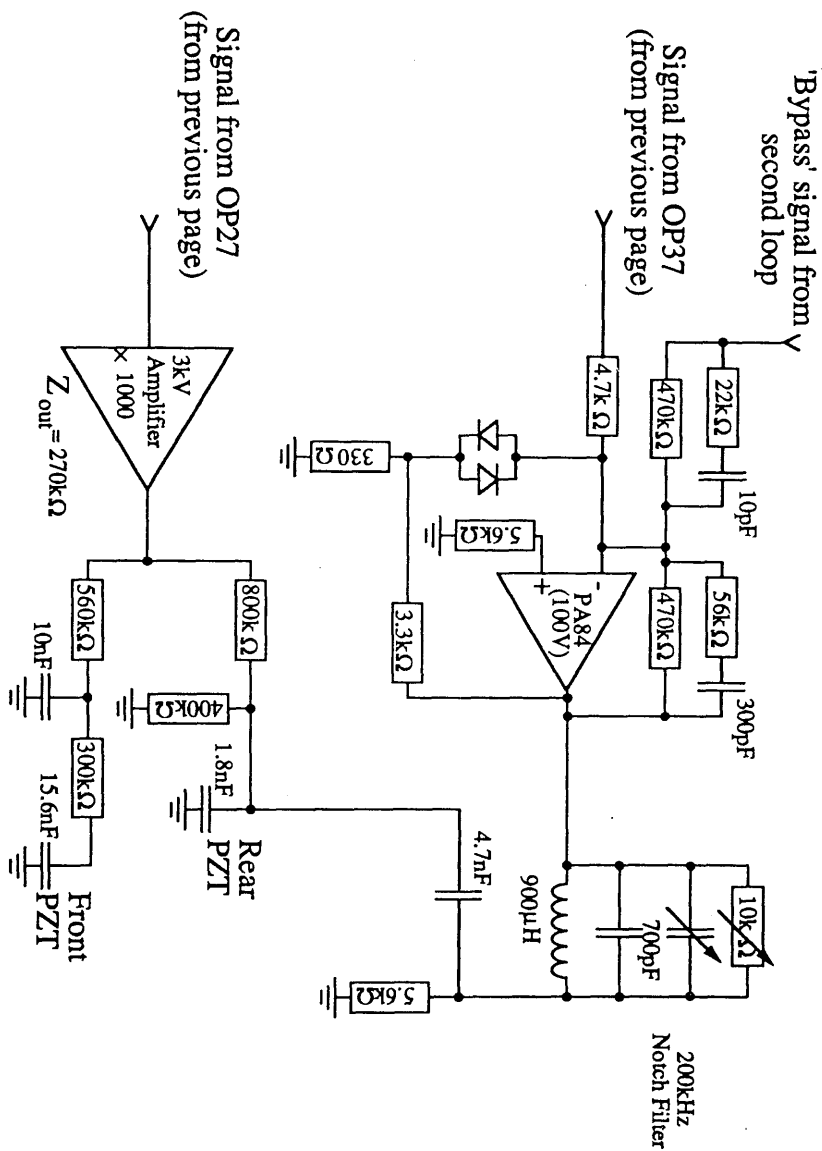


Figure A.3: The circuit diagram of the second part of the first servo loop (continued from the previous page).

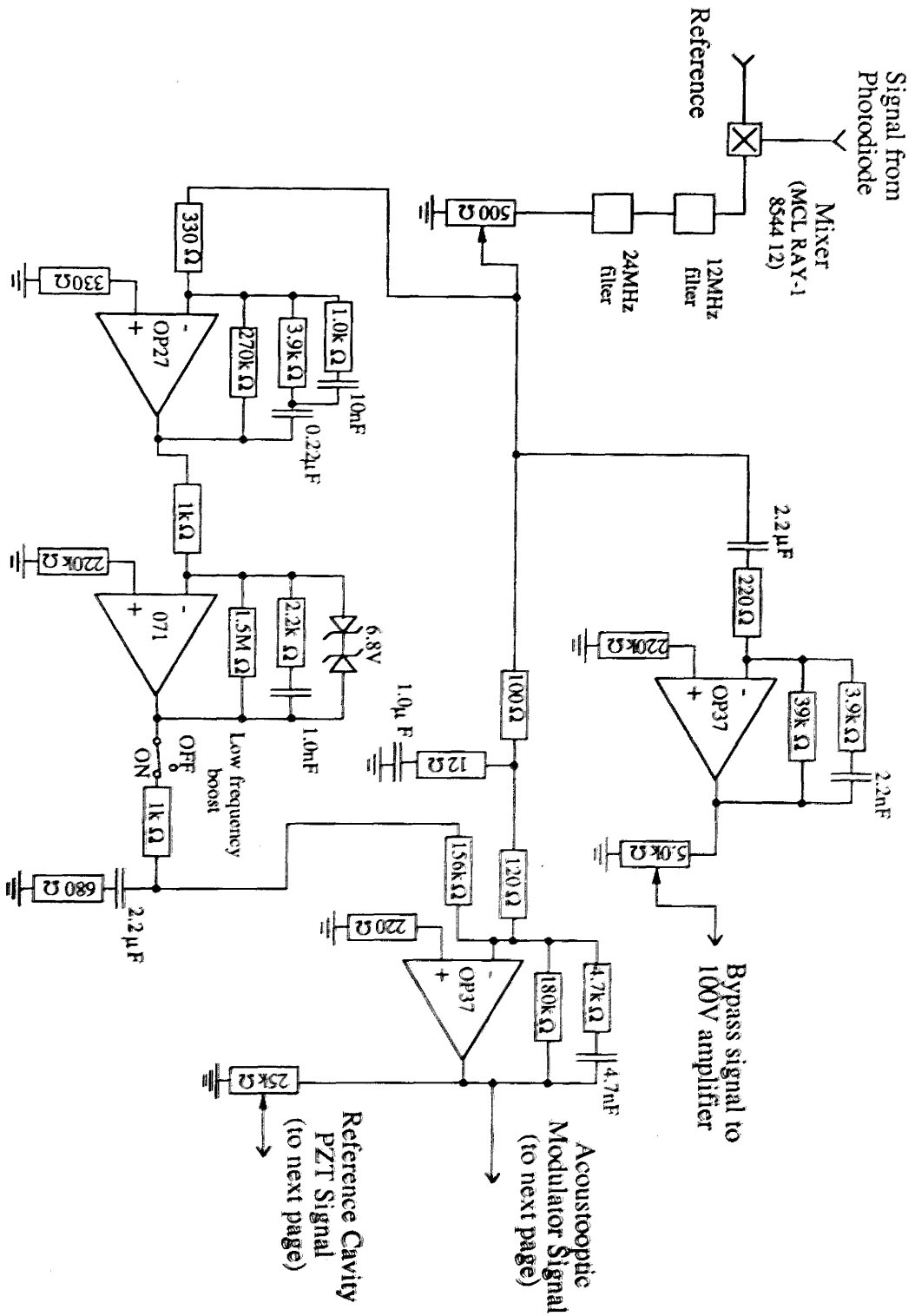


Figure A.4: The circuit diagram of the first part of second loop (continued on next page).

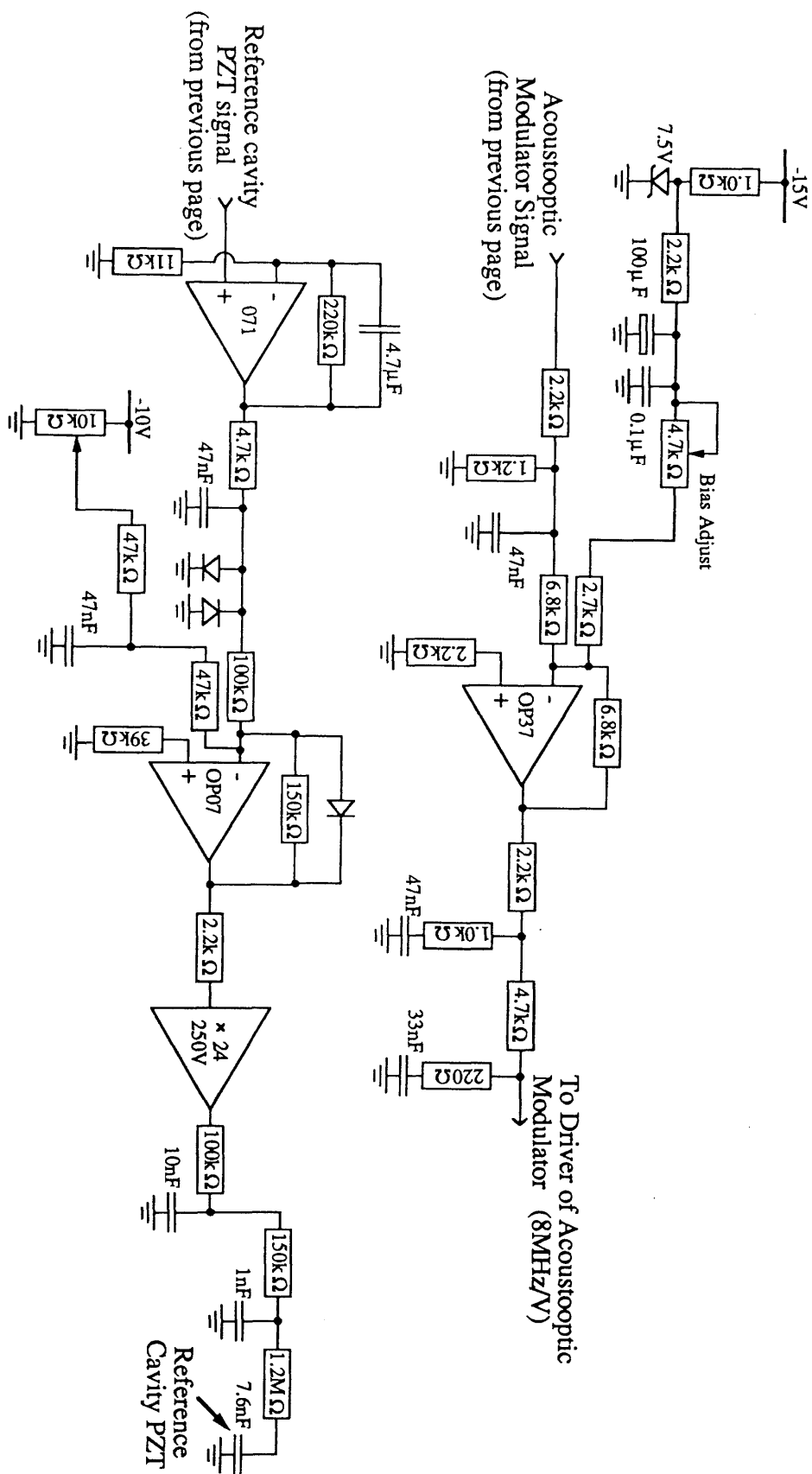


Figure A.5: The circuit diagram of the second part of the second servo loop (continued from the previous page).

Appendix B

Intensity Noise Measurements in some Large Frame Argon Ion Lasers

In the prototype detector at Glasgow the laser is frequency locked to an optical cavity using the RF reflection locking technique. The noise characteristics of the laser, the amount of light power used in the locking scheme and the loop gain of the servo system will determine how accurately the two are locked together. An important assumption in the scheme is that the frequency noise of the laser at the modulation frequency is less than the shot noise limit to frequency fluctuations in the detected light. If this condition does not hold then the ultimate stability of lock that can be achieved will depend on the frequency noise of the laser at the modulation frequency. It is therefore important to ensure that laser frequency noise above, say, 7MHz is low enough to avoid any problems.

The argon ion laser used to illuminate the prototype detector (a Spectra-Physics 171) is a discontinued model and will eventually have to be replaced. We therefore wanted to get some measure of the high frequency frequency noise of it and other large frame argon ion lasers. From previous experience we know that the frequency and intensity noise of argon ion lasers arise from the same processes and that the level of intensity noise is a good indicator of the level of frequency noise. Intensity measurements are also considerably less complicated than frequency ones. An intensity noise measuring system was built to test the intensity noise level of various different lasers. The lasers were installed in different buildings and it was therefore important to have an easily portable system.

The intensity noise was measured using a reverse-biased, low capacity photodiode which had a $1k\Omega$ load resistor. The signal, suitably amplified, was measured on an RF spectrum analyser. With this system shot noise in 6mA of photocurrent was at least 7dB clear of noise in the measuring system up to 7MHz.

The lasers tested were the Spectra-Physics 171, a Coherent CR18 (fitted with an 18W Innova tube) and a Spectra-Physics 2035. The intensity noise of each of these lasers was measured over a frequency span of some MHz.

All the lasers were running with a rear prism/mirror arrangement so that they lased only in the green ($\lambda = 514\text{nm}$). None had an etalon in and so all were running multi-longitudinal mode.

In some cases the lasers were running transverse modes other than TEM_{00} . This produced large, broad peaks in the intensity noise spectrum. These peaks could appear at frequencies below 4MHz but the most persistent ones were around 15–18MHz. In these cases the diameter of the laser aperture was reduced until these peaks were no longer present. This did not necessarily mean that the lasers were not running some ‘illegal’ transverse modes but it was found that their possible presence did not affect the results obtained in the 7MHz frequency span.

Measurements were taken in the following states

- | | |
|---------------|---|
| Spectra 171 | 28A laser current, 4W output power reduced to 2.4W
by closing the aperture to eliminate extra modes. |
| Coherent CR18 | 42A laser current, 4W output power reduced to 2.2W
by closing the aperture to eliminate extra modes. |
| Spectra 2035 | 26A laser current, 4W output power. |

In each case light was split from the main beam by reflection from a glass microscope slide and the intensity reduced by further reflections or neutral density filters so that in each case the light entering the photodiode was 30mW - giving 6mA photocurrent.

The results are shown in Figure B.1. It can be easily seen that the newer lasers (Coherent CR18 and Spectra-Physics 2035) are much noisier than the older

INTENSITY
NOISE
 $\Delta I / I (\sqrt{\text{Hz}})$

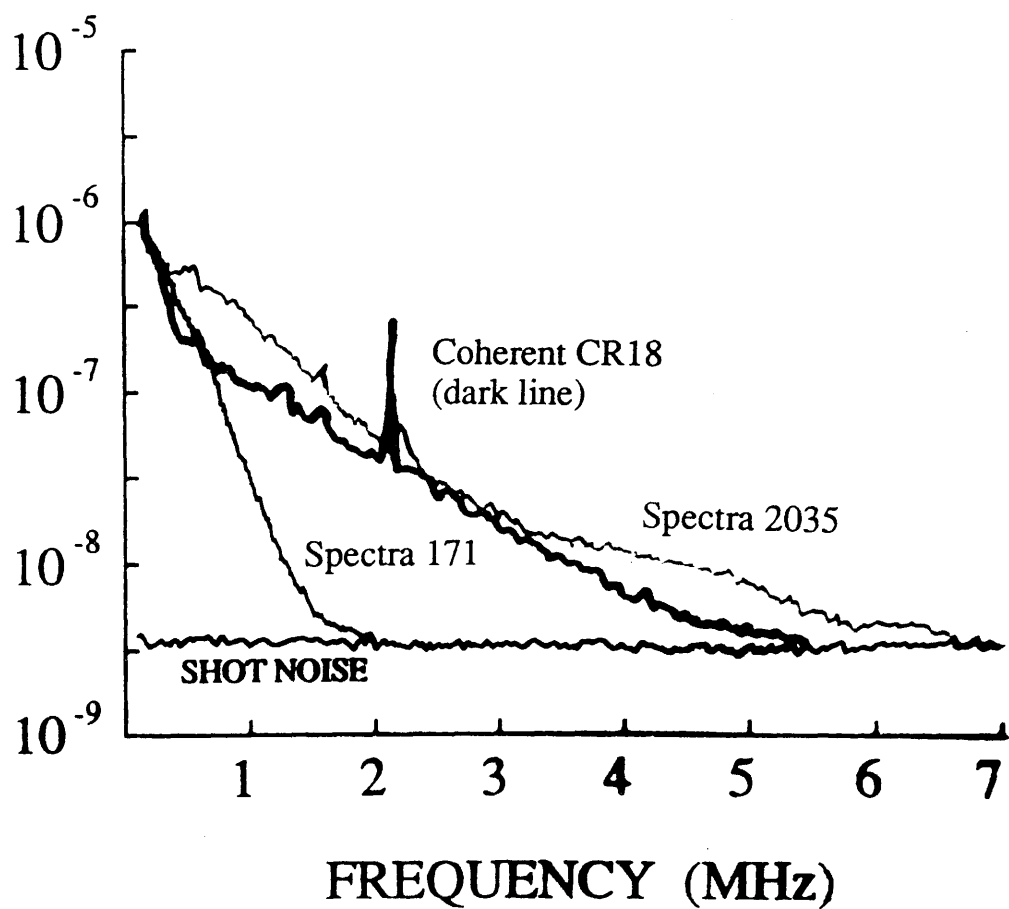


Figure B.1: A graph of intensity noise against frequency for the three lasers mentioned in the text.

Spectra-Physics 171 in the range 1-7MHz, with the Spectra-Physics 2035 being generally noisier than the Coherent over most of the frequency span. The Coherent has a peak in its noise spectrum at 2.1MHz, this peak occasionally disappeared or greatly reduced in height. Another peak at 1.8MHz was occasionally seen. Both of these effects happened on timescales of less than 10ms and occurred at a rate of once every few seconds. There seemed to be no correlation between the appearance of the 1.8MHz peak and the disappearance of the 2.1MHz peak. A similar effect may have been seen in the Spectra-Physics 2035 but at a much lower level. No such effect was seen in the Spectra-Physics 171. These peaks were unlike those caused by extra transverse modes and are likely to be caused by instabilities in the laser plasma.

In the Spectra-Physics 2035 the intensity noise was amplitude modulated at 100Hz, similar effects were seen in the Coherent CR18 but at a much lower level and no such effect was seen in the Spectra-Physics 171. This modulation is an undesirable effect; it is probably associated with the cathode heater in the laser which is driven by a 50Hz current. It should be possible to eliminate the modulation by using a DC current source to heat the cathode [Schilling].

Appendix C

Two Data Analysis Programs

This appendix contains two of the programs used in the Data Analysis chapter. The programs are those used to produce the pulse height graph (Figure 6.5) and the coherence graph between the seismometer signal and the output of the detector. The programs are written in Microsoft FORTRAN(4.1). They are both described in the Data Analysis chapter.

Pulse Height Statistics

This program is described in section 6.5.1. The function SECSTAT and the sub-routines such as GTMICR were written by Norman Mackenzie.

```

PROGRAM BNDPASP
C -to bandpass and histogram the sec. error point data from the
C -16 mins of data on the hard disk
  DIMENSION IHISTS[FAR](8,0:450), IHISTD[FAR](8,0:450), RDAT(1024)
  +, JHISTS[FAR](8,0:450), JHISTD[FAR](8,0:450)
  DIMENSION SCALED[FAR](32768)
  INTEGER*1 INDATA(32768)
  LOGICAL EOTAPE, SPLIT
  CHARACTER*11 FNAMES, FNAMED
  COMMON NBLKS, SPLIT, EOTAPE, LAME, INDATA, KOUNT, IDEAD
C -open data file
  OPEN(7, FILE='COPYC12.TSB', ACCESS='DIRECT', RECL=32768)
C -open output file for non-normalised data (Static)
  OPEN(9, FILE='BDPASS.DSC', ACCESS='SEQUENTIAL',
  +   FORM='FORMATTED')
C -open output file for normalised data (Dynamic)
  OPEN(19, FILE='BDPASP.DSC', ACCESS='SEQUENTIAL',
  +   FORM='FORMATTED')
  CALL GETTIM(IH1, IM1, ISE1, I100TH)
  KOUNT=0
  EOTAPE=.FALSE.
  ITHRESHS=175
  WRITE(9,*) 'Threshold set at', ITHRESHS
  ITHRESHD=175
  WRITE(19,*) 'Threshold set at', ITHRESHD
C -set dead time (number of blocks ignored after the veto signal)
  IDEAD=100
  WRITE(9,*) 'Dead time set at', IDEAD, ' Blocks'
  WRITE(19,*) 'Dead time set at', IDEAD, ' Blocks'
  FNAMES='HISTS00.DSC'
  FNAMED='HISTD00.DSC'
C -zero overall accumulators
  DO 4 J=1,8
  DO 4 I=0,450
    JHISTS(J,I)=0
    JHISTD(J,I)=0
  4 CONTINUE
C
  DO 60 ILP=0,0
  NSTART=NBLKS
  NTOTAL=0
  DO 5 J=1,8
  DO 5 I=0,450
    IHISTS(J,I)=0
    IHISTD(J,I)=0
  5 CONTINUE
  FNAMES(6:6)=CHAR(48+ILP)
  FNAMED(6:6)=CHAR(48+ILP)
C
  DO 40 ISTEPS=1, 1800*3276/1024
  DO 53 IFILL=0,31
C -get 32k continuous points
  6 CONTINUE
  SPLIT=.FALSE.
  DO 10 I=1,1024
    IF(SPLIT) GOTO 6
    IF(EOTAPE) GOTO 90
    RDAT(I)=SECDAT(1)
C -get the next point
  10 CONTINUE
  NTOTAL=NTOTAL+128
C -bandpass the data between 272*5000/1024 Hz and 400*5000/1024 Hz
  CALL REALFT(RDAT,512,1)
  DO 20 I=1,272
    RDAT(I)=0.0

```

```

20 CONTINUE
  DO 30 I=401,1024
    RDAT(I)=0.0
30 CONTINUE
  CALL REALFT(RDAT,512,-1)
  DO 53 I=1,1024
    SCALED(I+1024*IFILL)=RDAT(I)
53 CONTINUE
C -now have 32k bandpassed data
  SIGMA=0.0
  DO 21 I=1,32768
    SIGMA=SIGMA+SCALED(I)*SCALED(I)
21 CONTINUE
  SIGMA=1.0/SQRT(SIGMA/32768)
C
C  sigma is of order 5.5e+11
C
  DO 40 I=0,4095
    DO 40 KK=1,8
C -normalise the data to a sigma of order 7.0(static) or exactly 7.0(dynamic)
C -and bin it according to energy (amplitude)**2
    RS=SCALED(I*8+KK)*5.2E-5
    RD=SCALED(I*8+KK)*SIGMA
    JS=RS*RS*7.0
    JD=RD*RD*7.0
    IF(JS.GT.450) JS=450
    IF(JD.GT.450) JD=450
    IHISTS(KK,JS)=IHISTS(KK,JS)+1
    IHISTD(KK,JD)=IHISTD(KK,JD)+1
    IF (JS.GE.ITHRESHS) THEN
930  WRITE(6,930) JS,(NBLKS-1)*3276+LAME-32768+I*8+KK,NBLKS-1
      FORMAT(1X'S Size ',I3,', sample ',I9,',Block',I5)
      ENDIF
    IF (JD.GE.ITHRESHD) THEN
931  WRITE(6,931) JD,(NBLKS-1)*3276+LAME-32768+I*8+KK,NBLKS-1
      FORMAT(1X'D Size ',I3,', sample ',I9,',Block',I5)
      ENDIF
40 CONTINUE
90 CONTINUE
  NEND=NBLKS
60 CONTINUE
C -write the output to the appropriate files
C -(with bit for the graphing routines)
  FNAMES='STOTLS0.DSC'
  FNAMED='DTOTLS0.DSC'
  WRITE(9,*)'nend',NEND,' nstart',NSTART
  WRITE(19,*)'nend',NEND,' nstart',NSTART
  DO 52 KK=1,8
    FNAMES(7:7)=CHAR(47+KK)
    FNAMED(7:7)=CHAR(47+KK)
    OPEN(1,FILE=FNAMES,ACCESS='SEQUENTIAL',
+      FORM='FORMATTED')
    OPEN(2,FILE=FNAMED,ACCESS='SEQUENTIAL',
+      FORM='FORMATTED')
    WRITE(1,*) '451'
    WRITE(1,*) '451'
    WRITE(1,*) '451'
    WRITE(1,*) '''AMPLITUDE''',NTOTAL
    WRITE(1,*) '''FREQUENCY'''
    WRITE(2,*) '451'
    WRITE(2,*) '451'
    WRITE(2,*) '451'
    WRITE(2,*) '''AMPLITUDE''',NTOTAL
    WRITE(2,*) '''FREQUENCY'''
    DO 51 I=0,450
      WRITE(1,*) I
      WRITE(2,*) I
      IF (IHISTS(KK,I).EQ.0) THEN
        WRITE(1,*) -1
      ELSE

```

```

        WRITE(1,*) LOG(SQRT(FLOAT(I)+.5)*IHISTS(KK,I))
    ENDIF
    IF (IHISTD(KK,I).EQ.0) THEN
        WRITE(2,*) -1
    ELSE
        WRITE(2,*) LOG(SQRT(FLOAT(I)+.5)*IHISTD(KK,I))
    ENDIF
51  CONTINUE
    CLOSE(1)
    CLOSE(2)
52  CONTINUE
    CALL GETTIM(IH2,IMI2,ISE2,I100TH)
    WRITE(6,905) IH1,IMI1,IH2,IMI2
905  FORMAT(' Program ran from ',I2,':',I2,' to ',I2,':',I2)
    CLOSE(9)
    CLOSE(19)
    STOP
    END
C
    REAL FUNCTION SECDAT(I)
C -this function gets the next point in the time series, reading in new block
C -where appropriate. It discards any block in which one of the veto signals
C -is set and returns SPLIT=.TRUE.
    INTEGER*1 INDATA(32768),DIGITS[FAR](3276),BLK(4)
    INTEGER*2 SECDEF[FAR](3276),SECVIS[FAR](546)
    INTEGER*4 NBLK
    EQUIVALENCE (NBLK,BLK(1))
    LOGICAL GOOD,FILMRK,AVOID,CALIB,VETO,EOTAPE,MANPLS,SPLIT,MISSED
    COMMON NBLKS,SPLIT,EOTAPE,LAME,INDATA,KOUNT,IDEAD
    BLK(3)=0
    BLK(4)=0
    IF(I.EQ.1) THEN
        LAME=LAME+1
        SECDEF=SECDEF(LAME)/16
C -the recorded data is only 12 bit- the 4 least sig. bits do not exist
        IF(LAME.GE.3276) GOTO 10
        RETURN
    ENDIF
    10 CONTINUE
C -read a new block and check for any of the veto signals in it
    READ(7,END=998,ERR=999,IOSTAT=IOERR)INDATA
    BLK(1)=INDATA(32765)
    BLK(2)=INDATA(32766)
    KOUNT=KOUNT+1
    CALL GTMICR(INDATA,SECDEF)
    CALL GTDIGT(INDATA,DIGITS)
    CALL GTSVIS(INDATA,SECVIS)
    AVOID=.FALSE.
    DO 20 I=1,546
        IF(CALIB(DIGITS(I))) THEN
            WRITE(6,*) NBLK,' CALIBRATION'
            WRITE(9,*) NBLK,' CALIBRATION'
            WRITE(19,*) NBLK,' CALIBRATION'
            SPLIT=.TRUE.
            GOTO 10
        ENDIF
        IF(MANPLS(DIGITS(I))) THEN
            WRITE(6,*) NBLK,' MAINS'
            WRITE(9,*) NBLK,' MAINS'
            WRITE(19,*) NBLK,' MAINS'
            SPLIT=.TRUE.
            GOTO 10
        ENDIF
        IF(VETO(DIGITS(I))) THEN
            WRITE(6,*) NBLK,' VETO BOX'
            WRITE(9,*) NBLK,' VETO BOX'
            WRITE(19,*) NBLK,' VETO BOX'
            SPLIT=.TRUE.
            KOUNT=-IDEAD
            GOTO 10
        ENDIF
    END DO

```

```

ENDIF
IF (SECVIS(I).GT.3000) THEN
    WRITE(6,*) NBLK,' SEC VIS'
    WRITE(9,*) NBLK,' SEC VIS'
    WRITE(19,*) NBLK,' SEC VIS'
    SPLIT=.TRUE.
    GOTO 10
ENDIF
20 CONTINUE
DO 21 I=547,3276
IF (CALIB(DIGITS(I))) THEN
    WRITE(6,*) NBLK,' CALIBRATION'
    WRITE(9,*) NBLK,' CALIBRATION'
    WRITE(19,*) NBLK,' CALIBRATION'
    SPLIT=.TRUE.
    GOTO 10
ENDIF
IF (MANPLS(DIGITS(I))) THEN
    WRITE(6,*) NBLK,' MAINS'
    WRITE(9,*) NBLK,' MAINS'
    WRITE(19,*) NBLK,' MAINS'
    SPLIT=.TRUE.
    GOTO 10
ENDIF
IF (VETO(DIGITS(I))) THEN
    WRITE(6,*) NBLK,' VETO BOX'
    WRITE(9,*) NBLK,' VETO BOX'
    WRITE(19,*) NBLK,' VETO BOX'
    KOUNT=-IDEAD
    SPLIT=.TRUE.
    GOTO 10
ENDIF
21 CONTINUE
IF (KOUNT.LE.0) THEN
    WRITE(6,*) NBLK,' Dead time'
    WRITE(9,*) NBLK,' Dead time'
    WRITE(19,*) NBLK,' Dead time'
    GOTO 10
ENDIF
LAME=0
NBLKS=NBLK
RETURN
998 WRITE(6,*) ' end of file'
EOTAPE=.TRUE.
RETURN
999 WRITE(6,*) ' error in reading IOSTAT=',IOSTAT
EOTAPE=.TRUE.
RETURN
END

```

Coherence Function

This program calculates the coherence function between the seismometer signal and the output of the detector. It is described in section 6.6. The program used to calculate the coherence between the microphone signal and the output of the detector was similar but did not include the filtering of the detector signal that was necessary in this case. The function TWODAT is based on SECDAT above.

```
PROGRAM COHERS2
C to test the coherence between the seismometer signal and data
REAL RDAT(1024),MDAT(1024),A(6),DMMY[far](6144),DMMY2[far](1024)
REAL GRR(512),GMM(512),GRMR(512),GRMI(512),CROSS(512)
INTEGER*1 INDATA[FAR](32768)
LOGICAL EOTAPE,SPLIT
COMMON NBLKS,SPLIT,EOTAPE,LAME,INDATA,KOUNT,IDEAD
OPEN(7,FILE='COPYC12.TSB',ACCESS='DIRECT',RECL=32768)
C -the data file
OPEN(1,FILE='COHER.SL2',ACCESS='SEQUENTIAL')
OPEN(3,FILE='FBACK.SL2',ACCESS='SEQUENTIAL')
OPEN(4,FILE='SEIS.SL2',ACCESS='SEQUENTIAL')
OPEN(9,FILE='BUMF.SL2',ACCESS='SEQUENTIAL')
CALL GETTIM(IH1,IMI1,ISE1,I100TH)
KOUNT=0
IACC=0
EOTAPE=.FALSE.
IDEAD=100
C -used for dead time count
WRITE(6,*) 'Dead time set at',IDEAD,' Blocks'
CALL TWODAT(2,A,B)
C -initialise twodat
C NAVE -number of spectra to average
WRITE(6,*) 'How many averages?'
READ(6,*) NAVE
WRITE(6,*) NAVE,' Averages'
C -zero accumulators
DO 10 I=1,512
  GRR(I)=0.0
  GMM(I)=0.0
  GRMR(I)=0.0
  GRMI(I)=0.0
10 CONTINUE
  NSTART=NBLKS
  NTOTAL=0
C
  DO 50 IAVE=1,NAVE
20 CONTINUE
  SPLIT=.FALSE.
C -fill arrays
  DO 30 I=1,1024
    IF(SPLIT) GOTO 20
    IF(EOTAPE) GOTO 51
    CALL TWODAT(1,A,B)
    DO 25 IK=1,6
      DMMY((I-1)*6+IK)=A(IK)
25 CONTINUE
    MDAT(I)=B
30 CONTINUE
C -now have two data sets,each continuous and from the same time space
```

```

C -time to bandpass the detector data
  DO 34 IK=0,5
    DO 31 IKK=1,1024
      DMMY2(IKK)=DMMY(IK*1024+IKK)
31    CONTINUE
      CALL REALFT(DMMY2,512,1)
      DO 32 IKK=171,1024
        DMMY2(IKK)=0.0
32    CONTINUE
      CALL REALFT(DMMY2,512,-1)
      DO 33 IKK=1,1024
        DMMY(IK*1024+IKK)=DMMY2(IKK)
33    CONTINUE
34    CONTINUE
C now have bandpassed time series, 6* oversampled in DMMY
  DO 35 IK=1,1024
    RDAT(IK)=DMMY(IK*6-3)
35  CONTINUE
C all should now be well (give or take end effects)
  IACC=IACC+1
  CALL REALFT(RDAT,512,1)
  CALL REALFT(MDAT,512,1)
C for each frequency bin calculate
  DO 40 I=1,512
    GRR(I)=RDAT(2*I-1)*RDAT(2*I-1)+RDAT(2*I)*RDAT(2*I)+GRR(I)
    GMM(I)=MDAT(2*I-1)*MDAT(2*I-1)+MDAT(2*I)*MDAT(2*I)+GMM(I)
    GRMR(I)=GRMR(I)+RDAT(2*I-1)*MDAT(2*I-1)+RDAT(2*I)*MDAT(2*I)
    GRMI(I)=GRMI(I)+RDAT(2*I)*MDAT(2*I-1)-RDAT(2*I-1)*MDAT(2*I)
40  CONTINUE
50  CONTINUE
51  CONTINUE
C -calculate the coherence function for each frequency bin
  DO 60 I=1,512
    CROSS(I)=GRMR(I)*GRMR(I)+GRMI(I)*GRMI(I)
60  CONTINUE
C
  WRITE(1,*) '514'
  WRITE(1,*) '514'
  WRITE(1,*) '514'
  WRITE(1,*) 'FREQUENCY',IACC
  WRITE(1,*) 'COHERENCE'
C -to set the correct limits for the coherence fn graph
  WRITE(1,*) '-2.0'
  WRITE(1,*) '1.0'
  WRITE(1,*) '-1.0'
  WRITE(1,*) '0.0'
C
  WRITE(3,*) '512'
  WRITE(3,*) '512'
  WRITE(3,*) '512'
  WRITE(3,*) 'FREQUENCY',IACC
  WRITE(3,*) 'amplitude(dB) feedback'
C
  WRITE(4,*) '512'
  WRITE(4,*) '512'
  WRITE(4,*) '512'
  WRITE(4,*) 'FREQUENCY',IACC
  WRITE(4,*) 'amplitude(dB)seis'
C
  DO 70 I=1,512
    WRITE(1,*) (I-1)*1.627604
    WRITE(1,*) CROSS(I)/(GRR(I)*GMM(I))
70  CONTINUE
  NEND=NBLKS
  WRITE(6,*) ' nstart',NSTART,' nend',NEND
  CALL GETTIM(IH2,IMI2,ISE2,I100TH)
  WRITE(6,905) IH1,IMI1,IH2,IMI2
905  FORMAT(' Program ran from ',I2,',',I2,' to ',I2,',',I2)
  CLOSE(1)
  CLOSE(3)
  CLOSE(4)

```

```

CLOSE(7)
CLOSE(9)
STOP
END

```

```

SUBROUTINE TWODAT(N,A,B)

```

```

C -returns the sec. feedback signal (A(6)) and the seismometer signal B
C -making sure that no veto signals are set and SPLIT=.TRUE. if the data
C -is not continuous in time

```

```

      INTEGER*1 INDATA[FAR](32768),DIGITS[FAR](3276),BLK(4)
      INTEGER*2 SECDEF[FAR](3276),SECVIS[FAR](546),MICR[FAR](3276)
      INTEGER*4 NBLK
      EQUIVALENCE (NBLK,BLK(1))
      REAL A(6)
      LOGICAL GOOD,FILMRK,AVOID,CALIB,VETO,EOTAPE,MANPLS,SPLIT,MISSED
      COMMON NBLKS,SPLIT,EOTAPE,LAME,INDATA,KOUNT,IDEAD
      BLK(3)=0
      BLK(4)=0
      IF(N.EQ.1) THEN
        LAME=LAME+1
        DO 8 I=1,6
          A(I)=SECDEF(6*(LAME-1)+I)/16
        8 CONTINUE
        B=MICR(LAME)/16
        IF(LAME.GE.546) GOTO 10
        RETURN
      ENDIF
    10 CONTINUE
      READ(7,END=998,ERR=999,IOSTAT=IOERR)INDATA
      BLK(1)=INDATA(32765)
      BLK(2)=INDATA(32766)
      KOUNT=KOUNT+1
      CALL GTSFED(INDATA,SECDEF)
      CALL GTSEIS(INDATA,MICR)
      CALL GTDIGT(INDATA,DIGITS)
      CALL GTSVIS(INDATA,SECVIS)
      AVOID=.FALSE.
      DO 20 I=1,546
        IF(CALIB(DIGITS(I))) THEN
          WRITE(6,*) NBLK,' CALIBRATION'
          WRITE(9,*) NBLK,' CALIBRATION'
          SPLIT=.TRUE.
          GOTO 10
        ENDIF
        IF(MANPLS(DIGITS(I))) THEN
          WRITE(6,*) NBLK,' MAINS'
          WRITE(9,*) NBLK,' MAINS'
          SPLIT=.TRUE.
          GOTO 10
        ENDIF
        IF(VETO(DIGITS(I))) THEN
          WRITE(6,*) NBLK,' VETO BOX'
          WRITE(9,*) NBLK,' VETO BOX'
          SPLIT=.TRUE.
          KOUNT=-IDEAD
          GOTO 10
        ENDIF
        IF(SECVIS(I).GT.3000) THEN
          WRITE(6,*) NBLK,' SEC VIS'
          WRITE(9,*) NBLK,' SEC VIS'
          SPLIT=.TRUE.
          GOTO 10
        ENDIF
    20 CONTINUE

```

```

DO 21 I=547,3276
IF(CALIB(DIGITS(I))) THEN
    WRITE(6,*) NBLK,' CALIBRATION'
    WRITE(9,*) NBLK,' CALIBRATION'
    SPLIT=.TRUE.
    GOTO 10
ENDIF
IF(MANPLS(DIGITS(I))) THEN
    WRITE(6,*) NBLK,' MAINS'
    WRITE(9,*) NBLK,' MAINS'
    SPLIT=.TRUE.
    GOTO 10
ENDIF
IF(VETO(DIGITS(I))) THEN
    WRITE(6,*) NBLK,' VETO BOX'
    WRITE(9,*) NBLK,' VETO BOX'
    KOUNT=-IDEAD
    SPLIT=.TRUE.
    GOTO 10
ENDIF
21 CONTINUE
IF (KOUNT.LE.0) THEN
    WRITE(6,*) NBLK,' Dead time'
    WRITE(9,*) NBLK,' Dead time'
    GOTO 10
ENDIF
LAME=0
NBLKS=NBLK
RETURN
998 WRITE(6,*)' end of file'
EOTAPE=.TRUE.
RETURN
999 WRITE(6,*)' error in reading IOSTAT=',IOSTAT
EOTAPE=.TRUE.
RETURN
END

```


References

Allen 1988

B. Allen. Stochastic gravity-wave background in inflationary universe models. *Physical Review D*, 37(8):2078 – 2085, 1988.

Anderson *et al.* 1984

Dana Z. Anderson, Josef C. Frisch and Carl S. Masser. Mirror reflectometer based on optical cavity decay time. *Applied Optics*, 23(8):1238 – 1245, 1984.

Baer *et al.* 1980

T. Baer, F. V. Kowalski and J. L. Hall. Frequency stabilisation of a 0.633 μ m He-Ne longitudinal Zeeman laser. *Applied Optics*, 19(18):3173–3177, 1980.

Blackman and Tukey 1959

R. B. Blackman and J. W. Tukey. *The Measurement of Power Spectra*. Constable and Company, Ltd, London, 1959.

Blair 1990

D. Blair, editor. *The Detection of Gravitational Radiation*. Cambridge University Press, Cambridge, England, 1990. (in press).

Blair *et al.* 1989

D. Blair, J. Ferreira, P. Veitch, R. J. Sandeman, H. A. Bachor, D. McClelland and A. Wrightson. Proposal for the Australian International Gravitational Observatory, 1989.

Brillet 1986

A. Brillet. CNRS Orsay. Private communication, 1986.

Caves 1980

C. M. Caves. Quantum-mechanical radiation-pressure fluctuations in an interferometer. *Physical Review Letters*, 45:75 – 79, 1980.

Caves *et al.* 1980

C. M. Caves, K. S. Thorne, R. W. P. Drever, V. D. Sandberg and M. Zimmerman. On the measurement of a weak classical force coupled to a quantum-mechanical oscillator. I. Issues of principle. *Reviews of Modern Physics*, 52(2):341, 1980.

Chandrasekhar 1970

S. Chandrasekhar. Solutions of two problems in the theory of gravitational radiation. *Physical Review Letters*, 24(11):611, 1970.

DelFabbro *et al.* 1988

R. Del Fabbro, A. Di Virgilio, A. Giazotto, H. Kautzky, V. Montelatici and D. Passuello. First results from the Pisa seismic noise superattenuator for low frequency gravitational wave detection. *Physics Letters A*, 132(5):237 – 240, October 1988.

Drever *et al.* 1983a

R. W. P. Drever, J. L. Hall, F. V. Kowalski, J. Hough, G. M. Ford, A. J. Munley and H. Ward. Laser phase and frequency stabilisation using an optical resonator. *Applied Physics B*, 31:97 – 105, 1983.

Drever *et al.* 1983b

R. W. P. Drever, J. Hough, A. J. Munley, S. A. Lee, R. Spero, S. E. Whitcomb, H. Ward, G. M. Ford, M. Hereld, N. A. Robertson, G. Kerr, J. R. Pugh, G. P. Newton, B. Meers, E. D. Brooks III and Y. Gursel. Gravitational wave detectors using laser interferometers and optical cavities: Ideas, principles and prospects. In P. Meystre and M. O. Scully, editors, *Quantum Optics, Experimental Gravitation, and Measurement Theory*. Plenum Press, 1983.

Einstein 1916

A. Einstein. *Sitzungsber Preuss. Akad. Wiss.*, page 688, 1916.

Forward 1978

R. L. Forward. Wideband laser-interferometer gravitational radiation experiment. *Physical Review D*, 17(2):379, 1978.

Friedman and Schutz 1978

J. L. Friedman and B. Schutz. Secular Instability of Rotating Newtonian Stars. *Astrophysical Journal*, 222:281 – 296, 1978.

GeaBanacloche and Leuchs 1990

J. Gea-Banacloche and G. Leuchs. Use of squeezed states in interferometric gravitational wave detectors. In Blair [Blair 1990]. (in press).

Giazotto *et al.* 1989

A. Giazotto, A. Brillet and colleagues. The VIRGO Project, 1989.

Hackel *et al.* 1977

L. A. Hackel, R. P. Hackel and S. Ezekiel. Molecular beam stabilized multiwatt argon lasers. *Metrologia*, 13:141 – 143, 1977.

Hall and Hänsch 1984

J. L. Hall and T. W. Hänsch. External dye-laser frequency stabilizer. *Optics Letters*, 9(11):502 – 504, 1984.

Hall *et al.* 1977

J. L. Hall, H. P. Layer and R. D. Deslattes. An acoustooptic frequency and intensity control system for cw lasers. *IEEE Journal of Quantum Electronics*, 13:45D – 46D, 1977.

Hänsch and Couillaud 1980

T. W. Hänsch and B. Couillaud. Laser frequency stabilisation by polarisation spectroscopy of a reflecting reference cavity. *Optics Communications*, 35(3):441 – 444, 1980.

Hereld 1984

M. Hereld. *A search for gravitational radiation from PSR1937 + 214*. PhD thesis, California Institute of Technology, 1984.

Hewlett Packard

Hewlett Packard. *Measuring the coherence function with the HP 3582A spectrum analyser*. Application Note 245-2.

Hough *et al.* 1986

J. Hough, B. J. Meers, G. P. Newton, N. A. Robertson, H. Ward, B. F. Schutz, R. W. P. Drever, R. Mason, C. Pollard, R. Tolcher, D. W. Bellenger, J. R. J. Bennett, I. F. Corbett and M. D. Percival. A British Long Baseline Gravitational Wave Observatory (Design Study Report). Technical Report GWD/RAL/86-001, May 1986.

Hough *et al.* 1989

J. Hough, B. J. Meers, G. P. Newton, N. A. Robertson, H. Ward, G. Leuchs, T. M. Niebauer, A. Rüdiger, R. Schilling, L. Schnupp, H. Walther, W. Winkler, B. F. Schutz, J. Ehlers, P. Kafka, G. Schäfer, M. W. Hamilton, I. Schütz, H. Welling, J. R. J. Bennett, I. F. Corbett, B. H. W. Edwards, R. J. S. Greenhalgh and V. Kose. Proposal for a Joint German-British Interferometric Gravitational Wave Detector. Technical Report M P Q 147 and GWD/137/JH(89), September 1989.

Hough *et al.* 1990

J. Hough, H. Ward, G. A. Kerr, N. L. Mackenzie, B. J. Meers, G. P. Newton, D. I. Robertson, N. A. Robertson and (R. Schilling). The detection of gravitational radiation. In Blair [Blair 1990], chapter The Stabilisation of Lasers for Interferometric Gravitational Wave Detectors. (in press).

Jitschin and Meisel 1979

W. Jitschin and G. Meisel. Fast frequency control of a cw dye jet laser. *Applied Physics*, 19:181 – 184, 1979.

Kerr *et al.* 1985

G. A. Kerr, N. A. Robertson, J. Hough and C. N. Man. Fast frequency stabilisation of an argon laser to an optical resonator using an extra-cavity electro-optic modulator. *Applied Physics B*, 37:11 – 16, 1985.

Lamb 1964

W. E. Lamb, Jr. Theory of an optical maser. *Physical Review*, 134(6A):A1429 –A1450, 1964.

Livas 1987

Jeffrey Clark Livas. *Upper limits for Gravitational Radiation from some Astrophysical Sources*. PhD thesis, Massachusetts Institute of Technology, Cambridge, Massachusetts, May 1987.

Mackenzie 1989

Norman L. Mackenzie. *Experiments relevant to the development of laser interferometric gravitational wave detectors*. PhD thesis, Glasgow University, Glasgow, September 1989.

Mackenzie *et al.* 1987

N. L. Mackenzie, H. Ward, J. Hough, G. A. Kerr, J. B. Mangan, B. J. Meers, G. P. Newton, D. I. Robertson and N. A. Robertson. Data acquisition and analysis with the Glasgow prototype detector. In B. F. Shutz, editor, *Gravitational Wave Data Analysis*. Kluwer Academic Publishers, 1987.

Mangan 1987

John B. Mangan. *Some techniques relevant to the development of a long baseline gravitational wave detector using laser interferometry*. PhD thesis, Glasgow University, Glasgow, September 1987.

Marshall 1978

S. A. Marshall. *Introduction to control theory*. Macmillan Education Ltd., London, first edition, 1978.

Meers 1983

Brian J. Meers. *Some aspects of the development of an optically sensed gravitational-wave detector*. PhD thesis, Glasgow University, Glasgow, December 1983.

Meers 1988

B. J. Meers. Recycling in laser interferometric gravitational wave detectors. *Physical Review D*, 38(8):2317–2326, 1988.

Niebauer *et al.* 1988

T. M. Niebauer, J. E. Faller, H. M. Godwin, J. L. Hall and R. L. Barger. Frequency stability measurements on polarisation-stabilized He-Ne lasers. *Applied Optics*, 27(7):1285 – 1289, 1988.

Pandharipande *et al.* 1976

V. R. Pandharipande, D. Pines and R. A. Smith. Neutron star structure: Theory, observation and speculation. *The Astrophysical Journal*, 208:550 – 566, 1976.

Press *et al.* 1986

William H. Press, Brian P. Flannery, Saul A. Teukolsky and William T. Vetterling. *Numerical Recipes: The art of scientific computing*. Cambridge University Press, Cambridge, 1986.

Robertson *et al.* 1986

N. A. Robertson, S. Hoggan, J. B. Mangan and J. Hough. Intensity stabilisation of an argon laser using an electro-optic modulator – performance and limitations. *Applied Physics B*, 39:149–153, 1986.

Rüdiger *et al.* 1981

A. Rüdiger, R. Schilling, L. Schnupp, W. Winkler, H. Billing and K. Maischberger. *Optica Acta*, 28:641 – 658, 1981.

Saenz and Shapiro 1981

R. A. Saenz and S. L. Shapiro. Gravitational Radiation from Stellar Core Collapse. III. Damped Ellipsoidal Oscillations. *Astrophysical Journal*, 244(1033), 1981.

Schilling

R. Schilling. Private communication.

Schilling 1986

R. Schilling. Private communication, 1986. in Hough *et al.* 89.

Schutz 1986

B. F. Schutz. Determining the Hubble constant from gravitational wave observations. *Nature*, 323:310–311, 1986.

Shoemaker *et al.* 1988

D. Shoemaker, R. Schilling, L. Schnupp, W. Winkler, K. Maischberger and A. Rüdiger. Noise behaviour of the Garching 30m prototype gravitational wave detector. *Physical Review D*, 38(2):423 – 432, 1988.

Taylor and Weisberg 1982

J. H. Taylor and J. M. Weisberg. A New Test of General Relativity: Gravitational Radiation and the Binary Pulsar PSR1913+16. *The Astrophysical Journal*, 253:908–920, 1982.

Thorne 1987

K. Thorne. Gravitational radiation. In S. W. Hawking and W. Israel, editors, *300 Years of Gravitation*. Cambridge University Press, 1987.

Umeda *et al.* 1980

N. Umeda, M. Tsukiji and H. Takasaki. Stabilised $^3\text{He} - ^{20}\text{Ne}$ transverse Zeeman laser. *Applied Optics*, 19(3):442 – 450, 1980.

Veitch 1990

P. Veitch. Parametric transducers. In Blair [Blair 1990]. (in press).

Vogt *et al.* 1989

R. E. Vogt, R. W. P. Drever, K. S. Thorne, F. J. Raab and R. Weiss. *A laser interferometer gravitational-wave observatory*. California Institute of Technology and Massachusetts Institute of Technology, 1989.

Wallard 1972

A. J. Wallard. Frequency stabilisation of the helium-neon laser by saturated absorption in iodine vapour. *Journal of Physics E*, 5:926–930, 1972.

Ward 1983

Henry Ward. *Experiments and Techniques relevant to a search for Gravitational Radiation using a Broadband Laser Interferometric Detector*. PhD thesis, Glasgow University, Glasgow, May 1983.

Weber 1960

J. Weber. Detection and generation of gravitational waves. *Physical Review*, 117(1):306 – 313, 1960.

Weiss 1972

R. Weiss. Electromagnetically coupled broadband gravitational antenna. *Quarterly Progress Report, Research Laboratory of Electronics, MIT*, 105:54-76, 1972.

White 1965

A. D. White. Frequency stabilisation of gas lasers. *IEEE Journal of Quantum Electronics*, 1(8):349 - 357, 1965.

Yariv 1985

Amnon Yariv. *Optical Electronics*. Holt, Reinhart and Winston, New York, third edition, 1985.

Zimmerman 1978

M. Zimmerman. Revised estimate of gravitational radiation from Crab and Vela pulsars. *Nature*, 271(524 - 525), 1978.

